

2

NAVAL POSTGRADUATE SCHOOL

Monterey, California



THESIS

EVALUATION OF
GEOMAGNETIC ACTIVITY IN THE MAD
FREQUENCY BAND (.04 to 0.6 Hz)

by

Jeffrey Mark Schweiger

October 1982

Thesis Advisor:

O. Heinz

Approved for public release; distribution unlimited

REPRODUCED FROM
BEST AVAILABLE COPY

DTIC
ELECTE
MAR 14 1983

AD A125641

DTIC FILE COPY

Unclassified

SECURITY CLASSIFICATION OF THIS PAGE (When Data Entered)

REPORT DOCUMENTATION PAGE		READ INSTRUCTIONS BEFORE COMPLETING FORM
1. REPORT NUMBER	2. GOVT ACCESSION NO. A125 641	3. RECIPIENT'S CATALOG NUMBER
4. TITLE (and Subtitle) "Evaluation of Geomagnetic Activity in the MAD Frequency Band (.04 to 0.6 Hz)"		5. TYPE OF REPORT & PERIOD COVERED Master's Thesis October 1982
7. AUTHOR(s) Jeffrey Mark Schweiger		8. CONTRACT OR GRANT NUMBER(s)
9. PERFORMING ORGANIZATION NAME AND ADDRESS Naval Postgraduate School Monterey, California 93940		10. PROGRAM ELEMENT, PROJECT, TASK AREA & WORK UNIT NUMBERS
11. CONTROLLING OFFICE NAME AND ADDRESS Naval Postgraduate School Monterey, California 93940		12. REPORT DATE October 1982
		13. NUMBER OF PAGES 116
14. MONITORING AGENCY NAME & ADDRESS (if different from Controlling Office)		15. SECURITY CLASS. (of this report)
		15a. DECLASSIFICATION/DOWNGRADING SCHEDULE
16. DISTRIBUTION STATEMENT (of this Report) Approved for public release; distribution unlimited		
17. DISTRIBUTION STATEMENT (of the abstract entered in Block 20, if different from Report)		
18. SUPPLEMENTARY NOTES		
19. KEY WORDS (Continue on reverse side if necessary and identify by block number) Magnetic Anomaly Detection Geomagnetic Indices MAD Noise MAD Geomagnetism Geomagnetic Fluctuations Geomagnetic Activity Geomagnetic Noise Low frequency geomagnetic measure- Geomagnetic Index ment		
20. ABSTRACT (Continue on reverse side if necessary and identify by block number) After defining geomagnetic noise as it applies to MAD, the geomagnetic indices currently used by the fleet to predict MAD geomagnetic noise are reviewed to determine their actual applicability. The current indices are determined to be insufficient, methods are proposed for establishing a new MAD index, and a developmental MAD— (continued)		

DD FORM 1473

EDITION OF 1 NOV 68 IS OBSOLETE
S/N 1102-014-5601

Unclassified
SECURITY CLASSIFICATION OF THIS PAGE (When Data Entered)

Unclassified

SECURITY CLASSIFICATION OF THIS PAGE (When Data Entered)

Item 20 (Continued)

index system was tested. Geomagnetic fluctuations in the .04 to 2.0 Hz frequency band was recorded at Monterey, California, and used for a preliminary test of the proposed MAD index.

Accession For	
NTIS GRA&I	<input checked="checked" type="checkbox"/>
DTIC TAB	<input type="checkbox"/>
Unannounced	<input type="checkbox"/>
Justification	
By	
Distribution/	
Availability Codes	
Dist	Avail and/or Special
A	



Approved for public release, distribution unlimited

Evaluation of Geomagnetic Activity in the MAD Frequency Band
(.04 to 0.6 Hz)

by

Jeffrey Mark Schweiger
Lieutenant, United States Navy
S. B., Massachusetts Institute of Technology, 1975

Submitted in partial fulfillment of the
requirements for the degree of

MASTER OF SCIENCE IN SYSTEMS TECHNOLOGY
from the
NAVAL POSTGRADUATE SCHOOL
October 1982

Author

Jeffrey Mark Schweiger

Approved by:

Olaf Heinz

Thesis Advisor

Andrew B. Ochelski Jr.

Second Reader

W. F. Funt

Chairman, ASW Academic Group

H. Shroy

Academic Dean

ABSTRACT

After defining geomagnetic noise as it applies to MAD, the geomagnetic indices currently used by the fleet to predict MAD geomagnetic noise are reviewed to determine their actual applicability. The current indices are determined to be insufficient, methods are proposed for establishing a new MAD index, and a developmental MAD index system was tested. Geomagnetic fluctuations in the .04 to 2.0 Hz frequency band were recorded at Monterey, California, and used for a preliminary test of the proposed MAD index.

TABLE OF CONTENTS

I.	GEOMAGNETICS REVIEW	11
A.	HISTORY OF GEOMAGNETICS	11
B.	EARTH'S MAGNETIC FIELD	12
	1. Constituents of the Geomagnetic Field . .	12
	2. Models of the Main Field	13
	3. Sources of the Geomagnetic Field	16
	4. Magnetosphere	19
	5. Time Variations of the Geomagnetic Field .	20
	a. Quiet Variation Fields	21
	b. Disturbed Variation Fields	25
	6. Elements of the Magnetic Field Vector . .	27
II.	INTRODUCTION TO MAGNETIC ANOMALY DETECTION (MAD) .	29
A.	DEFINITION OF A MAGNETIC ANOMALY	29
B.	HISTORICAL DEVELOPMENT OF THE MAGNETIC DETECTION OF SUBMARINES	29
	1. Early Detection Systems	29
	2. Early Operational Usage	32
	3. Current Systems	33
	4. Future Developments	35
C.	MAD SIGNAL AND BANDPASS	36
	1. Source of the Signal	36
	2. Anderson Functions	38
	3. The MAD Filter Bandpass	45
III.	SOURCES OF MAD NOISE	48
A.	INTRODUCTION	48
B.	SENSOR, PLATFORM AND MANUEVER NOISE	48
C.	GRADIENT NOISE	49
D.	ENVIRONMENTAL NOISE	50
E.	GEOMAGNETIC NOISE	52
	1. Geomagnetic Micropulsations	52

IV.	METHODS OF EVALUATING GEOMAGNETIC ACTIVITY	55
A.	INTRODUCTION	55
B.	GEOMAGNETIC INDICES	55
1.	K, a, and A Indices	56
C.	GEOMAGNETIC INDICES IN FLEET USE	58
1.	Current Usage	58
2.	Theoretical Applicability of A and K Indices to MAD	58
3.	Experimental Correlation of A and K Indices with MAD Band Noise	59
a.	ASQ-10A Study	59
b.	ASQ-81 Study	60
c.	Power Spectral Density Evaluation	63
d.	Correlation Conclusions	65
D.	PROPOSED GEOMAGNETIC INDICES FOR MAD	66
1.	Time Series Analysis	66
2.	Frequency Domain Index	66
3.	Predictions of Geomagnetic Activity	68
V.	DEVELOPMENTAL MAD INDEX SYSTEM AT NPS	69
A.	EQUIPMENT CONFIGURATION	69
1.	Data Collection System	69
a.	Coil Antenna Sensors	71
b.	Preamplifier	71
c.	Signal Conditioners	73
d.	Pulse Code Modulation (PCM) System	73
e.	Transmission and Recording	74
2.	Data Analysis Equipment	74
B.	DATA ANALYSIS SOFTWARE	74
1.	Data Input	75
2.	Fourier Analysis	75
3.	Application of Transfer Function and Total Field Projection	75
4.	Data Averaging	76

5.	MAD Index Calculation	76
6.	Plotting of Power Spectral Density	77
C.	INITIAL SYSTEM OPERATION	77
VI.	CONCLUSION AND RECOMMENDATIONS	84
A.	CONCLUSION	84
B.	RECOMMENDATIONS	84
	APPENDIX A: MAD INDEX DATA ANALYSIS SOFTWARE	85
	LIST OF REFERENCES	110
	BIBLIOGRAPHY	114
	INITIAL DISTRIBUTION LIST	115

LIST OF TABLES

I.	Quiet Day Variation in La Mesa Village, February, 26, 1979	24
II.	Geomagnetic Micropulsation Classes	53
III.	Conversion from Range to K for Fredericksburg, Va.	57
IV.	Equivalent Range ak for Given K	57
V.	Observed AUTECH Data and Indices, April 11-18, 1976.	61
VI.	Observed AUTECH Data and Indices, April 19-24, 1976.	62
VII.	Single Coil RMS Noise Data and Indices	64
VIII.	Cs Vapor RMS Noise Data and Indices, Jul-Oct, 1980	65
IX.	MAD Noise 2037-2206Z, 25 JUL 82, Monterey, CA	78
X.	MAD Noise 0921-1050Z, 18 AUG 82, Monterey, CA	80
XI.	MAD Noise 1307-1436Z, 18 AUG 82, Monterey, CA	82

LIST OF FIGURES

1.1	Dipole Appearance of Geomagnetic Field	14
1.2	Eccentric Dipole Model of Geomagnetic Field	15
1.3	Simple Disk Dynamo	17
1.4	Twin Disk Dynamo	18
1.5	Configuration of The Magnetosphere	21
1.6	Variation of Total Geomagnetic Field Intensity, February 26, 1979	23
1.7	Typical Midlatitude Geomagnetic Storm	26
1.8	Magnetic Field Elements	28
2.1	Element of Fluxgate Magnetometer	31
2.2	Magnetization Versus Exciting Current	32
2.3	Metastable Helium Magnetometer	34
2.4	Formation of Submarine Caused Magnetic Anomaly (Simplified View Near Equator)	37
2.5	Qualitative Aspects of MAD Signal	39
2.6	Basic MAD Component $f_0(b)$	41
2.7	Basic MAD Component $f_1(b)$	42
2.8	Basic MAD Component $f_2(b)$	43
2.9	Frequency Spectrum (Fourier Transform) of MAD Signal Components	44
2.10	ASQ-81 Filter Characteristics: 0.06 - 0.6 Hz	46
3.1	Induced Magnetic Field per Meter of Waveheight	51
5.1	Data Collection System	70
5.2	Sensor Dimensions	71
5.3	Sensor Mounting Block	72
5.4	PSD 25 JUL 82, 2037-2206Z, La Mesa Village	79
5.5	PSD 18 AUG 82, 0921-1050Z, La Mesa Village	81
5.6	PSD 18 AUG 82, 1307-1436Z, La Mesa Village	83

ACKNOWLEDGEMENTS

Although many people contributed directly and indirectly to this thesis, I owe a special gratitude to my advisors, Dr. Otto Heinz and Dr. Andrew R. Ochadlick, Jr. for their guidance, cooperation and assistance. I am also deeply indebted to Mr. David F. Norman of the W. R. Church Computer Center, and other center personnel for assistance in the debugging of my computer software. Thanks is also due to Dr. Paul H. Moose and Dr. Michael Thomas for general guidance, to CPT Edward Pogue, USA, for assistance in data collection, and to LCDR Arnold Gritzke, USN, and LT Robert Johnson, USN for their assembly of and assistance in documenting the PCM system.

I. GEOMAGNETICS REVIEW

A. HISTORY OF GEOMAGNETICS

The beginnings of the study of geomagnetism lie back in prehistory when magnetic attraction between iron and certain minerals was first observed. Exactly when this phenomenon was first noticed is not known, but the properties of magnetite, then called lodestone, appeared in Greek literature around 600 B. C. (Brennan and Davis). [Ref. 1]

Chapman [Ref. 2] indicates that the directional property of magnets was known and used in Europe prior to 1200 A. D. and possibly in China before then. E. N. Parker [Ref. 3] noted "It is an interesting fact that the ancient walls of Peking were lined up with magnetic north rather than geographic north, a difference at that time of about 10. We may presume that the surveyor found it easier to work with his compass needle by day than to sight on the pole star by night." This property allows the use of the Earth's geomagnetic field for navigational purposes.

By the mid-fifteenth century it was determined in Europe that the magnetic compass does not point to true north. The angle between true north and the direction indicated by the compass is now known as magnetic declination by the geophysicist and as variation by the navigator.

The magnetic field dip, or magnetic inclination is the angle, in a vertical plane, between the horizontal and the direction of the earth's magnetic field vector. It was observed in 1544 by an instrument maker in Nuremberg named Hartmann, and again by Robert Norman in London in 1581.

These discoveries or observations gave rise to the study of geomagnetics as a specialty which gained its cornerstone

with William Gilbert in 1600. After comparing his experimental results with the previous work of others such as Norman, Gilbert, in his book, "De Magnete," concluded that "magnus magnes ipse est globus terrestris (the earth globe itself is a great magnet)" [Ref. 2]. It is this concept, that the earth is itself a magnet, that is the basis of the science of geomagnetics.

Gilbert felt that the Earth's magnetism must remain constant except for geological changes, but it was soon determined that this was not the case. A 'secular variation' of the Earth's was found to exist.

Shorter term changes in the geomagnetic field were observed and it was eventually realized that geomagnetism is dynamic. In 1722 George Graham discovered that daily, or diurnal, variations exist [Ref. 2]. During the early Nineteenth century magnetic observatories began to be established to record the changes in the geomagnetic field in a systematic fashion (Knecht) [Ref. 4].

B. EARTH'S MAGNETIC FIELD

1. Constituents of the Geomagnetic Field

There are various ways of breaking down the constituting parts of the geomagnetic field. One way is to divide the field in terms of distance from the center of the earth. Doing this yields these three parts: internal, crustal, and external (AFGL) [Ref. 5]. The internal field originates in the core region and is the more stable field, containing only extremely low frequency temporal variations. The crustal (or anomalous) field arises from modifications made on the internal field by materials and structures in the Earth's crust. These variations are not spatially constant and give rise to some of what is known as geological

variations. The external field is the most dynamic and arises from many sources including the interaction between the solar wind and the terrestrial magnetic field.

Another way of describing the components of the geomagnetic field is by time variation. This division is accomplished by considering that part of the field which varies with periodicities greater than about one year as the steady field and what is left as the variation field (Knecht). [Ref. 4]

The steady field consists of the above named internal field, also referred to as the main field. Slow variations in the main field with periods of years or longer are referred to as secular variations.

2. Models of the Main Field

Various models of the main geomagnetic field make use of a geocentric dipole. Gauss, in 1839, demonstrated that, as a fairly good first approximation to the geomagnetic field, the field of a uniformly magnetized sphere (for points outside the sphere) is equivalent to the field of a magnetic dipole located at the center of the sphere (Jacobs). [Ref. 6]

The simplest of the present approximations of the geomagnetic field is that of a short bar magnet or dipole located at the center of the earth with an axis inclined approximately 11.5° from the Earth's axis of rotation. The sense of the field lines is from south to north (Figure 1.1).

The axis of this dipole intersects the earth at the geomagnetic north pole, 78.5°N , 291.0°E in geographic coordinates, and at the geomagnetic south pole, 78.5°S , 110.0°E . The moment of the geomagnetic dipole is 8.1×10^{22} amp-m². It is these poles that are used to define the geomagnetic

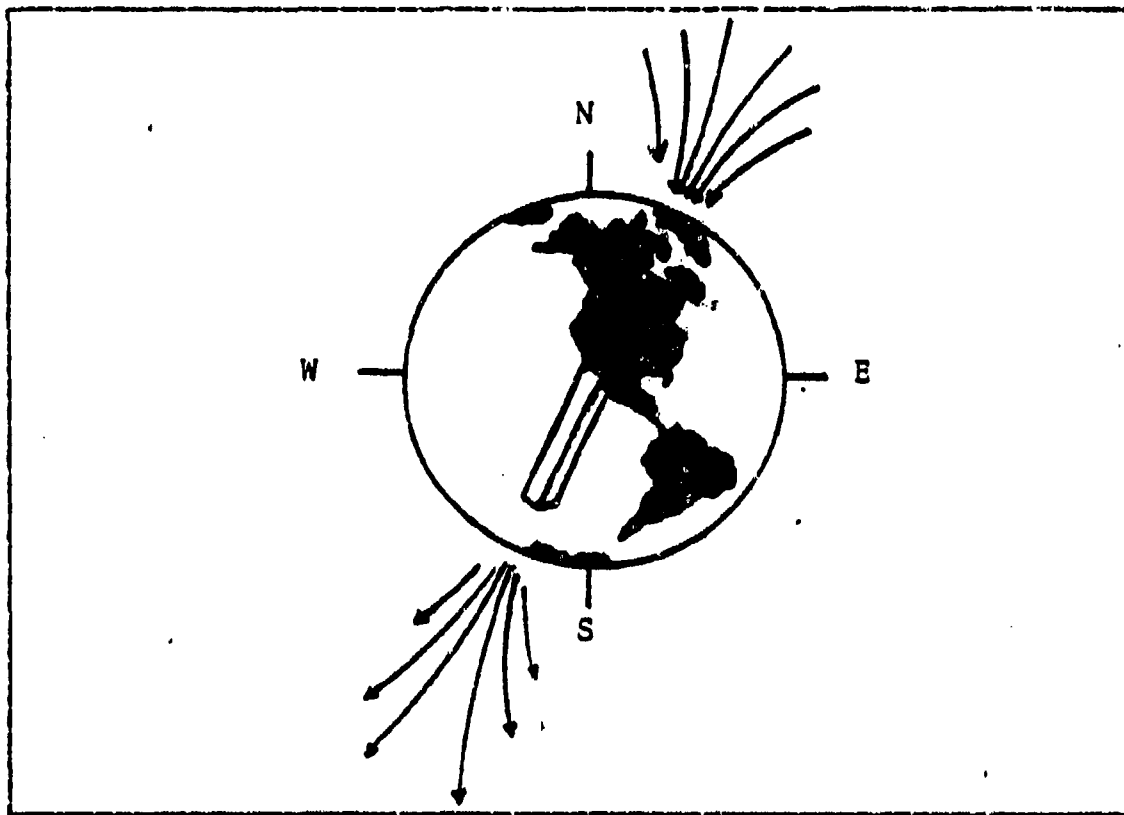


Figure 1.1 Dipole Appearance of Geomagnetic Field

coordinate system (Knecht) [Ref. 4]. The geomagnetic coordinate system is a spherical polar system similar to the geographic coordinate system with a geomagnetic equator defined 90 degrees away from either geomagnetic pole in latitude. This tilted geocentric dipole model describes the main geomagnetic field to an accuracy of about 10%.

In 1940 Chapman and Bartels defined an off-center dipole in the earth's interior, called the eccentric dipole. This dipole is displaced 0.0685 earth radii (436 km) in magnitude from the center and in the direction of the point 15.6°N, 150.9°E (geographic coordinates) (Vestine) [Ref. 7].

The intersections of the eccentric dipole axis at the earth's surface are 81.0°N , 84.7°W and 75.0°S , 120.4°E (Figure 1.2) (Haynes) [Ref. 8]. This approximation is accurate to within a few percent.

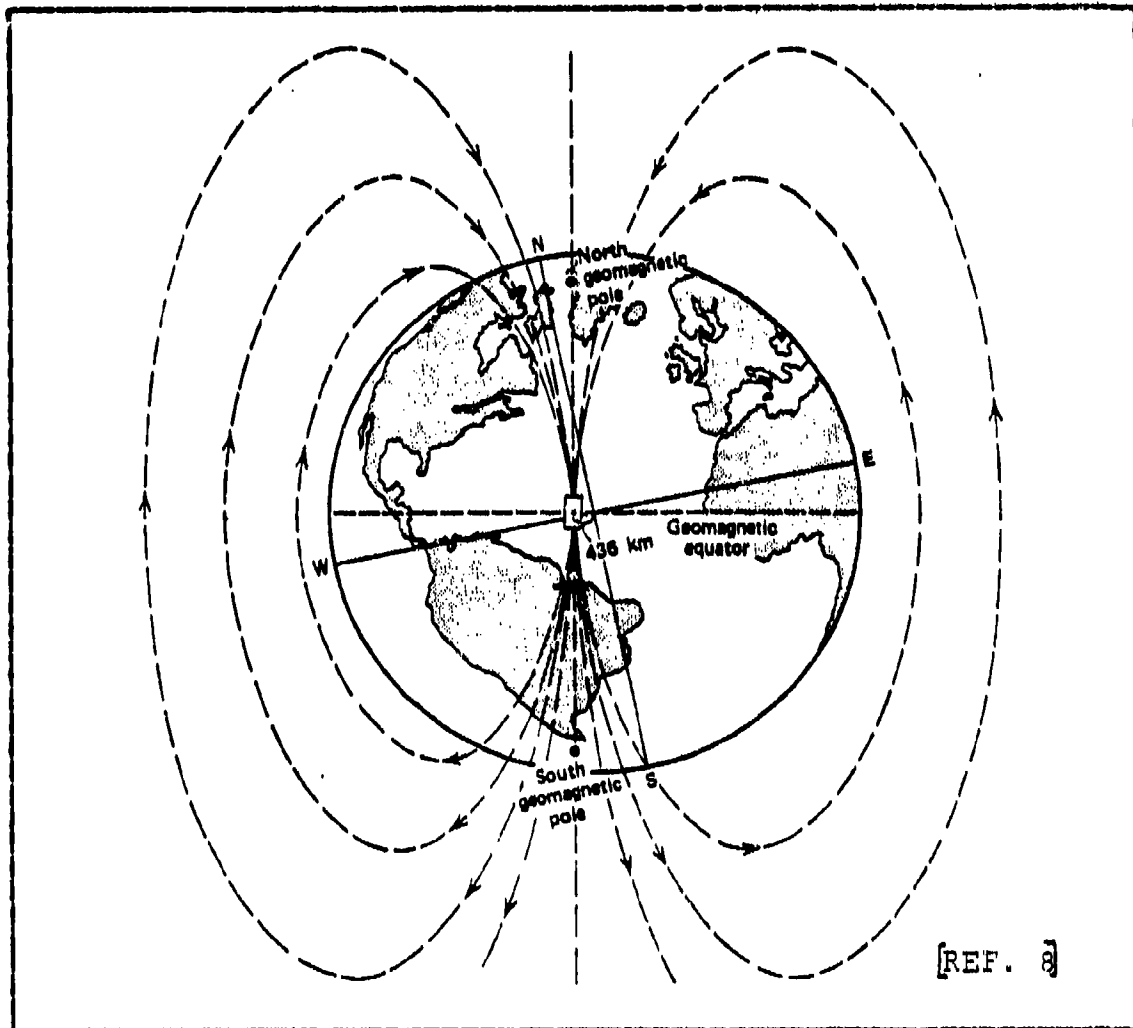


Figure 1.2 Eccentric Dipole Model of Geomagnetic Field

The field has additionally been modeled to an accuracy of about 1% by determining Gaussian coefficients by a least-squares fit of experimental measurements of the

geomagnetic field. These coefficients are used in a spherical harmonic series representing the scalar potential of the field. This accuracy implies that the internal contribution to the total main field is at least on the order of 99%.

The International Geomagnetic Reference Field (IGRF) yields values which differ by only parts per thousand from measured values.

3. Sources of the Geomagnetic Field

There are various elements that contribute to the geomagnetic field, some external to the earth's surface and some internal. As previously mentioned, the external contributions make up only a small fraction of the steady field, playing a more important role in the variation field.

These external sources include current systems in the earth's upper atmosphere affected by solar electromagnetic radiation and gravitation, solar corpuscular radiation or the interaction of solar plasma with the main field, and the effect of the solar interplanetary field. [Ref. 4]

Various magnetic surveys of the world, including those conducted at ground level, by airborne instruments, and by satellite, have pointed to the fact that the largest source of the earth's magnetic field is internal to it. While there exists residual permanent magnetism in the earth's crust, this cannot be the principal internal source of the geomagnetic field due to temperature and material properties known to exist in the earth's interior (Nagata and Ozima). [Ref. 9]

Permanent magnetism is generated by microscopic electric currents, since a changing electric field will generate a magnetic field. Another way to generate a magnetic field is by the motion of electric charges in a

macroscopic current. Convective motion of the electrically conducting fluid core of the earth, resulting in a macroscopic current system, is considered to be the principal source of the main field.

The most promising present theory of the generation of the geomagnetic field is that of some sort of a self-exciting dynamo system. This means that the motion of a conductor, such as the molten iron in the earth's core, in a magnetic field produces a current which in turn induces a magnetic field in support of the original magnetic field [Ref. 4, 7]. A very simple model of such a dynamo is shown in Figure 1.3 .

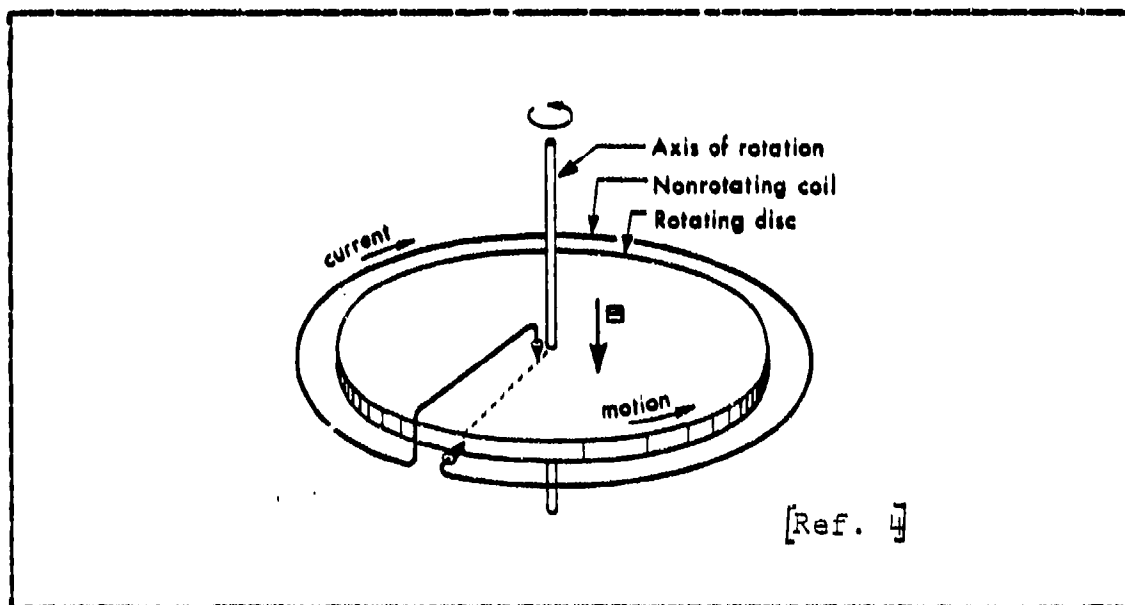


Figure 1.3 Simple Disk Dynamo

The original excitation or seed field may be due to an external field line, perhaps from the solar interplanetary magnetic field. This original, poloidal, field line is wound up due to the differential rotation (rotation not

constant with latitude) in the molten core. The wound up line becomes an intense azimuthal field which is carried outward by the upwelling associated with convection and twisted by the action of the Coriolis force. The twisting generates a helical toroidal field which, by outward diffusion, generates the externally observed quasidipole geomagnetic field.

The combination and interaction of two (see Figure 1.4) or more disk dynamos can also explain the reversal of the geomagnetic field [Ref. 7, 9].

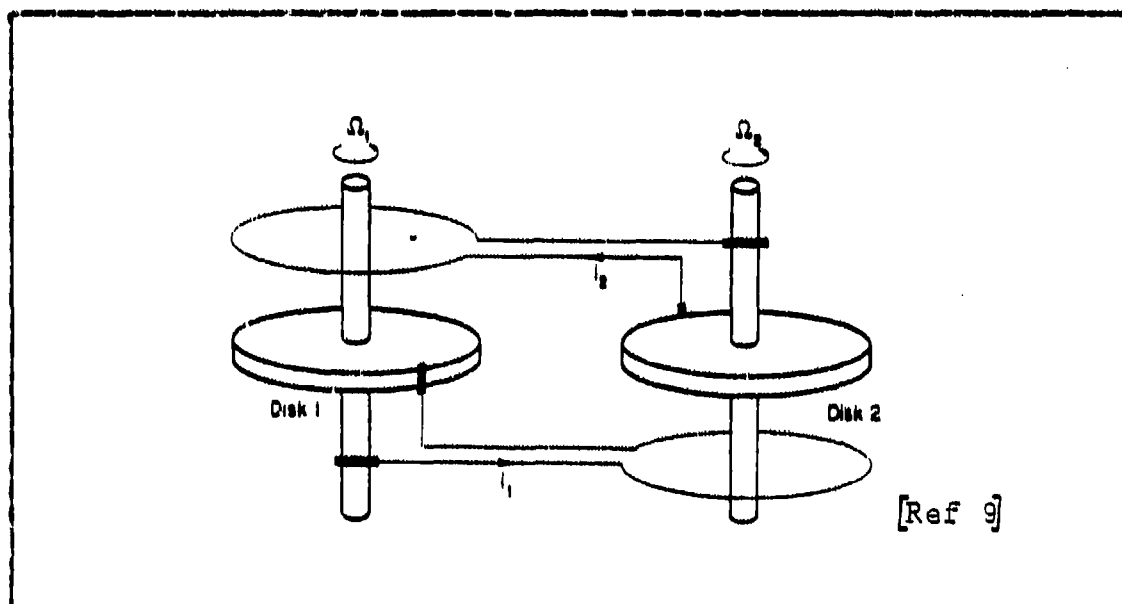


Figure 1.4 Twin Disk Dynamo

Regional anomalies that are nondipolar (do not conform to the dipole field) possibly arise from eddy circulations in the outer core [Ref. 4].

4. Magnetosphere

The magnetosphere can be defined to be that region (see Figure 1.5) occupied by the geomagnetic field above the ionosphere, a region where the field strongly influences the dynamics of ionized gas and charged particles (Kern) [Ref. 10].

If the space surrounding the earth were a perfect vacuum, the earth's magnetosphere and magnetic field might be more or less symmetric and extend outward until it merged with, and its strength became insignificant compared to the solar and other planetary magnetic fields. This turns out not to be the case.

Instead of being an island in a perfect vacuum, the earth encounters a continuous flow of hot, highly conductive ionized gas, or plasma, streaming outward from the sun. This continuous stream of charged particles is called the solar wind. The density of this 'wind' near earth is on the order of 10 particles per cm^3 , and has a velocity averaging 300-500 km per second (Jacobs). [Ref. 6]

Both the solar wind and the geomagnetic field exert pressure. The hot plasma of the solar wind pushes against the geomagnetic field deforming the field. At distances greater than about 13 or 14 earth radii, the pressure of the solar wind greatly exceeds that of the geomagnetic field and the geomagnetic field will be swept along with the wind. From 8 to 10 earth radii inward, the geomagnetic field pressure will predominate, excluding the solar wind, this being the region of the magnetosphere.

In the intermediate region, the magnitude of the solar wind and geomagnetic field pressures are comparable and the solar wind is compressed and flows around the geomagnetic field. This occurs when the magnetic energy density ahead of the plasma equals the kinetic energy

density of the streaming plasma. The solar wind is stopped at this point and forced to flow around the magnetosphere. This region where the magnetosphere starts is called the magnetopause. [Ref. 8]

The velocity of the undisturbed solar wind is analogous to a 'supersonic' velocity. Thus a shock front is formed between the magnetopause and the solar wind. The magnetosheath is the region of severe turbulence that exists between the shock front and the magnetopause.

Since the solar wind always travels outward from the sun, the effect of the wind on the earth's main field is not completely symmetric, although it is almost symmetric about an axis through the earth and sun. A geomagnetic tail is formed where the wind sweeps the geomagnetic field along with it on the nightside of the earth [Ref. 4]. Figure 1.5 pictorially represents the effects of the solar wind on the geomagnetic field.

5. Time Variations of the Geomagnetic Field

The geomagnetic field changes with time. As previously mentioned, very slow variations in the main field with periods on the order of years to thousands of years are referred to as secular variations. Secular variations are geologic or 'paleomagnetic' in origin. Secular variations are not caused by a strength or orientation change of the center dipole. Paleomagnetic studies are used to determine the secular variation. Geologic structure, especially conductivity structure, may partially mask the secular variation at one point on the earth as compared to that at another point.

Other time variations of the field can be categorized into quiet variation fields and disturbed variation fields. Disturbed variation fields include geomagnetic

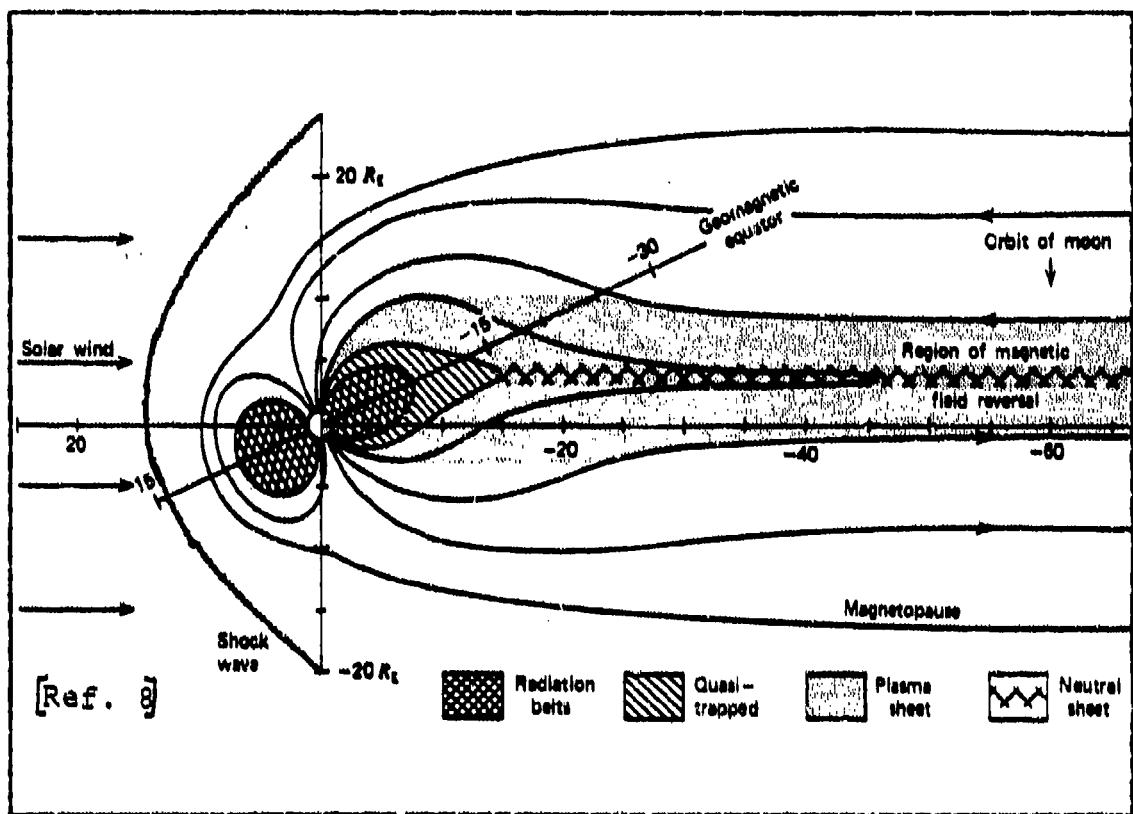


Figure 1.5 Configuration of The Magnetosphere

micropulsations which will be discussed separately, since they are of particular interest as a noise source for MAD sensors.

a. Quiet Variation Fields

Quiet variation fields are those which are not due to disturbances in the interplanetary environment and which vary slowly and regularly [Ref. 4].

There are several contributing fields to the quiet variation. These include the Solar Quiet Daily Variation (Sq), the Lunar Daily Variation (L), and the daily variation due to magnetospheric effects.

The Solar Quiet (Sq) variation is the name given to the pattern of diurnal field variation with respect to solar local time which is caused by currents flowing in the ionosphere (Matsushita) [Ref. 11]. The major portion (about two-thirds) of the Sq field is due to what is referred as an atmospheric dynamo. High speed tidal winds are generated by solar heating causing convection of the upper atmosphere [Ref. 4]. These winds produce a stationary current system by moving the conducting particles of the upper atmosphere across the geomagnetic field lines. The daily variation is caused by the earth rotating under the current system. The remaining third of the Sq variation is caused by currents in the earth induced by the primary currents in the ionosphere.

The Sq field can be shown to be latitude dependent reaching a maximum at the magnetic equator where a concentration of current, the equatorial electrojet, exists [Ref. 4]. The maximum horizontal component intensity is about 100 nT at the equator with 25 to 50 nT more likely at higher latitudes.

Longitudinal, seasonal, and solar cycle dependencies also occur for the Sq field.

An example of the quiet-day variation at Monterey, California is shown in Figure 1.6 and is summarized in Table I. This data was taken using a Cesium Vapor total field magnetometer in February, 1979.

The Lunar Daily Variation, L, is approximately one-tenth the magnitude of the Sq field and exhibits a semi-diurnal behavior in lunar time [Ref. 4]. The major difference is that the winds are caused by lunar-solar gravitational tides. The L field is dependent on seasonal influences, lunar phase, the solar cycle, and latitude.

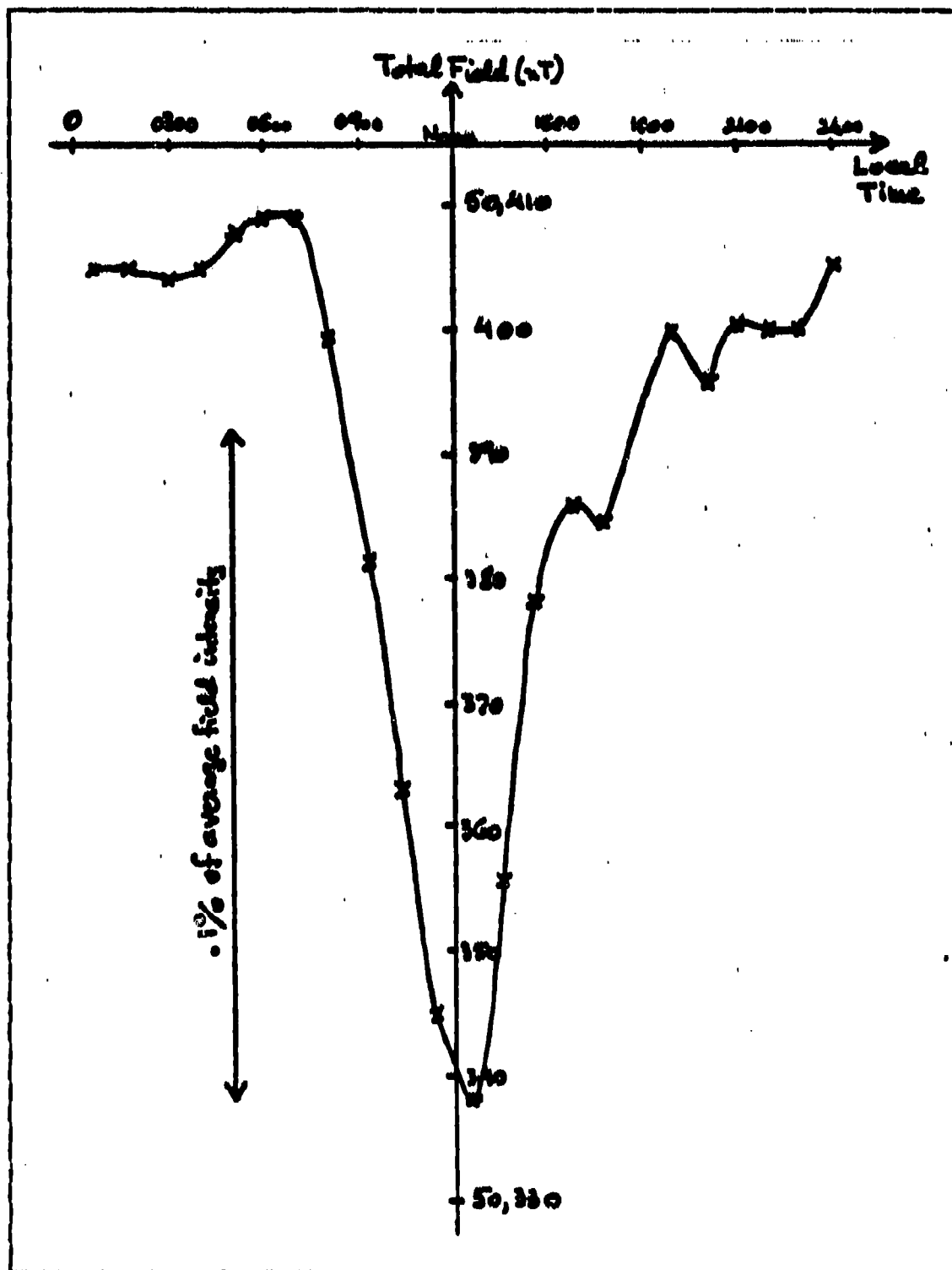


Figure 1.6 Variation of Total Geomagnetic Field Intensity, February 26, 1979

TABLE I

Quiet Day Variation in La Mesa Village, February, 26, 1979

POSITION 36°36'N, 121°51'W (LA MESA VILLAGE)

CALCULATED VALUES USING THE 1975 U.S. CHART MODEL (WORLD DATA CENTER A, BOULDER, COLORADO) FOR FEBRUARY 1979:

	D	I	H(NT)	Z(NT)	F(NT)
VALUE (FEB. 1979):	15.96°	60.74°	24,650	44,007	50,441
YEARLY CHANGE :	-2.3 '	-.8 '	-4.3	-32.1	-30.1

MEASURED VALUES OF TOTAL FIELD INTENSITY FOR FEB. 25, 1979

DATE	TIME	F(NT)
2/25/79	00:44	50,405.24
	01:48	50,405.79
	02:52	50,404.80
	03:56	50,405.48
	05:00	50,408.19
	06:04	50,409.15
	07:08	50,409.66
	08:12	50,399.69
	09:16	50,381.59
	10:20	50,363.68
	11:24	50,345.08
	12:28	50,338.51
	13:32	50,356.48
	14:36	50,378.86
	15:40	50,386.98
	16:44	50,384.30
	18:51	50,400.81
	19:55	50,396.91
	20:59	50,401.85
	22:03	50,400.80
2/26/79	23:07	50,400.54
	00:11	50,406.51

MID-DAY LOW

AVERAGE 50,390.50 ± 21.43 (NT)

$F_{\text{CALC}} - F_{\text{MEAS}} = 50.5 \text{ NT OR } .1\%$

A diurnal effect due to the dayside-nightside difference in compression by the solar wind of the geomagnetic field causes a small variation of the order of 3 nT [Ref. 4].

b. Disturbed Variation Fields

Disturbed variation fields are geomagnetic field variations that appear to be the result of interplanetary environmental changes and do not possess a simple periodicity. These variations include ionospheric disturbances, the aurora, geomagnetic storms, and geomagnetic micropulsations.

An ionospheric disturbance is a departure from the normal behavior of the ionosphere.

Solar flare effects (SFE) are magnetic disturbances produced by X-rays emitted from the solar flare. SFE's usually have a rapid onset, typically a few minutes in duration, followed by a slower return to normal. The entire event lasts on the order of an hour (Reid). [Ref. 12]

Auroras are caused by the precipitation of charged particles down magnetic field lines into the atmosphere and can be one of the brightest visual phenomena in the sky. The more intense and active auroras occur with geomagnetic disturbances and greatly increase ionization as well as creating the spectacular visual displays. [Ref. 4]

Geomagnetic storms are due to a change in the dynamic pressure of the solar wind. A typical storm begins with a compression of the magnetic field by an increase in solar wind dynamic pressure called a sudden commencement (SC), which increases the magnetic field (The so-called "gradual storm" begins with a gradual increase in field strength). The increase in field strength is on the order of several tens of nanoTeslas (nT) and takes about one to

six minutes to rise. If a disturbance starts with an SC but lacks the succeeding stages of a storm it is referred to as a sudden impulse (SI). Following the SC, the field remains compressed for two to eight hours in the initial phase of the storm. The main phase follows the initial phase. Over a period of hours to a day a westward ring current is set up at a distance of several earth radii whose magnetic field leads to a decrease in field strength on the order of 100 nT. This decrease overshoots the equilibrium field strength and leads into the recovery phase of a day or longer where the field returns towards its prestorm strength as the ring currents gradually dissipate [Ref. 4], (Matsushita) [Ref. 13]. A magnitude-time graph of a typical geomagnetic storm is shown in Figure 1.7.

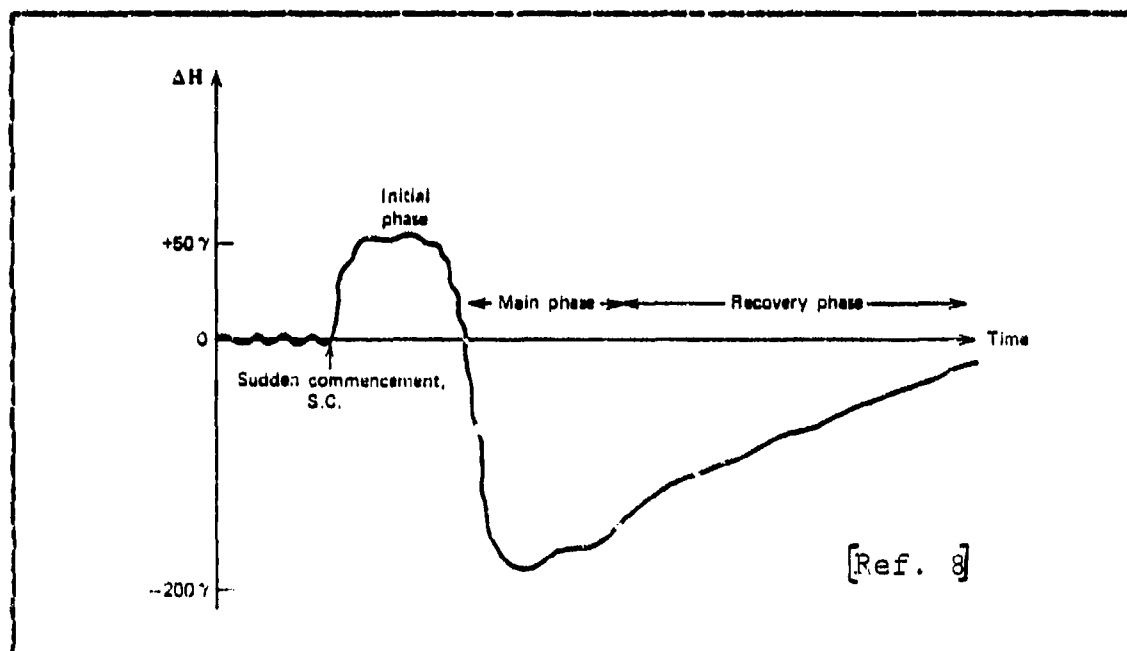


Figure 1.7 Typical Midlatitude Geomagnetic Storm

Geomagnetic micropulsations are rapid fluctuations in the surface magnetic field with periods of about 0.2 seconds to 10 minutes (frequencies about 0.0016 to 5.0 Hz). These are observed as a type of geomagnetic disturbance by ground based magnetometers [Ref. 4]. Micropulsations will be discussed in depth later.

6. Elements of the Magnetic Field Vector

The geomagnetic field vector is measured or characterized at any point by its direction and magnitude. This can be done in terms of some set of three independent parameters such as two direction angles and the magnitude, or three perpendicular components. [Ref. 4]

The system of coordinates commonly employed for describing the geomagnetic field on the surface of the earth is shown in Figure 1.8. The field is measured in terms of local (geodetic) coordinates with respect to True North.

The various coordinates are referred to as magnetic elements and are defined as follows:

B: Total Field Intensity (the symbol F is also used)

H: Horizontal Component

X: Northward, or North-South Component

Y: Eastward, or East-West Component

Z: Downward, or Vertical Component

D: Declination or magnetic variation. This is the angle between X and H and is measured positive eastward.

I: Inclination or dip angle. This is the angle between H and B and is measured positive downward.

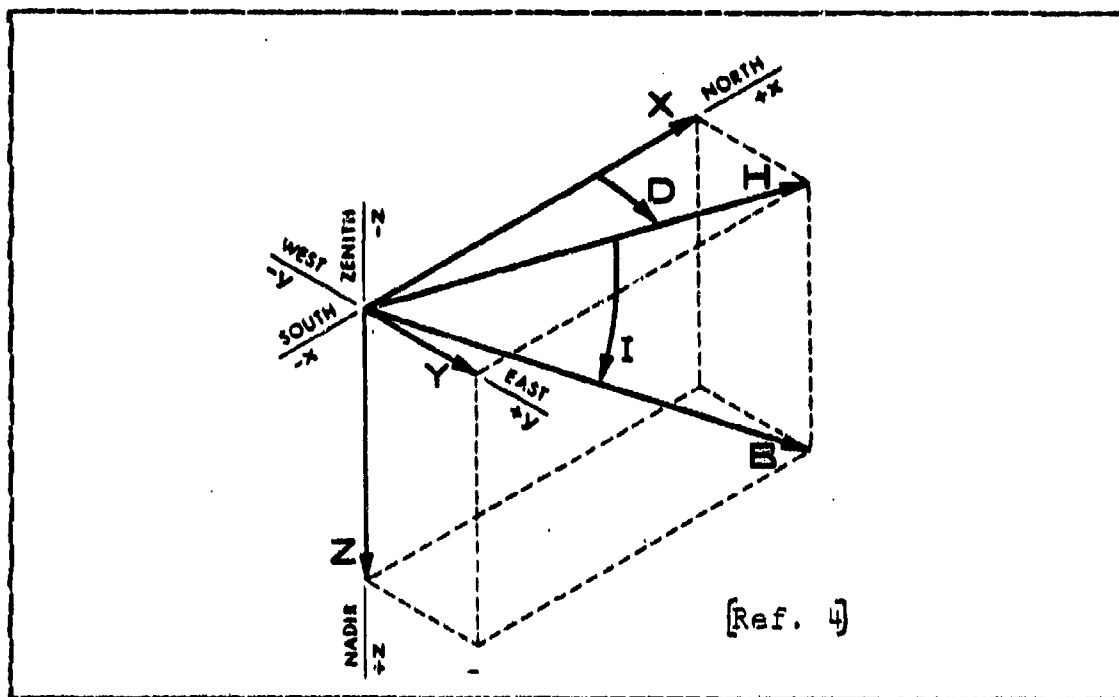


Figure 1.8 Magnetic Field Elements

II. INTRODUCTION TO MAGNETIC ANOMALY DETECTION (MAD)

A. DEFINITION OF A MAGNETIC ANOMALY

A magnetic anomaly is defined as any spatial variation or disturbance in the geomagnetic field which is due to local causes. Anomalies can be caused by waves, ore deposits, sea mounts, and magnetized objects such as surface ships and submarines (Anderson) [Ref. 14]. For the purposes of this research, magnetic anomalies due to a simple dipole field, such as those generated by submarines, will be regarded as signals, while other anomalies will be regarded as noise and will be discussed later.

B. HISTORICAL DEVELOPMENT OF THE MAGNETIC DETECTION OF SUBMARINES

1. Early Detection Systems

Attempts at finding submerged submarines by sensing disturbances in the geomagnetic field date back as least as far as World War I. In 1918, Earnest Merritt, at the Naval Experimental Station, New London studied the use of a fixed coil type of detector for use in moving boats and airplanes (Slichter). [Ref. 15]

MAD, originally known as Magnetic Airborne Detector, and now called Magnetic Anomaly Detection, had its beginnings as an airborne ASW sensor in late 1940 and early 1941.

Anomalies in the geomagnetic field caused by the presence of submarines, are on the order of one to a few nT (gammas) in magnitude. This is quite small compared to the magnitude of the field itself (30000 - 60000 nT). Two methods are generally employed to measure this small

disturbance. One is to use a gradiometer which measures the spatial rate of change of the magnetic field or its gradient. The second method, and the one presently used by U.S. Navy aircraft is to use a magnetometer to directly measure changes in the magnitude of the magnetic field.

The British investigated the use of a gradiometer for submarine detection, and by early 1941, had developed a two-coil gradiometer system which could detect a submarine at a range of 200 feet under favorable conditions. This range was considered to be too small to be of operational value and work on such a system was terminated when a magnetometer system showed promise (Coleman). [Ref. 16]

By late 1940, Victor V. Vacquier of the Gulf Research and Development Company had developed a sensitive saturable core magnetometer intended for geophysical (mineral) prospecting. The Vacquier magnetometer became the basis for further MAD development. The Airborne Instrument Laboratory of Columbia University continued the investigation of means of localizing submerged submarines by MAD.

The simplest saturable core or fluxgate magnetometer consists of a saturable or ferromagnetic core around which a coil of wire is wrapped (see Figure 2.1). This coil carries a sinusoidal current, $I(t)$, which is large enough to saturate the core during part of each cycle. The inductance of the coil will change as a function of the magnetization of the core. The core magnetization, in turn, depends on the instantaneous current in the coil, and, if present, the external magnetic field.

In the absence of an externally applied magnetic field, magnetization as a function of exciting current is symmetric around $I=0$ (Figure 2.2). An external magnetic field parallel to the core's axis will change the magnetization of the core and shift the magnetization curve. This

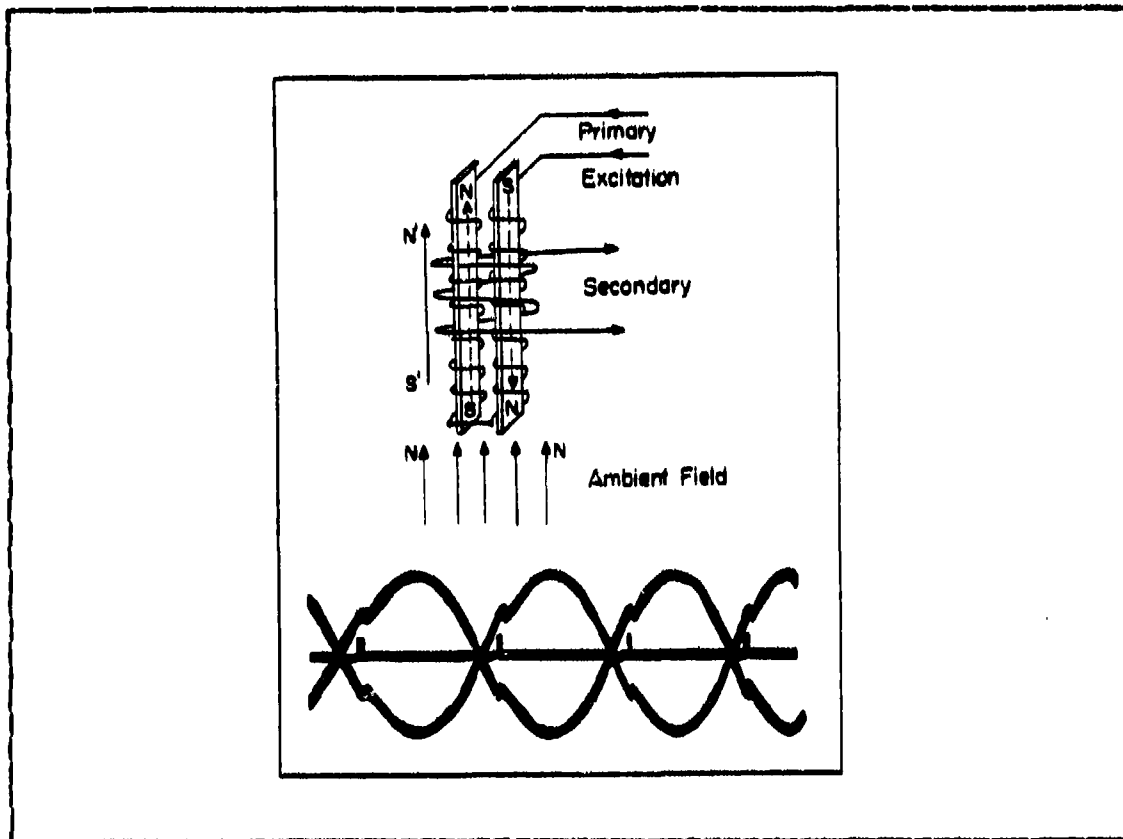


Figure 2.1 Element of Fluxgate Magnetometer

change will cause an asymmetry which can be sensed by analyzing the harmonic content of the signal. The coil can be combined with a stabilizer system, which keeps the detector element (coil) aligned with the geomagnetic field.

This was the basis of the MAD magnetometers used in World War II such as the AN/ASQ-1, ASQ-1A, and ASQ-2 [Ref. 16].

The fluxgate magnetometer measures only the component of the external field parallel to the axis of the ferromagnetic core. In order to measure the total field in this fashion it is necessary to align the ferromagnetic core along the earth's magnetic field or by using mutually

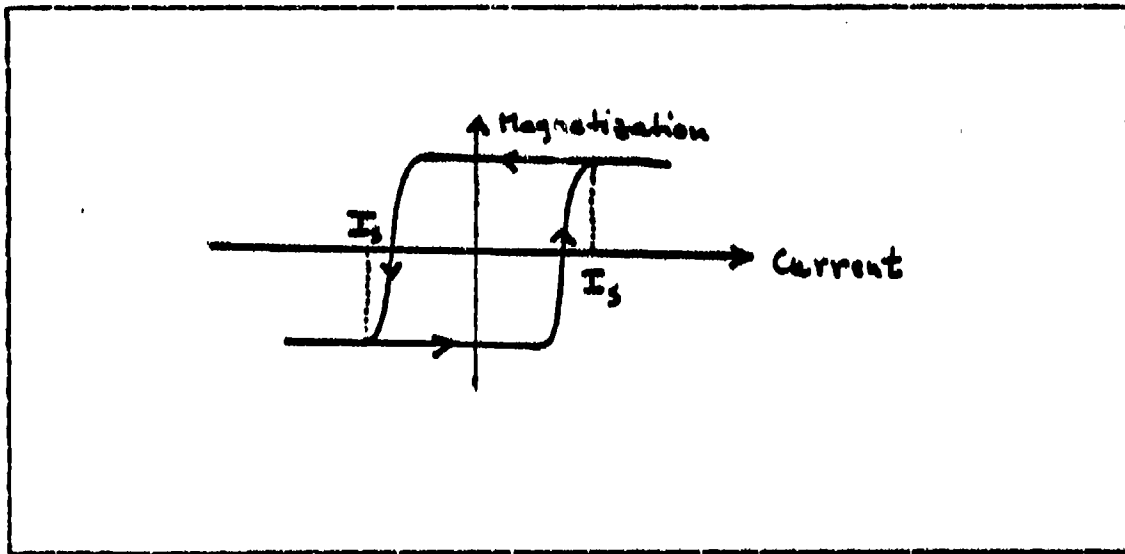


Figure 2.2 Magnetization Versus Exciting Current

perpendicular (orthogonal) cores. Precision requirements made this type of system difficult to realize during World War II but it has since found many years of operational usage and has found widespread use in geophysical exploration work and satellite mapping of the geomagnetic field.

2. Early Operational Usage

During World War II MAD provided a passive method of detection and tracking of submerged submarines. Within its range (then on the order of 500 feet) MAD gave a measure of surprise to the attacking aircrew. Until the first attack was delivered the crew of the submerged submarine might not even be aware of the aircraft hunting it.

Operational deployment of MAD began on a limited basis in December, 1941 with the installation of the early Mark I MAD in a blimp at Naval Air Station Lakehurst, New Jersey [Ref. 16].

By the end of 1942, MAD was operational on board PBY Catalina aircraft, nicknamed "Madcats." Even though MAD was operational at this time, it was not until February, 1944 that an initial contact by MAD led to the sinking of a submarine.

During February, 1944, the Madcats of Patrol Squadron 63 were assigned to fly a MAD barrier patrol of the Straits of Gibraltar. On 24 February 1944, a Madcat of VP-63 detected U-761 by use of MAD and commenced tracking to confirm the contact as a moving target. An attack was conducted in conjunction with another Catalina, two destroyers, and eventually two other aircraft, and U-761 was sunk. U-392 was sunk after a similar MAD contact on 16 March, and on 5 May, the third successful attack on a U-boat resulting from an initial MAD contact took place when U-731 was sunk (OEG No. 51, Price). [Ref. 17, 18]

The attacks at the Straits of Gibraltar demonstrated that though MAD has a limited search rate, there are scenarios where it can be employed effectively as a search sensor, such as providing a blockade across a restricted area without the presence of surface craft (OEG No. 54) [Ref. 19].

3. Current Systems

The magnetometer system in current operational use is the optically pumped magnetometer. The optically pumped magnetometer measures the external magnetic field by making use of the fact that when an atom is immersed in a magnetic field, its energy levels are split. This is known as the Zeeman effect. For the fields of interest, the amount of splitting of the levels is proportional to the intensity of the magnetic field. By measuring the separation between the levels the magnitude of the magnetic field can be determined.

This type of magnetometer usually makes use of Cesium or Rubidium vapors, or Helium gas. The current operational MAD system, the AN/ASQ-81, is a Helium gas optically pumped magnetometer.

In an optically pumped magnetometer (see Figure 2.3), the sample vapor or gas (such as Helium) is collected into an absorption cell. Circularly polarized light is passed through the cell giving up some of its energy in exciting or pumping the electrons of the sample gas to higher energy levels. These electrons then fluoresce to lower, metastable energy states. This is 'optical pumping.' A detector monitors the degree of optical pumping by measuring the transparency of the gas cell.

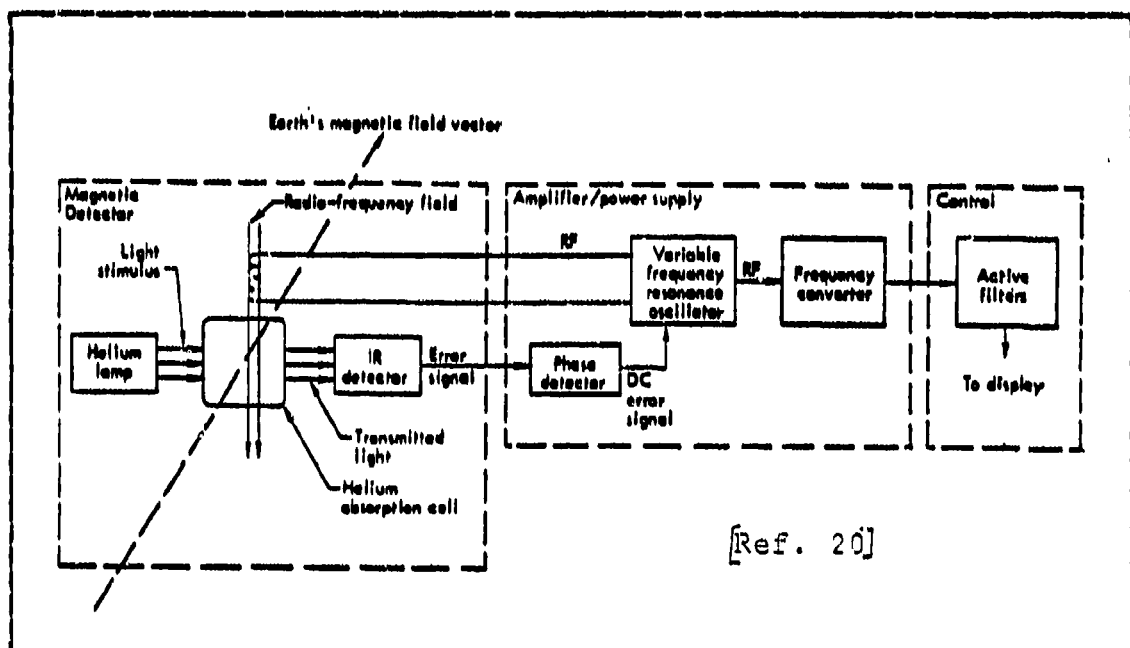


Figure 2.3 Metastable Helium Magnetometer

The actual separation of the energy levels is measured by applying a weak R. F. field which redistributes the

electrons among the ground state sublevels. These transitions will only occur when the R. F. field has a particular frequency (called the Larmor frequency) which is proportional to the separation between the levels and therefore to the external magnetic field [Ref. 20]. Thus measurement of this frequency yields a direct value of the magnetic field.

4. Future Developments

Optically pumped magnetometers are the most sensitive sensor for fleet usage today. Increasing capability to make use of the phenomenon of superconductivity will yield more sensitive MAD sensors. Superconducting Quantum Interference Devices (SQUIDS) which make use of the Josephson effect have a theoretical sensitivity of 10^{-7} nT as opposed to the theoretical value of 0.001 nT and the operationally realized value of 0.01 nT in current fleet systems (Chilton) [Ref. 20]. Field changes on the order of 10^{-5} nT have actually been measured. These SQUIDS are used in both superconducting magnetometers, and superconducting gradiometers.

A Josephson junction consists of a thin layer of insulator between two superconductors. This junction has the property that a current can flow across it without developing a voltage up to some maximum current. A voltage is developed for all current values greater than the maximum current.

In a superconducting magnetometer a superconducting ring containing a pair of Josephson junctions is used to measure the amount of magnetic flux penetrating the loop. This system is a vector magnetometer which measures variations in only one field component.

By using more than one superconducting loop, it is possible to measure magnetic field gradients, and construct a superconducting gradiometer. This is also a component, or vector, sensor.

These instruments have been used extensively in the laboratory and to some extent in geophysical work, but considerable engineering problems remain to be solved before operational Navy use can be contemplated.

C. MAD SIGNAL AND BANDPASS

1. Source of the Signal

The MAD signal results from moving a magnetometer through the magnetic field of a submarine, which can be approximated by the field of a magnetic dipole. Figure 2.4 depicts the formation of a submarine caused anomaly.

The magnetic moment of an object in the earth's magnetic field can be due to permanent magnetization, magnetization induced by the earth's magnetic field, or a combination of both. In the case of a submarine hull both causes are present with a small amount of permanent magnetization produced by hull stress in metal components during construction and stress caused by submarine diving and surfacing. This, however, is a minor contribution. The most important constituent of the submarine magnetic moment is due to magnetization induced in the hull by the presence of the geomagnetic field. [Ref. 21]

The induced field of a submarine depends on the effective permeability along the vertical, athwartships, and longitudinal axes of the submarine. This information, taken together with the strength and dip angle of the geomagnetic field, yields a fairly precise calculation of the magnetic anomaly produced by the submarine. 'Deperming'

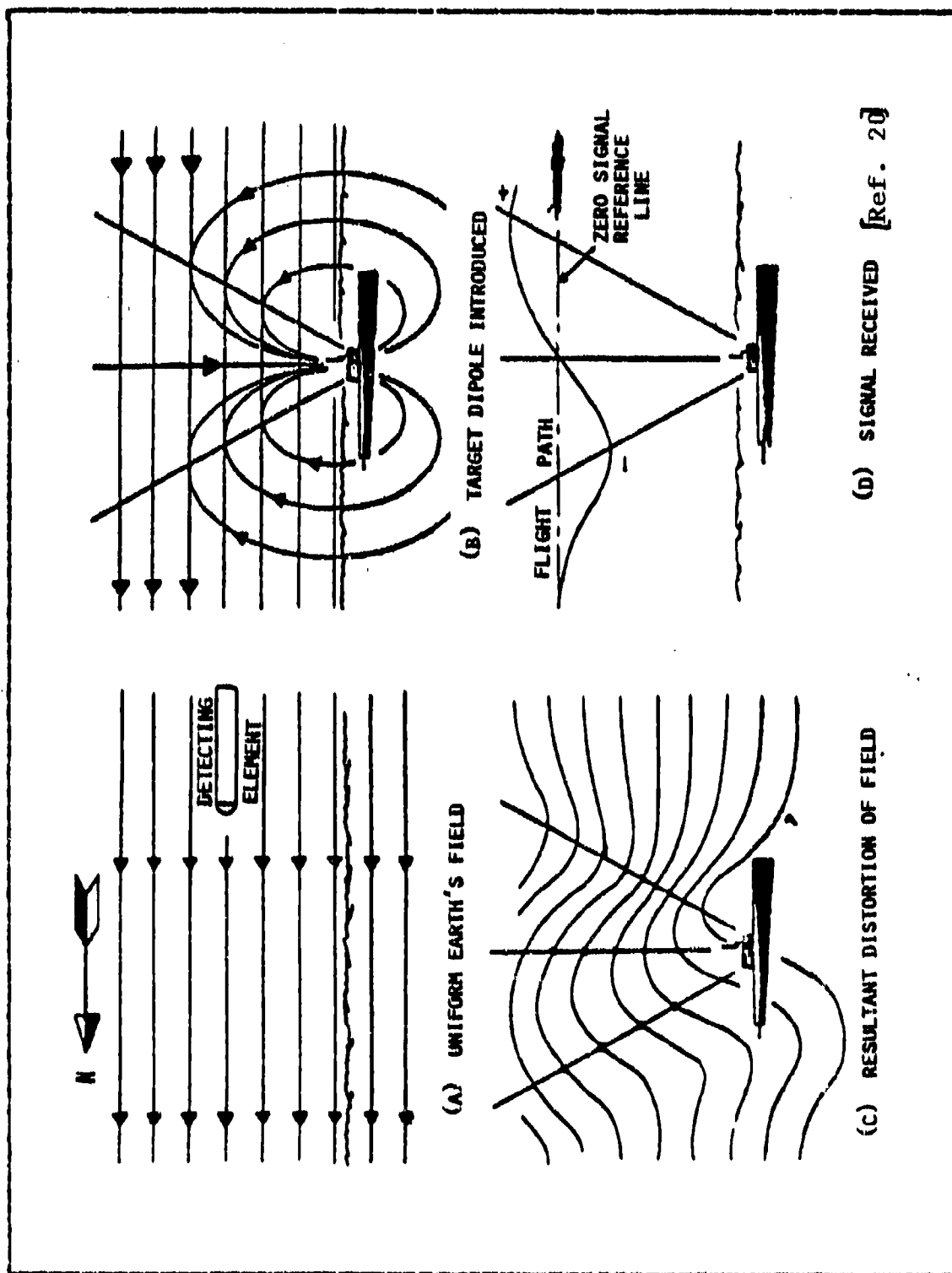


Figure 2.4 Formation of Submarine Caused Magnetic Anomaly (Simplified View Near Equator)

of the submarine hull cancels out the permanent hull magnetization leaving the induced magnetization as the principal signal source. [Ref. 21]

The MAD signal is approximated as the projection of the submarine dipole field onto the geomagnetic field vector. This approximation is good because the magnitude of the dipole field is very much smaller than the magnitude of the geomagnetic field (a few nanoTeslas as opposed to approximately 50000 nT). Therefore, whenever the dipole field is perpendicular to the earth's field a region of zero signal will result. The signal recorded by the AN/ASQ-81 or other MAD equipment is a mapping along the aircraft's flight path of this signal. Figure 2.5 qualitatively describes some aspects of the MAD signal.

2. Anderson Functions

The submarine anomaly signal shape is a function of the dip angle of the geomagnetic field, the magnetic heading of the aircraft, magnetic heading of the submarine dipole, and the lateral range between the aircraft and the submarine. These factors determine the 'A' coefficients for the Anderson functions below.

In 1949, J. E. Anderson of the Naval Air Development Center determined that the MAD signal, obtained along any course, consisted of a linear combination of three basic components. Different shaped signals could be obtained by changing the proportional contribution of these basic components. The mathematical representation of these components are now referred to as the Anderson functions. Using the dimensionless parameter 'b' (defined as the distance traveled along the aircraft track divided by the slant range at closest point of approach (CPA), $b=0$ at CPA) the anomaly can be represented by

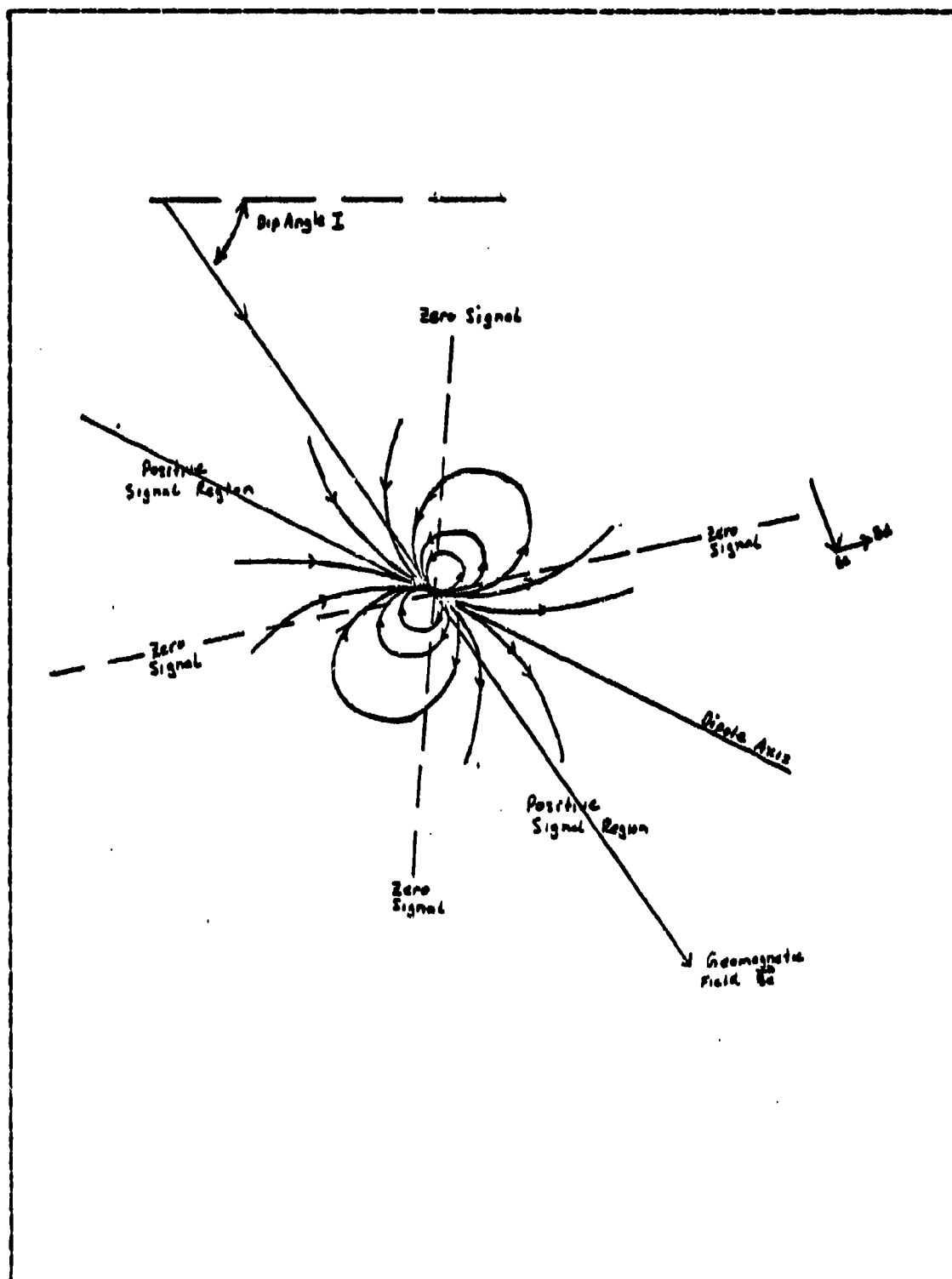


Figure 2.5 Qualitative Aspects of MAD Signal

$$B_s = \frac{M}{z^3} \frac{A_2 b^2 + A_1 b + A_0}{(b^2 + 1)^{5/2}} \quad (2-1a)$$

$$\text{or } B_s = \frac{M}{z^3} [A_0 f_0(b) + A_1 f_1(b) + A_2 f_2(b)] \quad (2-1b)$$

where M = magnetic moment of target dipole
 z = lateral range between target and plane at CPA

$$f_0(b) = \frac{1}{(b^2 + 1)^{5/2}}$$

$$f_1(b) = \frac{b}{(b^2 + 1)^{5/2}}$$

$$f_2(b) = \frac{b^2}{(b^2 + 1)^{5/2}}$$

The strength of the detected signal is seen to fall off as the cube of the distance between the aircraft and the target.

By analyzing the functions and their coefficients, it can be shown that the optimum orientation for maximum anomaly signal detection is when the aircraft, target dipole, and geomagnetic field are lined up together as closely as possible. Specifically, this occurs when the submarine moment and the aircraft's track are oriented North-South. [Ref. 14, 21]

The Fourier transform of the component functions were taken to determine the frequency distribution of energy in the MAD signal. The anomaly signal components are shown in Figures 2.6 through 2.8 (Anderson) [Ref. 14]. The Fourier transforms of the signal components with a platform velocity of 150 knots are shown in Figure 2.9.

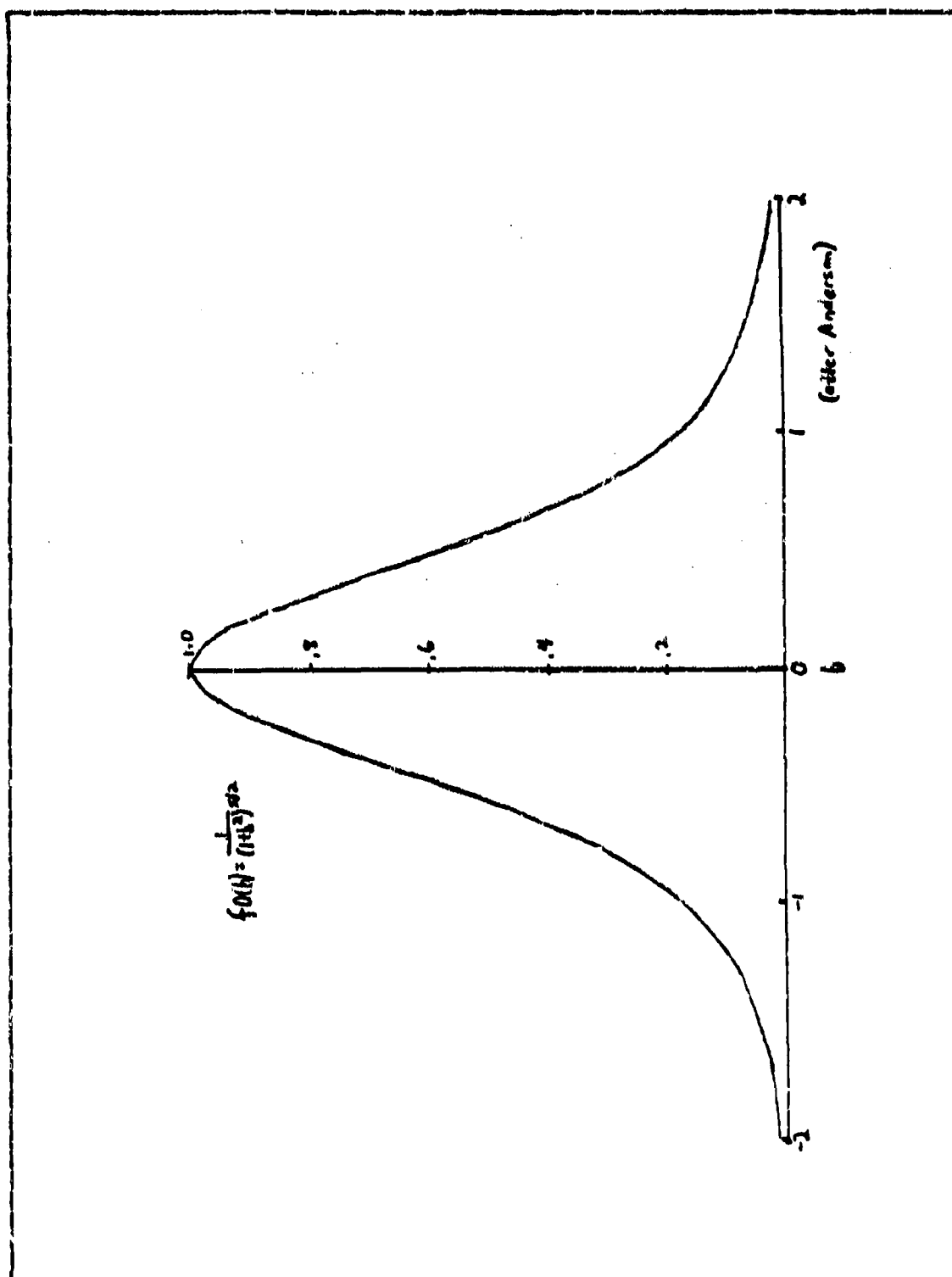


Figure 2.6 Basic MAD Component $f_0(b)$

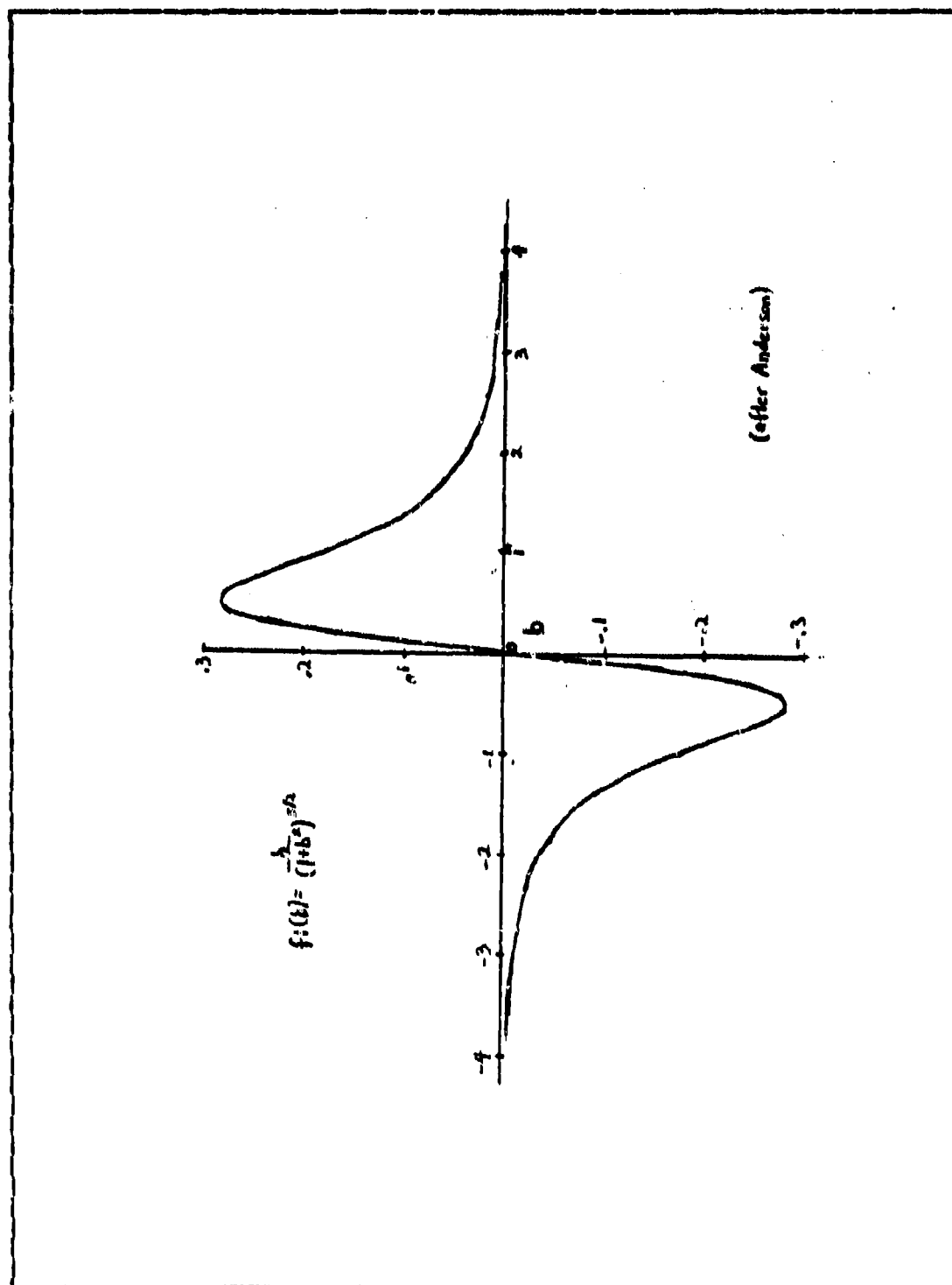


Figure 2.7 Basic MAD Component $f_1(b)$

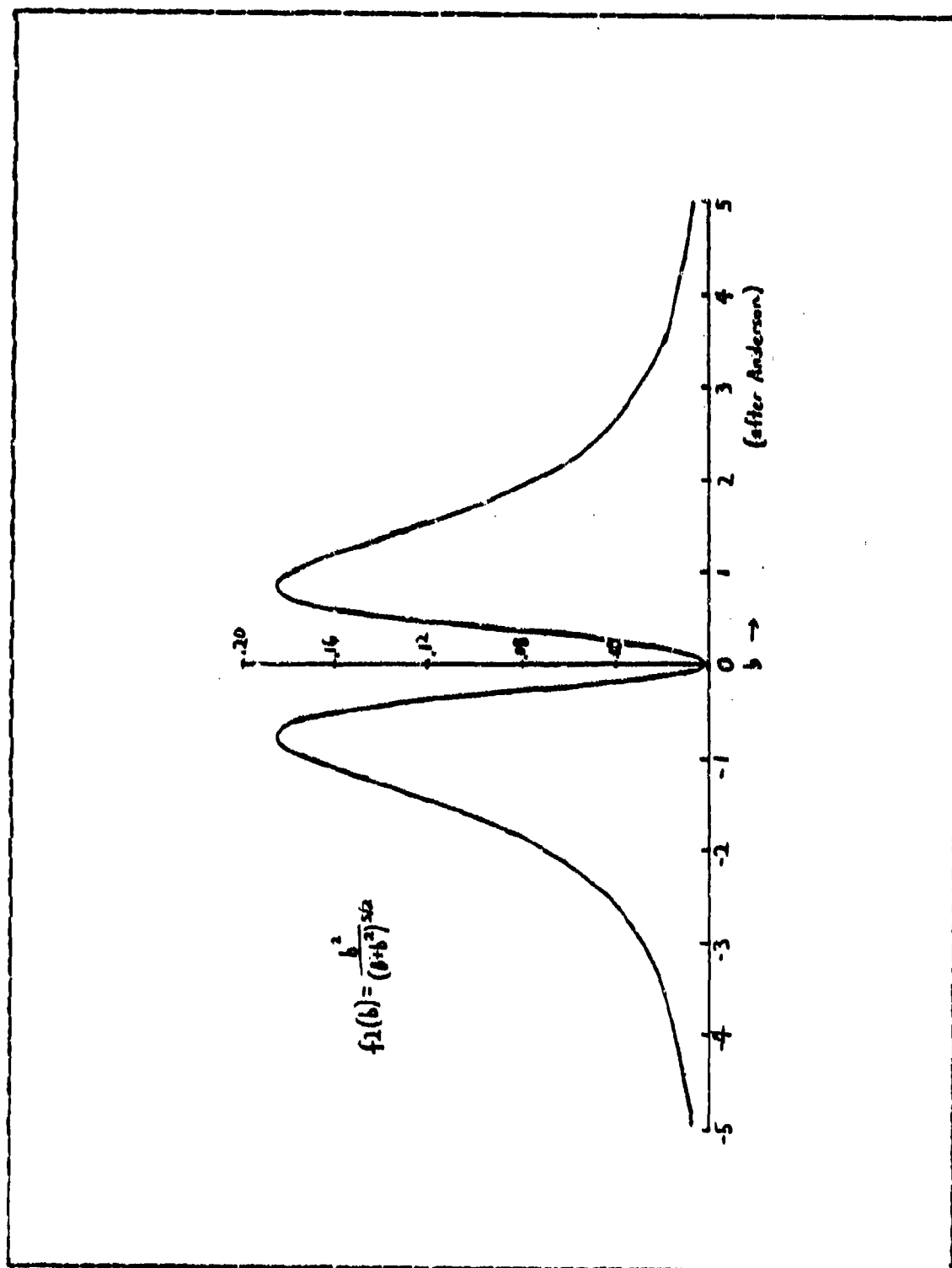


Figure 2.8 Basic MAD Component $f_2(b)$

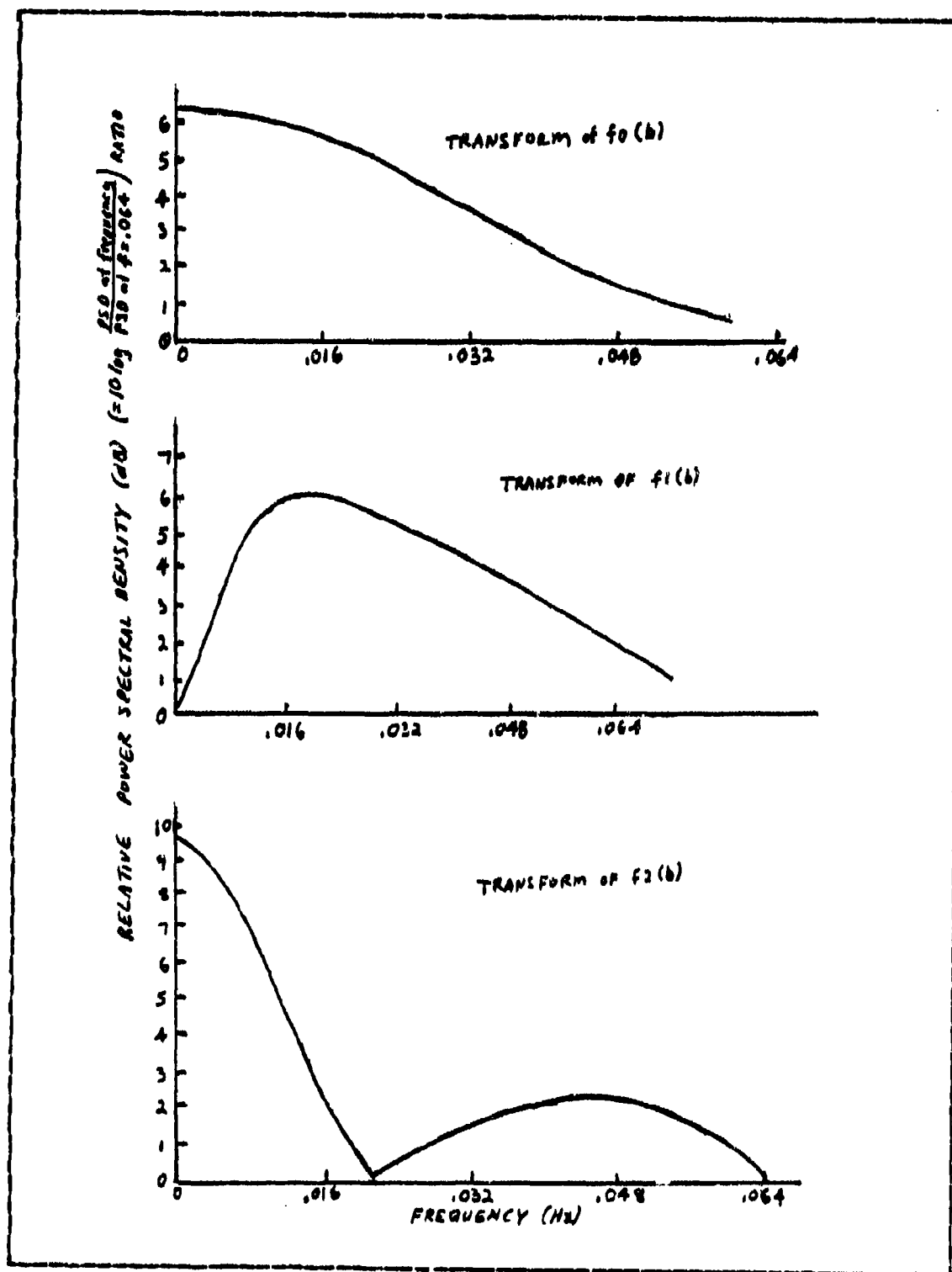


Figure 2.9 Frequency Spectrum (Fourier Transform) of MAD Signal Components

3. The MAD Filter Bandpass

The MAD signal, being a transient, is essentially a broadband (as opposed to a discrete frequency) signal. The frequency spectra of energy content shows how the signal is contained in a certain frequency range. In order to screen out unwanted noise, bandpass filtering is used in processing magnetic anomaly detections.

The major factors influencing the determination of an optimum MAD filter frequency are aircraft speed and the slant range from the aircraft to the target at CPA. Factors exerting a minor influence include dip angle, aircraft heading, and target dipole orientation.

The range in frequency variation is about an octave, with the higher values occurring when the passes are made parallel to the axis of the dipole and the lower when the pass is perpendicular to the dipole. Anderson empirically determined that the center frequency of the filter is given by

$$f = \frac{0.4 v}{Z} \quad (2-2)$$

where f = frequency in Hertz
 v = aircraft velocity in ft/sec
and Z = greatest anticipated CPA
 range in feet

The ASQ-81 Bandpass Filter has highpass settings of 0.04, 0.06, 0.08, and 0.1 Hz, and lowpass settings of 0.2, 0.4, 0.6, and 2.0 Hz (Orion Service Digest 26) [Ref. 22]. There are no recommended settings for normal operation since background noise varies. The filter characteristics for the 0.06 to 0.6 Hz settings are shown in Figure 2.10 (Orion Service Digest 28) [Ref. 23].

The figure is a representation of the adjustable band pass filter of the ASQ-81 by itself. Other parts of the ASQ-81 system add in an additional high pass filter which adds another 12 dB/octave roll off to the low frequency end in Figure 2.10. Thus Figure 2.10 would represent the characteristics of the entire ASQ-81 system if the roll off of 36 dB/octave is changed to 48 dB/octave. [Ref. 24]

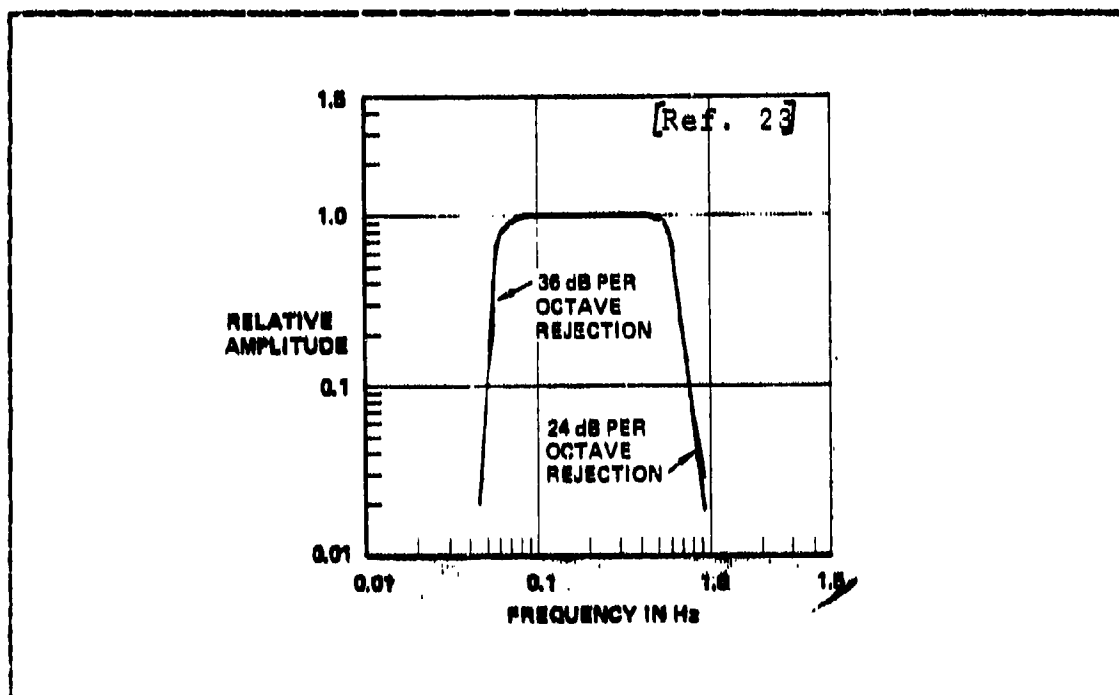


Figure 2.10 ASQ-81 Filter Characteristics: 0.06 - 0.6 Hz

Using equation 2-2, the center frequency for a MAD signal with a CPA slant range of 300 feet and aircraft velocity of 220 knots is 0.49 Hz. Using a lowpass filter setting above 0.6 Hz would not be very useful.

One reason the ASQ-81 filter extends up to 2.0 Hz instead of just 0.6 Hz is the following. The early Service Test Engineering Model (STEM) ASQ-81 that preceeded the

current ASQ-81 production model had two bandpass filters, one adjustable from .04 to .6 Hz, and the other fixed at .75 to 10 Hz. During tests, the .75 to 10 Hz channel proved to be helpful in monitoring the STEM ASQ-81 "system" noise level. During design reviews for the production ASQ-81, it was decided that it might be useful to retain the ability to monitor "system" noise. In order to do this easily, the .75 to 10 Hz band was dropped and a 2 Hz position was added to the adjustable filter. [Ref. 24]

The center frequency at 1200 feet and 160 knots is .09 Hz. Consequently, the highpass filter settings could affect slower, longer range MAD detections.

The choice of the highpass (lower end of bandpass) settings have to be made after considering the noise present at time of system operation.

III. SOURCES OF MAD NOISE

A. INTRODUCTION

On a practical level MAD noise is defined as magnetic disturbances falling within the MAD passband (0.04 to 2.0 Hz, or since 0.6 Hz is the normal upper limit, 0.04 to 0.6 Hz) and having an amplitude greater than 0.01 nanoteslas (the system sensitivity of the AN/ASQ-81 MAD system).

MAD noise sources can be divided into the following categories:

- Equipment Noise
- Aircraft Platform Noise
- Aircraft Maneuver Noise
- Gradient Noise Due to Aircraft Motion Through the Geomagnetic Field
- Geologic Noise
- Noise from Wind Waves and Swells
- Geomagnetic Noise

B. SENSOR, PLATFORM AND MANUEVER NOISE

Sensor noise is the self-noise generated by the operation of the equipment itself. This can be partially due to the fact that the detector element is misaligned with respect to the geomagnetic field vector. Changes in lamp intensity, photodetector noise and noise in the electronic circuits can also contribute to sensor noise [Ref. 21]. The self-noise limitation of the ASQ-81 is 0.01 nT.

Platform noise is generated by components fixed to the aircraft in the vicinity of the sensor [Ref. 23]. Permanent, induced and eddy-current magnetic fields are

associated with the airframe. Permanent magnetic fields are due to aircraft structure or equipment having ferromagnetic parts. This field changes its orientation with respect to the geomagnetic field vector as the aircraft maneuvers, causing field fluctuations near the magnetometer.

Platform noise is also induced in aircraft ferromagnetic structures by the geomagnetic field. Similarly, eddy-currents are induced in aircraft skin, ribs, and frames, and these currents, in turn, cause additional magnetic fields. Thus, rapid aircraft maneuvers will induce changes in the magnetic field sensed by the magnetometer.

Platform noise in aircraft mounted sensors is countered by applying equal and opposite magnetic fields to the sensor in a process called compensation. Towed MAD systems are essentially free from this type of noise.

C. GRADIENT NOISE

Gradient noise can be divided into turn noise and noise due to changes in altitude.

Turn noise is a problem when 'MAD trapping' or using MAD for tracking a target. The earth's magnetic field has a horizontal gradient (in this case the magnitude varying with latitude). As the aircraft moves in the direction of the gradient the field strength changes. The noise due to a MAD trapping or hunting circle is centered in frequency at the reciprocal of the time taken to complete one revolution. In the case of a two-minute circle, the noise would be centered at 0.00833 Hz, well below the filter used in the ASQ-81. The horizontal gradient noise due to flying a cloverleaf pattern, for the most part, also falls below the MAD passband. [Ref. 21]

Vertical gradient noise is due to changes in sensor altitude. An altitude gradient of up to 0.005 to 0.01 nT

per foot exists in the earth's main field. In areas of geological anomalies this gradient is even larger. Fast altitude or aircraft pitch changes can cause a magnetic field fluctuation of sufficient amplitude to be of concern. To avoid vertical gradient noise, altitude compensation equipment is used. [Ref. 23]

D. ENVIRONMENTAL NOISE

Magnetic noise from sources existing in the natural environment include geologic noise, temporal variation in the earth's magnetic field, and noise due to ocean waves and swells.

Geologic noise has its source in naturally occurring magnetic anomalies caused by magnetic material present in the earth's crust. When the sensor passes over geological anomalies, the relative motion causes a MAD-like signal to be recorded. Geologic noise is usually more pronounced in shallow water as the sensor is much closer to the source of the noise. Geological magnetic anomalies are often associated with such oceanographic features as seamounts and ocean ridges.

Sea water is a conducting medium which is transported by the physical motion of water waves in the presence of the geomagnetic field. This motion induces currents in the sea. These currents give rise to secondary magnetic fields, which add vectorially to the quasistatic, geomagnetic field (Weaver) [Ref. 25]. These fields can be detected at significant distances above the sea surface and fall off exponentially with altitude. Figure 3.1 is a plot for several surface wave periods of the induced magnetic field per meter amplitude of the surface wave. These induced fields can be a problem at the low altitudes where MAD is used.

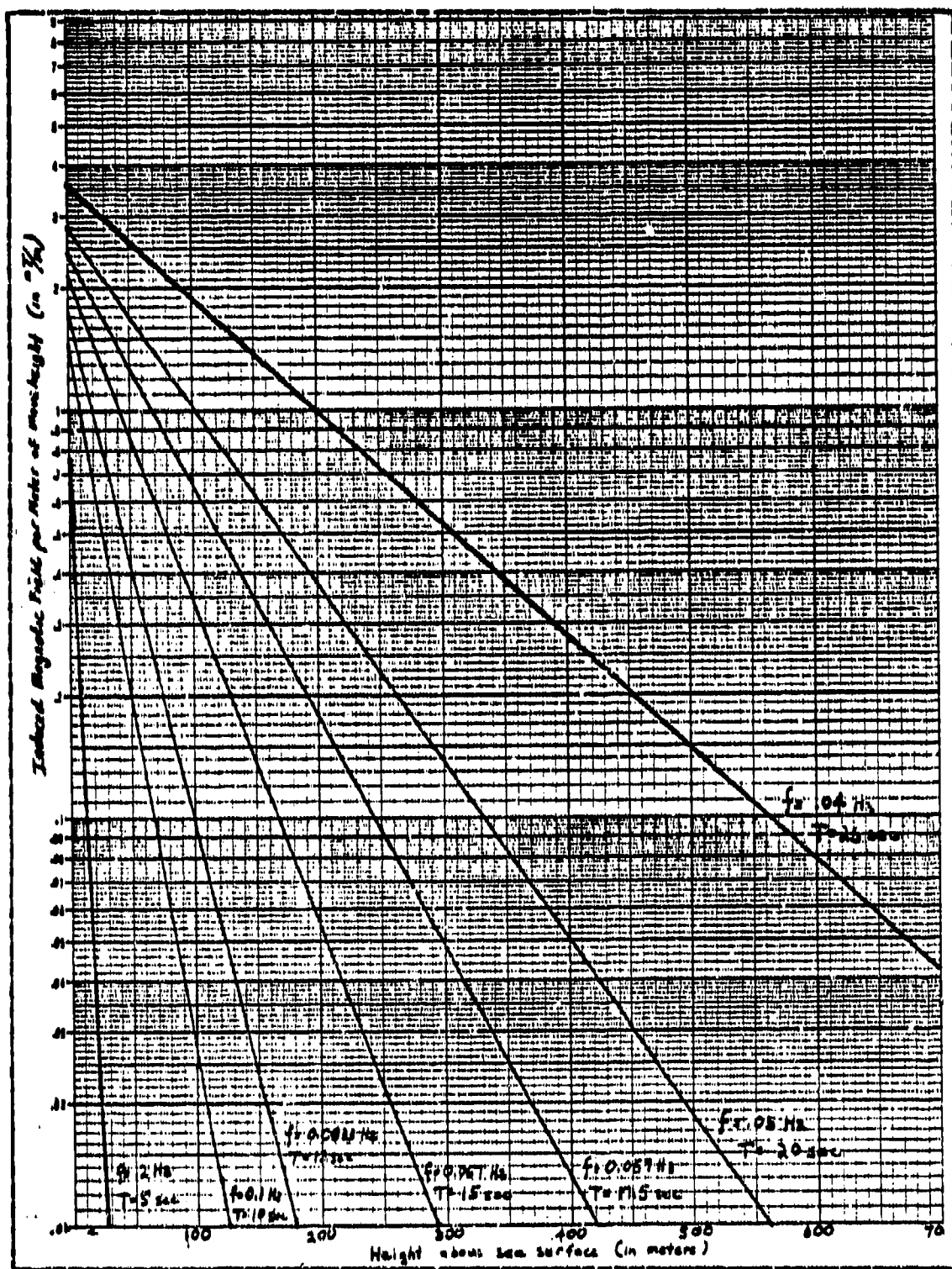


Figure 3.1 Induced Magnetic Field per Meter of Waveheight

E. GEOMAGNETIC NOISE

Temporal variations in the earth's magnetic field with frequencies in the MAD bandpass and amplitudes greater than 0.01 nT have become known as geomagnetic noise in the MAD literature.

Quiet daily variations, such as the Sq and L variations, have periods sufficiently long to fall far below the MAD passband.

Geomagnetic storms have been discussed previously. Rapid fluctuations with high amplitude and falling within the MAD passband occur in connection with geomagnetic storms.

Geomagnetic micropulsations comprise the last category of geomagnetic noise to be discussed.

1. Geomagnetic Micropulsations

Geomagnetic micropulsations are rapid fluctuations of the earth's magnetic field with periods from 0.2 seconds to 10 minutes and amplitudes from about 0.1 nT to as high as a few tens of nT's. These fluctuations are caused by electromagnetic perturbations propagating in the magnetosphere as hydromagnetic waves (Nishida). [Ref. 26]

Micropulsations are classified by morphology, that is, by examining periods, amplitudes, times of occurrence and other observed characteristics. Micropulsations have been placed into two broad categories: irregular and continuous. The irregular pulsations are represented by the symbol Pi, and the continuous pulsations by Pc. Table II shows the breakdown by period of the various micropulsation classes.

It can be seen that for MAD geomagnetic noise the lower frequency Pc1, Pc2, Pc3, and Pi1 pulsations are of interest.

TABLE II

Geomagnetic Micropulsation Classes

NOTATION	PERIOD (sec)	AVERAGE AMPLITUDE (nT)
PC1	0.2 - 5.0	0.05 - 0.1
PC2	5 - 10	0.1 - 1.0
PC3	10 - 45	0.1 - 1.0
PC4	45 - 150	0.1 - 1.0
PC5	150 - 600	0.1 - 1.0
PI1	1 - 40	0.05 - 0.1
PI2	40 - 150	1 - 5

(after Jacobs)

Pc1 pulsations are regular sinusoidal oscillations with periods normally falling in the 0.3 to 4 second (0.25 to 3.33 Hz frequency) range. Pc1's may start as separate bursts and gradually develop into a series of pulsations which could last for hours. They may also occur as consecutive groups of pulsations with sharply varying frequencies. The average amplitude of Pc1's is 0.05 to 0.1 nT and they tend to have a single well defined frequency. Pc1 pulsations with frequency less than 0.5 Hz are more common at high latitudes than at mid latitudes. These pulsations occur in the daytime in the auroral zone, and at night and early morning hours in lower latitudes. Pc1's are characteristic of the quiet and weakly disturbed states of the geomagnetic field and show an increase in activity one to two hours before, and four to seven days after, a magnetic storm. [Ref. 6]

Pc2 and Pc3 pulsations are grouped together in most characteristics. The amplitudes of the oscillations are usually under 0.5 nT and the typical frequency range is 0.03 to 0.2 Hz. These pulsations are normally found during the day with their activity reaching a maximum around noon. Pc3 pulsations show a seasonal variation with a minimum of activity occurring during winter.

Pc4 and Pc5 are large amplitude fluctuations, but fall below the frequency band of interest for MAD.

Pi1 pulsations have an irregular form with an average amplitude of 0.01 to 0.1 nT and a frequency mainly in the 0.10 to 0.17 Hz range. Spectral analysis of these pulsations show a broad band of frequencies. Pi1 amplitudes have maximum values in the auroral zones, with the intensity of the pulsations decreasing with decreasing latitude. Pi1's are normally observed in the late night and early morning hours, and show an increase in activity with increased geomagnetic field disturbance. [Ref. 6]

Geomagnetic micropulsations can be observed anywhere on the globe, at various times of day and year, and in both quiet and disturbed geomagnetic field conditions.

IV. METHODS OF EVALUATING GEOMAGNETIC ACTIVITY

A. INTRODUCTION

Previous chapters have defined geomagnetic activity as it applies to Magnetic Anomaly Detection. In this chapter, methods of evaluating that activity will be examined, including methods currently in use by the fleet.

B. GEOMAGNETIC INDICES

A geomagnetic index is simply a measure used to quantify and describe time variations of the earth's magnetic field resulting from solar-terrestrial relationships. These indices are commonly used to express the intensity and depict the character of geomagnetic activity throughout the day.

For the most part, geomagnetic indices developed as range indices, measuring the difference between the high and low values for different field components measured during the day by magnetic observatories (Lincoln) [Ref. 27]. Most current indices are of the range type, but other indices have been developed which are more subjective or qualitative in nature.

Geomagnetic indices are designated by a letter code such as: C, Ci, Cp, C9, Q, R, W measure, Dst, K, Ks, Kp, ak, Ak, ap, and Ap. There are additional indices in use.

The C, Ci, Cp, and C9 indices are daily magnetic field character figures. The C index is the daily character figure for a single observatory. In this scale, C=0 indicates a quiet day, C=1 a moderately disturbed day, and C=2 a heavily disturbed day. The daily international character

figure, C_i , is the arithmetic mean of the C indices reported by participating observatories around the world. C_p , the daily planetary character figure, is similar to C_i , except that it is derived from the values of K_p and a_p . C_9 is a contracted scale for C_i and C_p with single digit values running from 0 to 9 (Bartels). [Ref. 28].

The Q and R indices are quarter-hourly and hourly range indices respectively, taken at high latitude stations only.

The W measure is an index of the equatorial electrojet. Dst is a measure of ring current effect. They are both amplitude indices. [Ref. 27]

1. K, a , and A Indices

The K, K_s , K_p , a_k , A_k , a_p , and A_p indices comprise a group of related 3-hour range indices. The K index is a single station code using a quasi-logarithmic scale from 0 to 9 to measure geomagnetic activity. The value of K is determined by first determining the difference between the lowest and highest deviations from the regular daily variation (S_q) during a 3-hour period. This range (in nT) is converted to the K scale based on the historical activity ranges at the particular observatory involved [Ref. 27]. The conversion for the Fredericksburg, Virginia observatory is given in Table III. This conversion can also be applied to the USAF/NOAA observatory in Boulder, Colorado [Ref. 29].

The K_s index is a standardized K index which is freed from local variations and is then used to determine the planetary 3-hour index, K_p .

The equivalent three-hour-range, a_k , is a conversion of the K index as shown in Table IV. In order to determine the units of a_k for a particular observatory, divide the lower range limit of $K=9$ by 250. Thus for Fredericksburg and Boulder, a_k is in 2-nT units.

TABLE III

Conversion from Range to K for Fredericksburg, Va.

K	Range (nT)
0	5
1	10
2	20
3	40
4	70
5	120
6	200
7	330
8	500
9	> 500

(after Lincoln)

TABLE IV

Equivalent Range a_k for Given K

K	0	1	2	3	4	5	6	7	8	9
a_k	0	3	7	15	27	48	80	140	240	400

(after Lincoln)

A_k is the equivalent daily amplitude and is the average of the eight daily a_k values at a particular observatory. This index is promulgated using the name of the observatory, the A_k index for Fredericksburg is known as the A-Fredericksburg or A-Fred index.

The equivalent planetary amplitude, a_p , is determined from the K_p index in a fashion similar to that of determining a_k from the K indices. The eight a_p values for a given day can then be averaged into the daily equivalent planetary amplitude A_p . These two indices are given in 2-nT units.

C. GEOMAGNETIC INDICES IN FLEET USE

1. Current Usage

Geomagnetic indices of interest in connection with MAD operations are the K, Ak, and Ap indices.

Fleet operators utilize the "alpha Index" for predicting geomagnetic activity over the entire world [Ref. 30]. This index is promulgated by the Fleet Numerical Oceanographic Center, Monterey, California, in the environmental briefings received by aircrew personnel. This index is the Ap index as sent out from the Space Environmental Services Center, Boulder, Colorado in the Joint USAF/NOAA Report of Solar and Geophysical Activity [Ref. 31].

The Boulder K index is available to interested parties by telephone recording and in the WWV and WWVH radio broadcasts and is therefore available to fleet users [Ref. 32].

The Ak index for the Fredericksburg, Virginia observatory has been used in studies of geomagnetic activity as applied to Magnetic Anomaly Detection [Ref. 33].

2. Theoretical Applicability of A and K Indices to MAD

With the widest useful filter settings, the MAD bandpass ranges from 0.04 to 0.6 Hz (1.7 to 25 seconds in period). As such, in order for a geomagnetic index to be directly applicable for MAD use, it should be sensitive to that frequency range.

The K indices, and the K-derived A indices, are not especially sensitive to the MAD range. Mayaud [Ref. 34] indicates that these indices are mainly sensitive to fluctuations whose periods are much longer than the lower end of the frequency range analyzed, that is, a frequency corresponding to a period of 45 minutes (0.0004 Hz).

One reason for this lack of sensitivity for MAD bandpass geomagnetic noise is that the amplitude of geomagnetic fluctuations varies inversely with frequency, so that the amplitude of the fluctuation increases as the frequency decreases. It can therefore be seen that the fluctuations with periods of an hour or greater largely determine the variation range used to calculate the K index. The activity driving the K and A indices, will, because of band pass filtering, not even be observed by the MAD system, and the activity of interest to MAD might not influence the K or A indices at all. It can be concluded that there is no direct physical link between MAD geomagnetic noise and either the K or A indices. [Ref. 35]

3. Experimental Correlation of A and K Indices with MAD Band Noise

a. ASQ-10A Study

Brennan and Smits [Ref. 33] found that geomagnetic micropulsation activity was recorded at their ASQ-10A MAD magnetometer site in Maryland, when the A-Fredericksburg index was greater than 25. This occurred everytime they were recording data with A-Fred greater than 25. It is important to note that they observed additional activity during some periods when A-Fred was less than 25.

The Brennan and Smits study tends to validate the use of the A indices as at least qualitative indications of geomagnetic noise in the MAD bandpass. Their study, however, was specific to the ASQ-10A magnetometer system which has a sensitivity of 0.1 nT as opposed to the 0.01 nT sensitivity of the ASQ-81 system. The effect of the ASQ-10 sensitivity is to filter out most Pc1 pulsations. As Pc1 pulsations do not correlate well with the A and K indices, the filtering out of these pulsations would tend to increase

the reliability of the A-Fred or Ap indices as measures of MAD geomagnetic noise. Mason [Ref. 36] stated that the "occurrence of Pc1 is well known to be associated with low Kp values." It should be noted that an operational drawback of the filtering out of Pc1 pulsations by the ASQ-10A is that the system also filters out valid signals of less than 0.1 nT amplitude.

While information has been presented that suggests the the A-Fred index can be useful for MAD geomagnetic noise evaluation for the AN/ASQ-10A system, sufficient data was not presented to draw conclusions for index usage with the AN/ASQ-81 system.

b. ASQ-81 Study

For two weeks in April 1976, Naval Air Development Center personnel operated a geomagnetic observatory at the Atlantic Undersea Test and Evaluation Center in the Bahamas. The primary magnetometer used for this observatory was the ASQ-81 magnetometer. One purpose of this observatory was to compare the K index (as determined by the San Juan Observatory) with geomagnetic activity in the MAD band pass. The conclusion of this study was that the K-San Juan index did not correlate with geomagnetic noise in the MAD band pass. [Ref. 37]

We have undertaken a correlation analysis using the Fisher Z transformation [Ref. 38] of the NADC data furnished to us by Ochadlick. The data used is listed in Tables V and VI.

Observed AUTEC Data and Indices, April 11-18, 1976.

[illegible]

Observed AUTECH Data and Indices, April 19-24, 1976.

D
 K-SEA
 Juan
 A
 Amp
 Tia
 (nT)

62

being from 0.14 to 0.52. Sample size was 86. This indicates that there is at most a weak correlation between the observed data and the K-San Juan index. A much greater correlation would be required for the K index to be of any significant value for MAD operational use.

The coefficient of correlation has values from -1.0 to 1.0. A value of -1.0 or 1.0 indicates perfect negative or positive correlation, respectively. A value of zero signifies no correlation at all.

A similar correlation analysis against the Ap index was conducted. The sample correlation coefficient was 0.51 with the .95 confidence interval for the actual coefficient of correlation being from 0.32 to 0.65. Again, this signifies that only a weak correlation was observed.

The weak correlation between observed geomagnetic activity and the K-San Juan index suggests that this index would not be very useful in describing MAD geomagnetic noise, as this K index reflected activity similar to that in the band of interest only about one-third of the time. The stronger correlation of the Ap index indicates that it reflected activity similar to MAD geomagnetic noise about one-half of the time. This is still not a very good indication of what is going on in the MAD band pass.

c. Power Spectral Density Evaluation

As part of ongoing research at the Naval Postgraduate School, geomagnetic activity data in the range of the MAD band pass has been collected and analyzed in the form of power spectral density (PSD) curves.

A measure of MAD band activity has been developed by integrating under the PSD curve and using compromise band pass limits of 0.05 and 1.0 Hz. This type of index is discussed in depth later.

Two sets of data were analyzed. One set was taken using an induction coil to measure the fluctuations in one direction during May, 1980 [Ref. 39] and August to October, 1981 [Ref. 40]. The other data set was collected using a Cesium vapor total field magnetometer during the July to October, 1980 period [Ref. 41].

Correlation analysis of the single-coil system data yielded a sample correlation coefficient of 0.401 for the K-Fredericksburg index, 0.180 for the A-Fredericksburg index and 0.155 for the Ap index. Sample size was 9. The .95 confidence intervals for the correlation coefficient for K-Fred, A-Fred, and Ap were -.36 to .85, -.55 to .76, and -.56 to .75, respectively. The data for this test is presented in Table VII.

TABLE VII

Single Coil RMS Noise Data and Indices

	Date	Time (Z)	RMS Noise Amplitude (nr)	K-Fred	A-Fred	Ap
1	May 80	1800	0.10	3	1	1
2	May 80	2040	0.05	3	1	1
3	Aug 81	0233	0.12	3	1	1
4	Aug 81	0743	0.13	3	1	1
5	Aug 81	1318	0.05	3	1	1
6	Oct 81	1830	0.05	3	1	1
7	Oct 81	0155	0.12	3	1	1
8	Oct 81	0630	0.03	3	1	1
9	Oct 81	1530	0.02	3	1	1

The Cesium vapor magnetometer data yielded sample coefficients of correlation of 0.552, 0.374, and 0.444 for the K-Fred, A-Fred, and Ap indices, respectively. The sample size was 14. The .95 confidence intervals were for K-Fred from .03 to .84, A-Fred from -.20 to .76, and for Ap from -.12 to .79. The Cs vapor magnetometer data is presented in Table VIII.

TABLE VIII

Cs Vapor RMS Noise Data and Indices, Jul-Oct, 1980

Date	Time	RMS Noise		K-Fred	A-Fred	Ap
		Amplitude	(nT)			
11/01/80	11:00	0.00	0.10	22	31	45
11/01/80	11:05	0.00	0.06	22	7	45
11/01/80	11:10	0.00	0.07	22	7	45
11/01/80	11:15	0.00	0.05	22	6	45
11/01/80	11:20	0.00	0.05	22	6	45
11/01/80	11:25	0.00	0.04	22	199	45
11/01/80	11:30	0.00	0.04	22	177	45
11/01/80	11:35	0.00	0.06	22	177	45
11/01/80	11:40	0.00	0.04	22	177	45
11/01/80	11:45	0.00	0.04	22	177	45
11/01/80	11:50	0.00	0.04	22	177	45
11/01/80	11:55	0.00	0.04	22	177	45
11/01/80	12:00	0.00	0.04	22	177	45
11/01/80	12:05	0.00	0.04	22	177	45
11/01/80	12:10	0.00	0.04	22	177	45
11/01/80	12:15	0.00	0.04	22	177	45
11/01/80	12:20	0.00	0.04	22	177	45
11/01/80	12:25	0.00	0.04	22	177	45
11/01/80	12:30	0.00	0.04	22	177	45
11/01/80	12:35	0.00	0.04	22	177	45
11/01/80	12:40	0.00	0.04	22	177	45
11/01/80	12:45	0.00	0.04	22	177	45
11/01/80	12:50	0.00	0.04	22	177	45
11/01/80	12:55	0.00	0.04	22	177	45
11/01/80	13:00	0.00	0.04	22	177	45

Although the sample sizes used were too small to draw any meaningful conclusions, there is little evidence to suggest that any of the K-Fred, A-Fred, or Ap indices is a very accurate measure of geomagnetic noise in the ASQ-81 MAD band pass.

d. Correlation Conclusions

Although some weak correlation does exist between the K indices, the A-Fred index, the Ap index and geomagnetic noise in the MAD band pass, this correlation is incidental and indirect, being the result of a correlation between the activity in the MAD band and in the lower frequency activity that influences the K and A indices. These indices are not directly influenced by activity in the MAD band. The correlation that does exist does not appear to be sufficiently high to enable these indices to yield accurate indications of the actual MAD band activity. The use of these indices for anything except the roughest qualitative estimation of activity in the MAD band pass is not recommended.

D. PROPOSED GEOMAGNETIC INDICES FOR MAD

Overall geomagnetic activity is analyzed in both the time and frequency domains. Geomagnetic noise indices for the MAD band pass could be developed in either of these domains.

The spatial coherence of MAD geomagnetic noise has not yet been adequately determined. This information would be necessary in order to determine the number and location of mini-observatories for an operational MAD noise index.

1. Time Series Analysis

One way to develop an index of MAD geomagnetic activity would be to establish mini-observatories near bases from which MAD operations are conducted. These observatories would use ASQ-81 magnetometers or different magnetometers with ASQ-81 filter networks, and could in real time record the geomagnetic noise in the MAD band. A measure such as the maximum peak-to-peak (or possibly the average peak-to-peak) noise in a given time period could then be disseminated to flight crews operating in the area covered by that index. Obviously, the spatial coherence of MAD band activity is important in making such a system work. This type of mini-observatory has been suggested by References 31 and 35.

2. Frequency Domain Index

Present fleet procedures examine MAD noise such as system and maneuver noise in terms of the amplitude of the fluctuation [Ref. 30]. An index of geomagnetic noise in the MAD band pass would therefore be of greatest usefulness to the fleet operator if it were in units of the amplitude of the signal as seen by the MAD equipment.

The method proposed to derive a MAD noise index in the frequency domain begins with obtaining the power spectral density of the activity in the MAD band by Fourier analysis of the time series data input from the magnetometer.

By integrating under the PSD curve over the limits of the MAD bandpass, a value in units of amplitude² will result. Taking the square root of this value will yield an RMS amplitude. Equation 4-1 represents the derivation of this index.

$$\text{MAD Index} = \left(\int_1^u \text{PSD}(f) df \right)^{1/2} \quad (4-1)$$

where MAD Index is in nT (gammas)
 f = frequency (Hz)
 u = upper bandpass limit
 l = lower bandpass limit
 and $\text{PSD}(f)$ = power spectral density
 (nT²/hz)

The characteristics of the MAD filter (the filter not being an ideal bandpass filter) could be applied prior to the integration. The integration itself could be done by either a point-by-point numerical integration or by first modelling the PSD curve by polynomial curve fitting and then integrating the polynomial over the range of the band pass. It is anticipated that this could be done in close to real time by a digital computer, possibly by a desk top computer such as the HP9845.

The type of sensor utilized could be the ASQ-81 magnetometer, other total field magnetometer, or possibly an orthogonal 3-coil system whose signals can be combined to yield the projection on the total field vector of the fluctuations. A single coil system oriented in the direction of the earth's magnetic field vector could also be used.

A three coil system which is used to yield an RMS amplitude is currently in research use at the Naval Postgraduate School.

3. Predictions of Geomagnetic Activity

The proposed indices discussed above are intended to be real time measures of the geomagnetic noise in the MAD bandpass. Whether or not such activity can be predicted ahead of time needs to be looked into.

While there is no model for the background component of geomagnetic noise, work has been done on estimating the future activity of micropulsations, notably by Fraser-Smith in the case of Pc1 pulsations [Ref. 42, 43]. By extending the prediction technique for Pc1 pulsations to the Pc2, Pc3, and Pi1 pulsations, the occurrence of geomagnetic micropulsation activity in the MAD band might be predicted. Combining this prediction with real-time solar flare information should give the capability to disseminate real-time and estimated future MAD index values to fleet users.

Previous studies have led to the conclusion that the currently used geomagnetic indices are not accurate measures of geomagnetic noise in the MAD band pass. Experimental equipment has been utilized, and computer software written in order to confirm this conclusion, and to develop a replacement means of evaluating MAD geomagnetic noise.

A. EQUIPMENT CONFIGURATION

Experimental equipment, acquired as part of the Naval Postgraduate School geomagnetics research program, has been utilized in the effort to develop a usable MAD index. This equipment is in use in other projects of the geomagnetics research group. The sensors and associated equipment are set up for remote site operation with system monitoring and data analysis located at the Naval Postgraduate School. Descriptions of the data collection system and data analysis system follow below.

1. Data Collection System

The data acquisition system illustrated in Figure 5.1 reveals the following major components:

- coil antenna sensors (3)
- preamplifiers (3)
- signal conditioners (amplifiers) (3)
- pulse code modulation system (1)
- radio transmitter (1)
- radio receiver (1)
- instrumentation tape recorder (1)

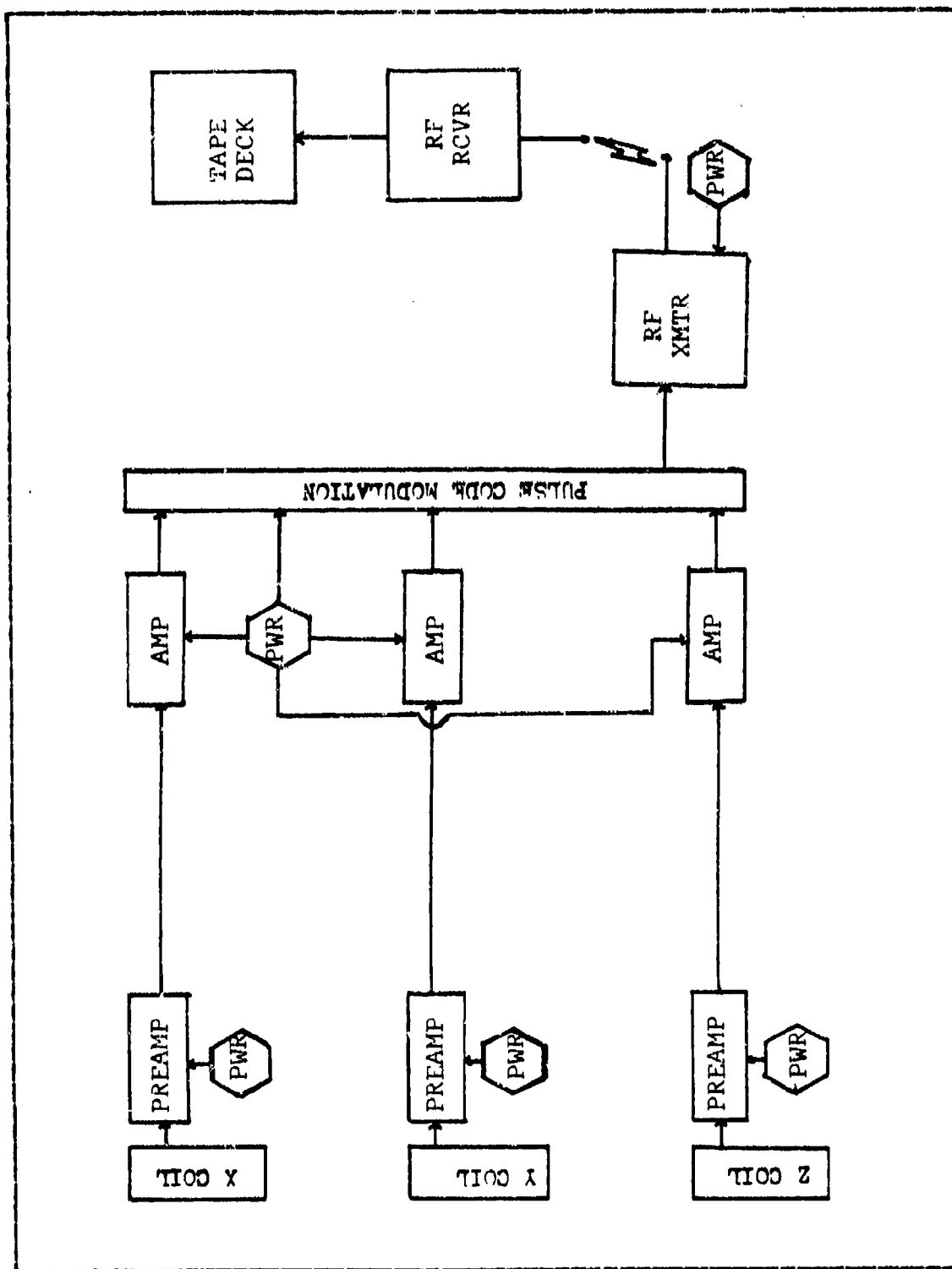


Figure 5.1 Data Collection System

a. Coil Antenna Sensors

Three coil sensors are used in this system. Each sensor is a self-supporting, continuously wound, non-center-tapped coil antenna manufactured by Elma Engineering, Palo Alto, California, from about 5460 turns of 18 gauge copper magnet wire. The coils weigh approximately 50 kg each with dimensions as depicted in Figure 5.2. The dimensions of the sensor are constrained by the dimensions of the largest glass sphere that is commercially available. These spheres are used to enclose the coils during underwater experiments. The coil resistance is 120 ohms and its self-inductance is approximately 9.31 henries. The three coils are mounted orthogonally on a nonmagnetic frame (Figure 5.3).

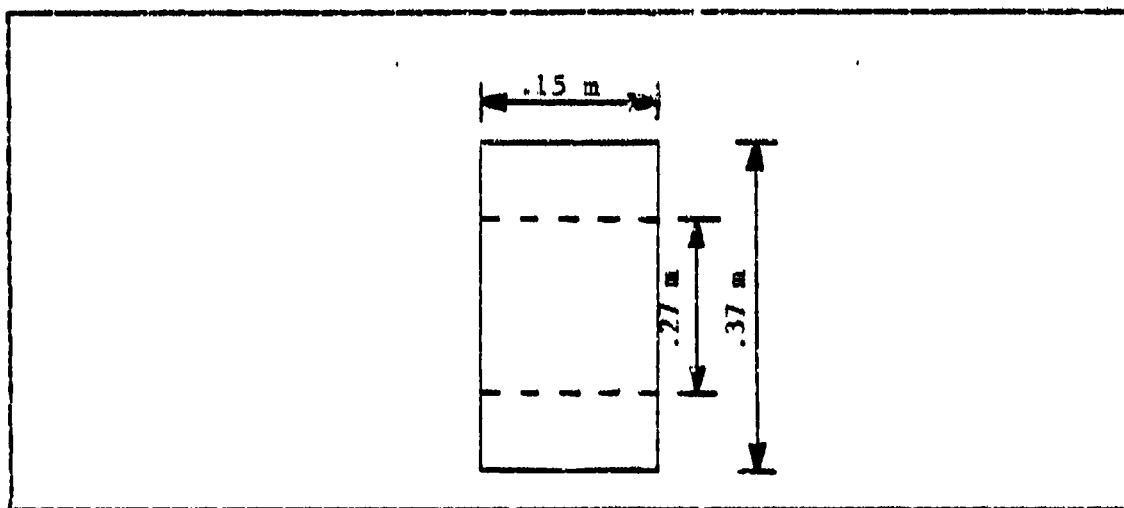


Figure 5.2 Sensor Dimensions

b. Preamplifier

The preamplifier used was the model 13-10A low noise ELF amplifier manufactured by Dr. Alan Phillips of SRI

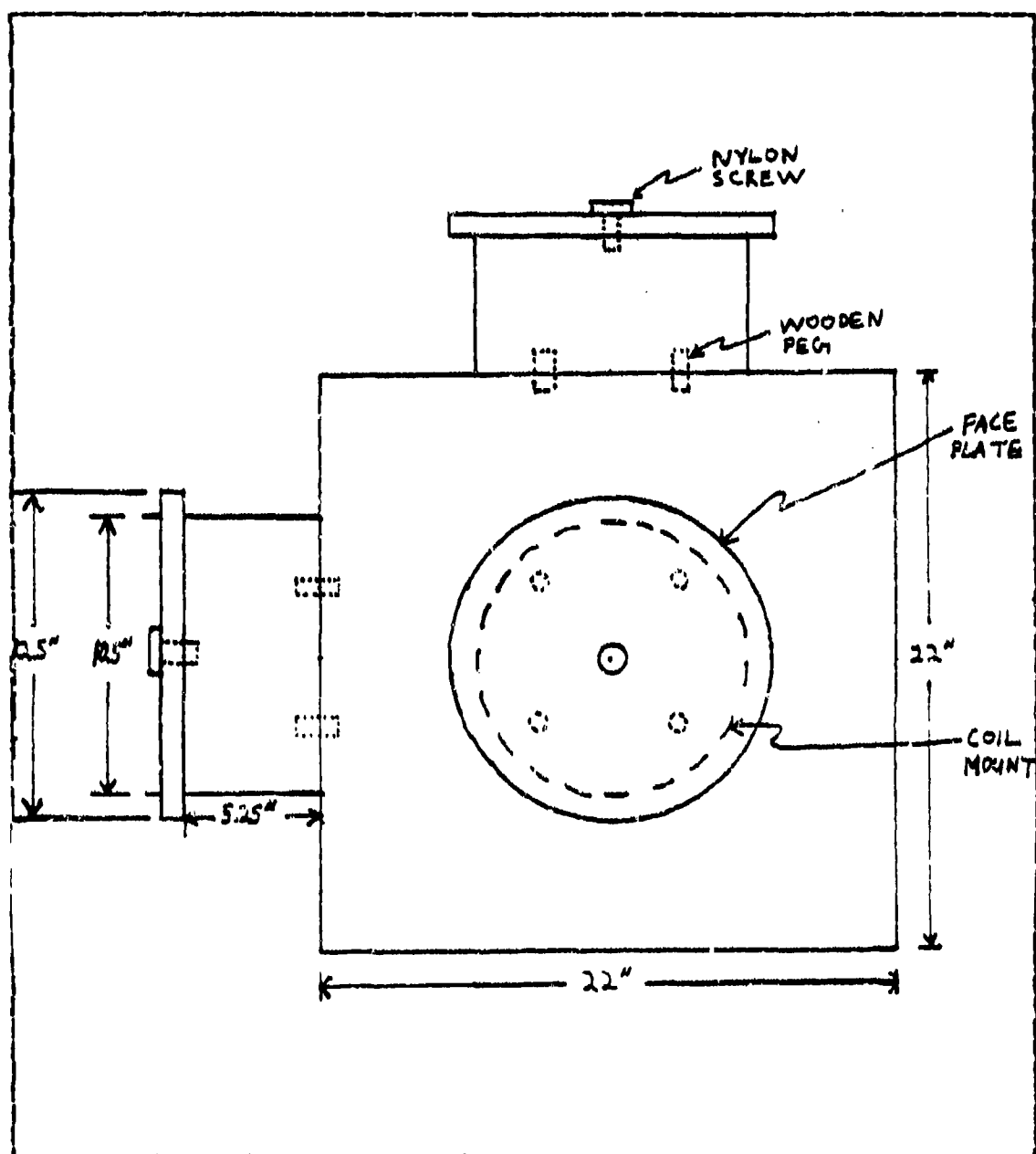


Figure 5.3 Sensor Mounting Block

International. The final stage of the amplifier contains an active low-pass filter which provides a sharp cutoff for frequencies above 20 Hz. The overall preamplifier gain for inputs of less than 2.5 millivolts is 60 dB.

c. Signal Conditioners

The signal conditioners receive the analog signals from the coil preamplifiers, amplify them on the order of 30 dB, and limits signals with peak amplitudes of 7.5 volts from entering the pulse code modulation system.

d. Pulse Code Modulation (PCM) System

The pulse code modulation system chosen for use is one designed and manufactured by Dr. Robert Lowe, Lowecom, Inc. The system features 15 channel analog input capability and offers selectable sampling rates of 2, 4, 8, 16, 32, 64, and 128 samples per second. By appropriately jumpering the analog input pins, the sampling rate may be increased by a factor of 5.

The PCM system incorporates a crystal oscillator, and associated CMOS integrated circuitry to develop the clocking pulses, and a 16 channel CMOS analog multiplexer, a 16 channel, 12 bit CMOS analog to digital converter and associated circuitry to provide the pulse coding. The crystal clock oscillator operating at a frequency of 24.576 kHz produces a square wave output with a loss rate of 1 bit in 10^6 . The clock pulses gate the analog multiplexer, analog to digital converter and associated follow on circuitry that form the pulse code words. The basic output is a Bi-phased pulse coded signal.

The data is organized in frames. Each frame is headed by a sync code word which is followed sequentially by the pulse coded samples from PCM channels 1 through 15. The sync code word is a pulse coded digital word with a decimal value between 0 and 4095. This word is preselected and hardwired on the circuit board. This code word is essential to the decoding process.

In the initial operation of this system, a sampling rate of 32 samples per second was utilized. Only one sample per coil per frame was analyzed, making use of PCM channels 2, 3, and 4 only.

e. Transmission and Recording

After the data has been PCM encoded, it is transmitted by a VHF radio link back to a receiver located at the Naval Postgraduate School, where it is currently recorded on an instrumentation tape recorder for later analysis.

2. Data Analysis Equipment

Currently, the recorded PCM data is played back into a PCM decoder and associated equipment which generates a nine-track 800 BPI computer tape containing the decoded sensor data. This computer tape is then input into the Naval Postgraduate School IBM 3033 computer for analysis. It is in the computer software that the sensor system transfer function is applied, spectral analysis performed, and the MAD index generated.

B. DATA ANALYSIS SOFTWARE

As was noted earlier, a mainframe computer was utilized to perform the spectral analysis, apply the transfer function, convert to power spectral density, plot the PSD and generate the RMS noise amplitude MAD index (using equation 4-1). This program is written in FORTRAN IV and is discussed in brief below. A copy of the program can be found in Appendix A.

The main program is divided into sections which perform the following functions:

- Data input
- Fourier analysis of time series data

- Application of system transfer function
- Projection of field components onto total field vector
- Data averaging
- Curve fitting and calculation of MAD index
- Calculation and plotting of power spectral density

1. Data Input

Data input is accomplished with the aid of a subroutine package supplied by Dr. Tim Stanton of the Naval Postgraduate School Department of Oceanography. His subroutine (called 'SUBROUTINE RD') serves as a FORTRAN 'READ' statement, taking the PCM data off the computer tape and converting it into integer format with a value between 0 and 4095. The data input section of the main program takes this integer value and converts it to a 'REAL' number and normalizes it to represent a voltage value between -5.0 and +5.0 volts. This section also sorts the input data matching the PCM channel to the data array representing the appropriate coil.

2. Fourier Analysis

The time series data is next converted to the frequency domain by utilizing a subroutine (called 'FOURT') which performs a Fast Fourier Transform (FFT). The subroutine is one available to users at the Naval Postgraduate School and utilizes the Cooley-Tukey FFT algorithm. Further information about this subroutine can be found in the program listing in Appendix A.

3. Application of Transfer Function and Total Field Projection

The next section of code applies the system transfer functions for the three coils to the frequency domain data.

The transfer functions are given as straight line segments which were found by least-squares approximation. The data enters this section in amplitude units of volts, and is converted into nanoTeslas by the transfer function.

Following the application of the system transfer function to the coil data, the program next calculates the projection of this data onto the earth's magnetic field vector (total field projection). This is done by first applying the local magnetic variation (declination) to the North-South (X) and East-West (Y) coil information to determine the horizontal field component. The local magnetic dip (inclination) angle is then used to project the vertical (Z-coil) and horizontal field fluctuations onto the total field fluctuation.

4. Data Averaging

The previous program sections exist inside of a do-loop which enables the analysis of a long period of data without a prohibitive need for storage space. This loop includes accumulator arrays for each field component and the total field projection. The fluctuation data is converted into power prior to storage. This is done by taking the magnitude of the fluctuation component, dividing by the number of sample points, and then squaring the value. After the program passes through the averaging loop for the last time, the arithmetic average is taken for each frequency point on the arrays. At this stage the power spectrum is multiplied by the sample period to determine power spectral density.

5. MAD Index Calculation

The next section computes the RMS MAD noise index previously discussed. A polynomial curve fit is performed on

the total field PSD using an available subroutine ('CHBFT'). The resulting polynomial is then integrated over the limits of the various ASQ-81 band pass settings.

6. Plotting of Power Spectral Density

Plots of the power spectral density of each of the field components and the total field projection are generated in the last section of the program. This is done by converting the fluctuation power spectral density to decibels (dB) referenced to 1 nanoTesla² per Hertz. A Versatec plotting subroutine ('PLOTP') is then called to actually generate the plots.

C. INITIAL SYSTEM OPERATION

The NPS MAD index system was initially placed into operation with the coil sensors located in the La Mesa Village housing area near the Naval Postgraduate School, Monterey, California. System checkout was accomplished in June, 1982. The full system was placed into operation on 25 July 1982 and 18 August 1982 in conjunction with similar measurements taken on the floor of Monterey Bay.

The MAD index output and power spectral density plots of the total field fluctuation for 25 July 1982, 1237-1406 local (2037-2206Z), and 18 August 1982, 0121-0250 local (0921-1050Z) and 0507-0636 local (1307-1436Z) are shown in Tables IX, X, XI, and Figures 5.4, 5.5, and 5.6 respectively.

TABLE IX

MAD Noise 2037-2206Z, 25 JUL 82, Monterey, CA

1 Gamma = 1 NanoTesla

MAD INDEX=	0.1083	GAMMAS
BANDPASS:	0.04 TO 0.20	HERTZ
MAD INDEX=	0.1148	GAMMAS
BANDPASS:	0.04 TO 0.40	HERTZ
MAD INDEX=	0.1169	GAMMAS
BANDPASS:	0.04 TO 0.60	HERTZ
MAD INDEX=	0.0888	GAMMAS
BANDPASS:	0.06 TO 0.20	HERTZ
MAD INDEX=	0.0966	GAMMAS
BANDPASS:	0.06 TO 0.40	HERTZ
MAD INDEX=	0.0991	GAMMAS
BANDPASS:	0.06 TO 0.60	HERTZ
MAD INDEX=	0.0729	GAMMAS
BANDPASS:	0.08 TO 0.20	HERTZ
MAD INDEX=	0.0822	GAMMAS
BANDPASS:	0.08 TO 0.40	HERTZ
MAD INDEX=	0.0852	GAMMAS
BANDPASS:	0.08 TO 0.60	HERTZ
MAD INDEX=	0.0598	GAMMAS
BANDPASS:	0.10 TO 0.20	HERTZ
MAD INDEX=	0.0708	GAMMAS
BANDPASS:	0.10 TO 0.40	HERTZ
MAD INDEX=	0.0743	GAMMAS
BANDPASS:	0.10 TO 0.60	HERTZ
MAD INDEX=	0.1234	GAMMAS
BANDPASS:	0.04 TO 2.00	HERTZ
MAD INDEX=	0.1122	GAMMAS
BANDPASS:	0.06 TO 2.00	HERTZ
MAD INDEX=	0.1018	GAMMAS
BANDPASS:	0.08 TO 2.00	HERTZ
MAD INDEX=	0.0923	GAMMAS
BANDPASS:	0.10 TO 2.00	HERTZ

POWER SPECTRAL DENSITY OF TOTAL
FIELD PROJECTION, LA MESA VILLAGE
25 JUL 1982, 1237-1406 LOCAL

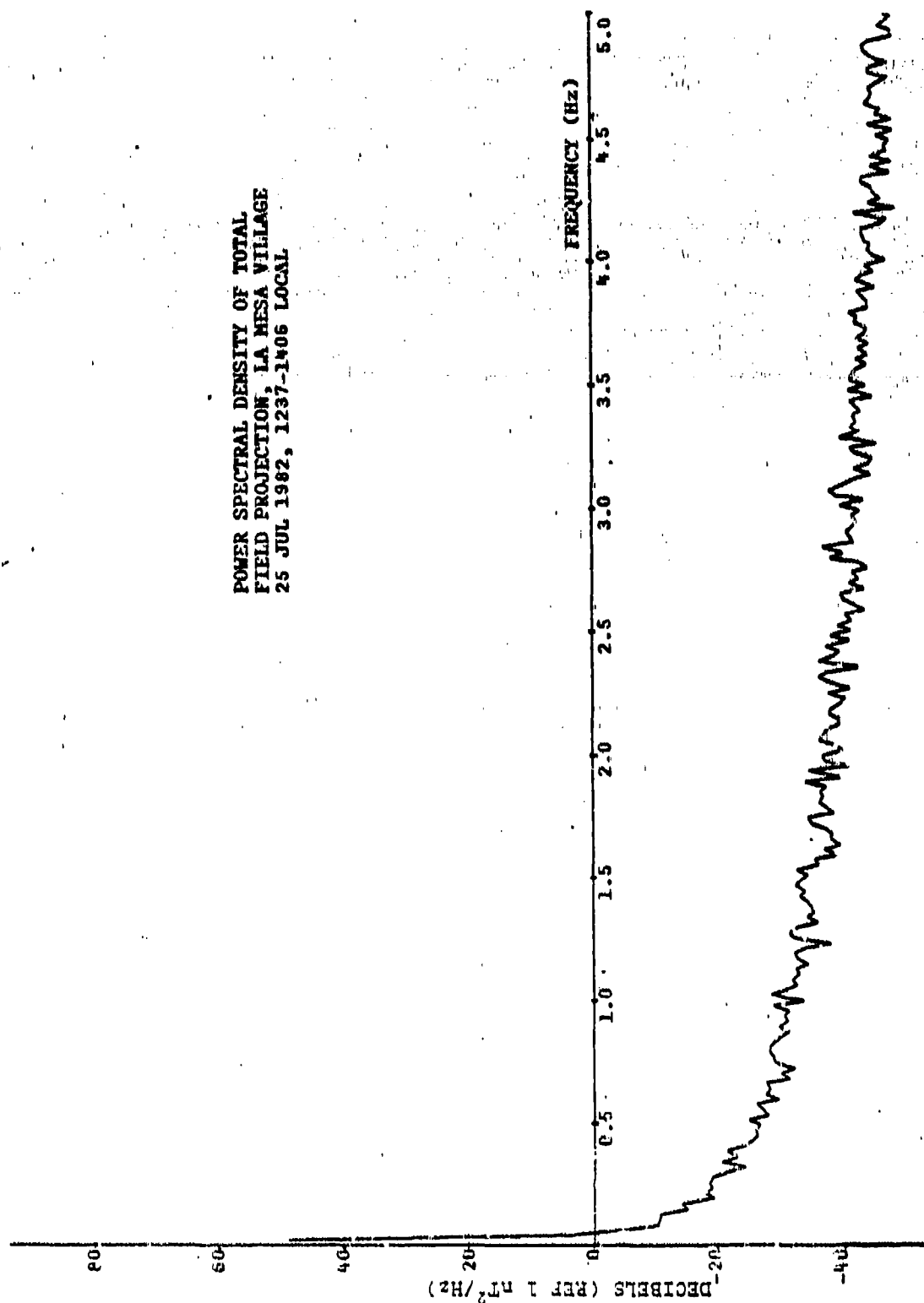


Figure 5.4 PSD 25 JUL 82, 2037-2206Z, La Mesa Village

TABLE X

MAD Noise 0921-1050Z, 18 AUG 82, Monterey, CA

1 Gamma = 1 NanoTesla

MAD INDEX=	0.3644	GAMMAS
BANDPASS:	0.04 TO 0.20	HERTZ
MAD INDEX=	0.3960	GAMMAS
BANDPASS:	0.04 TO 0.40	HERTZ
MAD INDEX=	0.4004	GAMMAS
BANDPASS:	0.04 TO 0.60	HERTZ
MAD INDEX=	0.3027	GAMMAS
BANDPASS:	0.06 TO 0.20	HERTZ
MAD INDEX=	0.3401	GAMMAS
BANDPASS:	0.06 TO 0.40	HERTZ
MAD INDEX=	0.3453	GAMMAS
BANDPASS:	0.06 TO 0.60	HERTZ
MAD INDEX=	0.2528	GAMMAS
BANDPASS:	0.08 TO 0.20	HERTZ
MAD INDEX=	0.2966	GAMMAS
BANDPASS:	0.08 TO 0.40	HERTZ
MAD INDEX=	0.3025	GAMMAS
BANDPASS:	0.08 TO 0.60	HERTZ
MAD INDEX=	0.2118	GAMMAS
BANDPASS:	0.10 TO 0.20	HERTZ
MAD INDEX=	0.2624	GAMMAS
BANDPASS:	0.10 TO 0.40	HERTZ
MAD INDEX=	0.2691	GAMMAS
BANDPASS:	0.10 TO 0.60	HERTZ
MAD INDEX=	0.4047	GAMMAS
BANDPASS:	0.04 TO 2.00	HERTZ
MAD INDEX=	0.3679	GAMMAS
BANDPASS:	0.06 TO 2.00	HERTZ
MAD INDEX=	0.3339	GAMMAS
BANDPASS:	0.08 TO 2.00	HERTZ
MAD INDEX=	0.3026	GAMMAS
BANDPASS:	0.10 TO 2.00	HERTZ

POWER SPECTRAL DENSITY OF TOTAL
FIELD PROJECTION, LA MESA VILLAGE
18 AUG 1982, 0121-0250 LOCAL

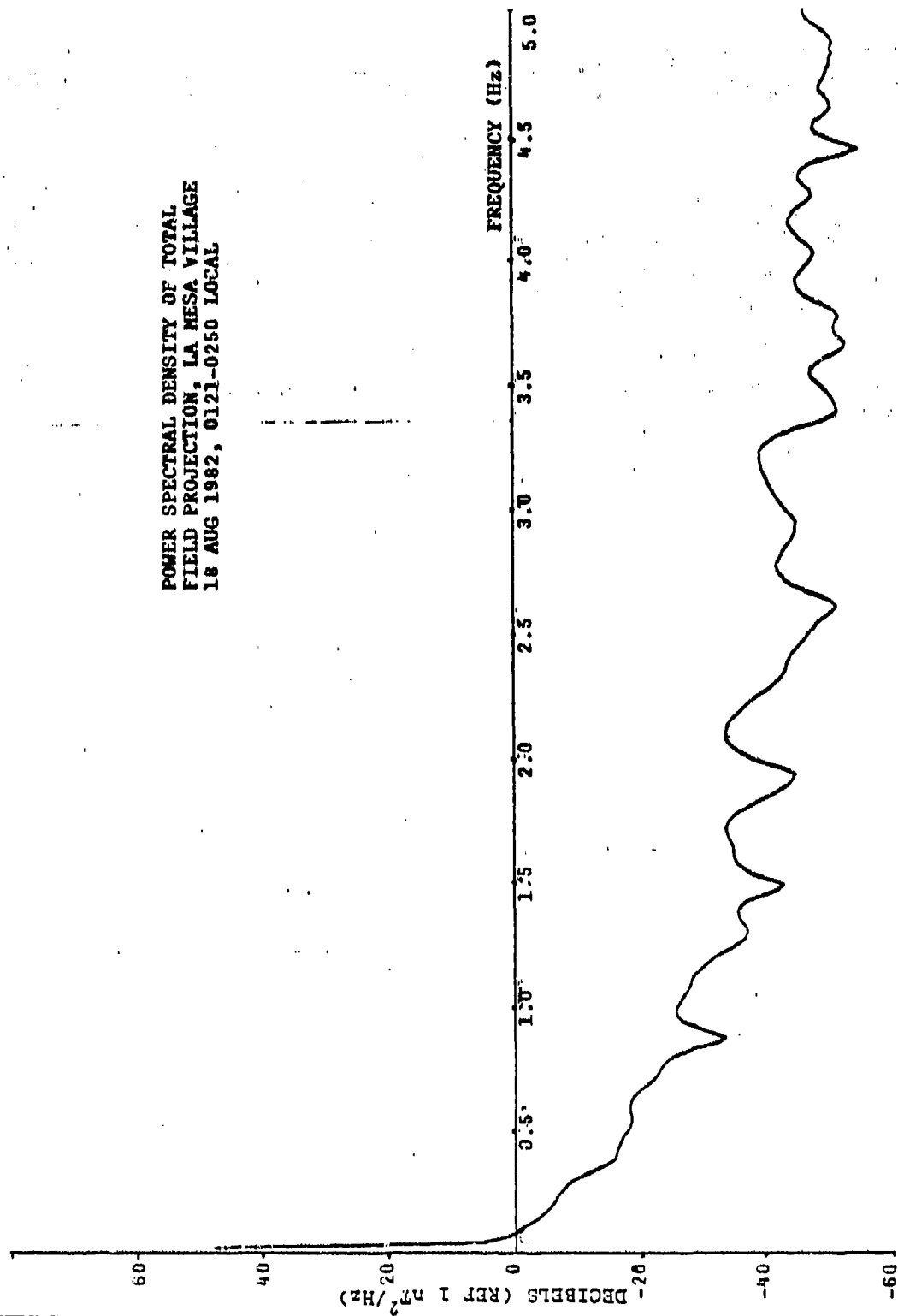


Figure 5.5 PSD 18 AUG 82, 0921-1050Z, La Mesa Village

TABLE XI

MAD Noise 1307-1436Z, 18 AUG 82, Monterey, CA

1 Gamma = 1 NanoTesla

MAD INDEX=	0.3188 GAMMAS
BANDPASS:	0.04 TO 0.20 HERTZ
MAD INDEX=	0.3246 GAMMAS
BANDPASS:	0.04 TO 0.40 HERTZ
MAD INDEX=	0.3267 GAMMAS
BANDPASS:	0.04 TO 0.60 HERTZ
MAD INDEX=	0.2297 GAMMAS
BANDPASS:	0.06 TO 0.20 HERTZ
MAD INDEX=	0.2376 GAMMAS
BANDPASS:	0.06 TO 0.40 HERTZ
MAD INDEX=	0.2405 GAMMAS
BANDPASS:	0.06 TO 0.60 HERTZ
MAD INDEX=	0.1585 GAMMAS
BANDPASS:	0.08 TO 0.20 HERTZ
MAD INDEX=	0.1699 GAMMAS
BANDPASS:	0.08 TO 0.40 HERTZ
MAD INDEX=	0.1738 GAMMAS
BANDPASS:	0.08 TO 0.60 HERTZ
MAD INDEX=	0.1031 GAMMAS
BANDPASS:	0.10 TO 0.20 HERTZ
MAD INDEX=	0.1199 GAMMAS
BANDPASS:	0.10 TO 0.40 HERTZ
MAD INDEX=	0.1254 GAMMAS
BANDPASS:	0.10 TO 0.60 HERTZ
MAD INDEX=	0.3504 GAMMAS
BANDPASS:	0.04 TO 2.00 HERTZ
MAD INDEX=	0.3137 GAMMAS
BANDPASS:	0.06 TO 2.00 HERTZ
MAD INDEX=	0.2801 GAMMAS
BANDPASS:	0.08 TO 2.00 HERTZ
MAD INDEX=	0.2495 GAMMAS
BANDPASS:	0.10 TO 2.00 HERTZ

POWER SPECTRAL DENSITY OF TOTAL
FIELD PROJECTION, LA MESA VILLAGE
18 AUG 1982, 0507-0636 LOCAL

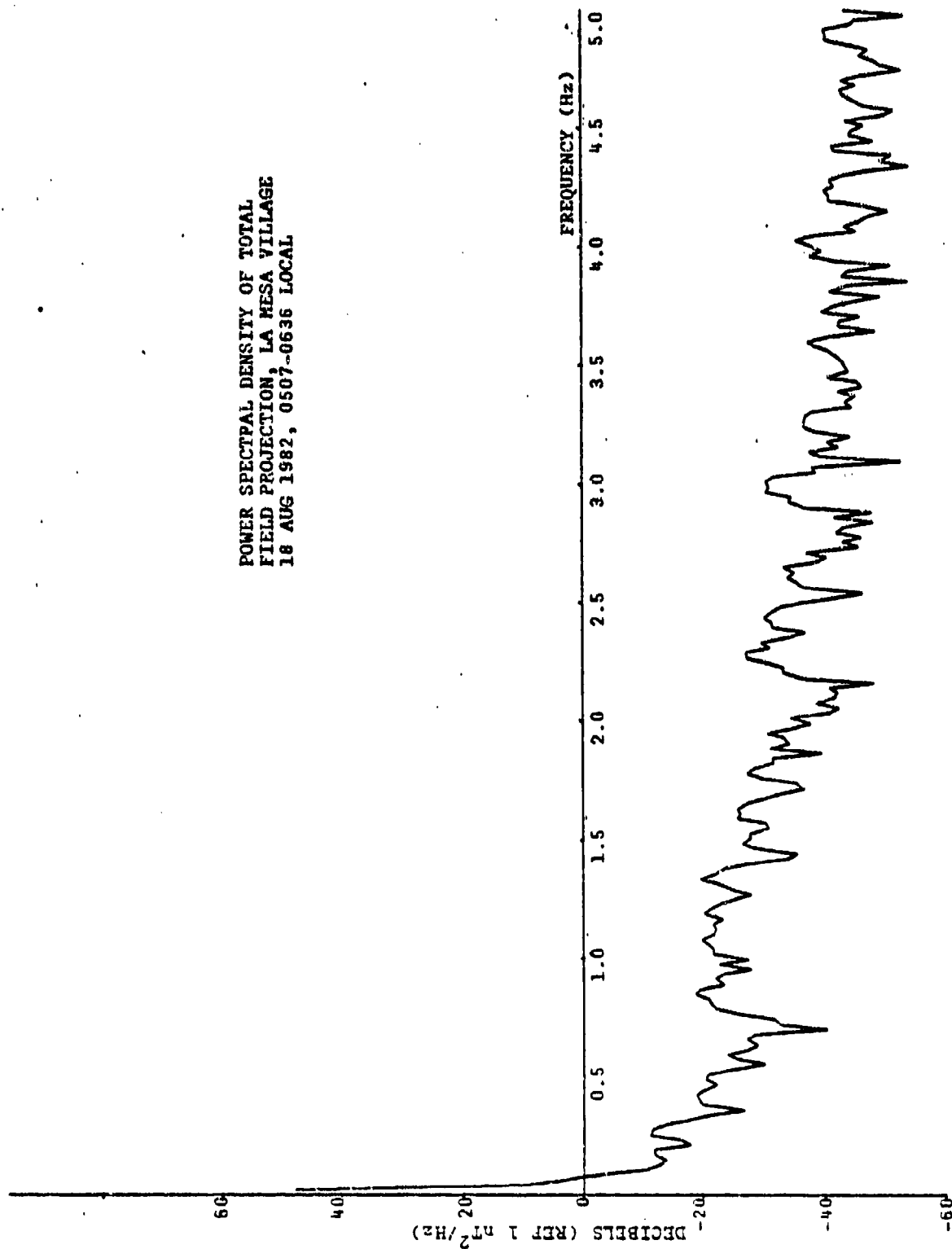


Figure 5.6 PSD 18 AUG 82, 1307-1436Z, La Mesa Village

VI. CONCLUSION AND RECOMMENDATIONS

A. CONCLUSION

Analysis of available information regarding current geomagnetic indices and the actual level of geomagnetic noise in the MAD bandpass indicates that the currently used indices, the K and Ap indices, are not valid for MAD operations. It is therefore desirable to derive a new index which more accurately represents the geomagnetic noise at frequencies of interest in MAD operations.

B. RECOMMENDATIONS

A tentative index was developed, tested, and sample data obtained. The data analysis for the preliminary system was accomplished using a mainframe computer. It is recommended that further work include improving the index and the setting up of a system to on-line decode the incoming data, and utilizing a desk top computer such as the HP9845 to enable real time determination of the MAD noise index.

The spatial coherence of MAD geomagnetic noise should also be investigated, with possible application to noise cancellation. Additionally, the feasibility of the prior estimation of geomagnetic noise should be evaluated, possibly by using the prediction methods proposed by Fraser-Smith [Ref. 42, 43].

APPENDIX A

MAD INDEX DATA ANALYSIS SOFTWARE

```

MAD000060
MAD000070
MAD000080
MAD000090
MAD000100
MAD000110
MAD000120
MAD000130
MAD000140
MAD000150
MAD000160
MAD000170
MAD000180
MAD000190
MAD000200
MAD000210
MAD000220
MAD000230
MAD000240
MAD000250
MAD000260
MAD000270
MAD000280
MAD000290
MAD000300
MAD000310
MAD000320
MAD000330
MAD000340
MAD000350
MAD000360
MAD000370
MAD000380
MAD000390
MAD000400
MAD000410
MAD000420
MAD000430
MAD000440
MAD000450
MAD000460
MAD000470
MAD000480
MAD000490
MAD000500
MAD000510
MAD000520
MAD000530

//JEFF$1L JOB (3224,0129),SCHWEIGER SMC 2239',CLASS=F
//*MAIN ORG=NPQVM1,3224P,LINES=(10)
//*FCRMAT PR,DDNAME=PL0T,SYSVECTR,DEST=LOCAL
// EXEC FRTXCLGP,PARM.LKED=LIST,MAP,XREF,REGION.G0=1200K
//FCRT SYSDN DD *
  INTEGER*2 IN(16)
  C ARRAY IN IS USED IN READING DATA FROM TAPE
  C COMPLEX*8 XX(9500),YY(9500),ZZ(9500),TF(9500)
  C THE COMPLEX*8 ARRAYS ARE USED TO ORDER INPUT DATA AND INITIALLY
  C REPRESENT VOLTAGE - TIME SERIES INFORMATION.
  C DIMENSION TIME(9500),FREQ(9500),WORK(19000),ERQ2(500)
  C DIMENSION ZX(9500),ZY(9500),ZV(9500),ZT(9500)
  C THE *Z* ARRAYS REPRESENT FREQUENCY DOMAIN (FF TRANSFORMED)
  C MAGNITUDE DATA AND ARE EVENTUALLY CONVERTED TO POWER SPECTRAL
  C DENSITY INFORMATION.
  C INTEGER R(10)
  C DIMENSION RX(10),PX(10),PY(10),PC(10),PD(9),PX(40),PY(40)
  C THE *R* AND *P* ARRAYS ARE USED IN CURVE FITTING THE
  C POWER SPECTRAL DENSITY OF THE ACTIVITY PROJECTION ON THE
  C TOTAL FIELD.
  C DIMENSION FL(4),FU(4)
  C INTEGER*4 ITB(12)/12*0/
  C REAL*4 RTB(28)/28*0.0/
  C REAL ALAB(4)/CH-X',CH-Y',CH-Z',TOT'/
  C REAL*8 TITLE(12)
  C EQUIVALENCE(TITLE(1),RTB(5))
  C ARRAYS *ITB*,*RTB*,*ALAB*,AND *TITLE* ARE USED IN GENERATING
  C THE VERTSATEC PLOTTER OUTPUT.
  C DATA XX,YY,ZZ,TF/38000*(0.,0.)//
  C DATA ZX,ZY,ZV,ZT/38000*0.0//
  C DATA FL,C4,.06,.08,.1/
  C DATA FU/.2,.4,.6,.2//
  C DATA TIME,FREQ/19000*0.0//
  C DATA PX,PY,PX1,PY1/268*0.0//
  C TWOPI=6.2831853
  C COS60=COS(TWOPI/6.)
  C COS30=COS(TWOPI/12.)
  C D=16.75*TWOPI/360.
  C COSD=COS(D)
  C COSD1=COS(90.-D)*TWOPI/360.)
  C D IS THE DECLINATION OR MAGNETIC VARIATION AT THE MAGNETOMETER
  C SITE.
  C THE NEXT FIVE LINES SERVE AS A TIME DELAY IN STARTING THE
  C DATA ANALYSIS
  C ISEC=3
  C ITL=1SEC*32
  C DC 55 JJ=1,ITL
  C CALL RD(20,IN,1000,IREF,IRR)

```

MAD000540
MAD000550
MAD000560
MAD000570
MAD000580
MAD000590
MAD000600
MAD000610
MAD000620
MAD000630
MAD000640
MAD000650
MAD000660
MAD000670
MAD000680
MAD000690
MAD000700
MAD000710
MAD000720
MAD000730
MAD000740
MAD000750
MAD000760
MAD000770
MAD000780
MAD000790
MAD000800
MAD000810
MAD000820
MAD000830
MAD000840
MAD000850
MAD000860
MAD000870
MAD000880
MAD000890
MAD000900
MAD000910
MAD000920
MAD000930
MAD000940
MAD000950
MAD000960
MAD000970
MAD000980
MAD000990
MAD001000
MAD001010

```

55  C CONTINUE
    IFRAME=9500
    NR=18
    FNR=FLOAT(NR)
    DO 70 LL=1, NR
      THE DO LOOP ENDING WITH STATEMENT 70 ENABLES THE PROGRAM TO
      PROCESS A LARGE AMOUNT OF DATA BY REPEATING THE PROCESS IN
      BLOCKS. THE DATA POINTS FROM EACH RUN THROUGH THE DO LOOP ARE
      ADDED TOGETHER AND EVENTUALLY AVERAGED BY THE NUMBER OF RUNS
      THROUGH THE DO LOOP.
      'NR' REPRESENTS THE NUMBER OF DATA SEQUENCES TO BE AVERAGED.
      I SEQUENCE CURRENTLY EQUALS 9500 DATA POINTS FOR EACH CHANNEL
      OR 296.88 SECONDS OF DATA.

      THE DO LOOP ENDING WITH 60 READS THE DATA FROM THE PCM FRAME
      STRIPS OUT THE SYNC CODE, AND SORTS OUT THE DATA BY COIL
      CHANNEL
      DO 60 JJ=1, IFRAME
        CALL RD(20, IN, 1000, IREC, IRR)
        XX(JJ)=IN(2)
        YY(JJ)=IN(3)
        ZZ(JJ)=IN(4)
      CONTINUE
      WRITE(6, 200) IRR, IREC
      FORMAT(10X, 'IRREC=', I6, '/')
      THE FOLLOWING SECTION GENERATES THE TIME AND FREQUENCY
      ARRAYS AND NORMALIZES THE INPUT PCM DATA TO VOLTAGE FORM
      IN PREPARATION FOR FAST FOURIER TRANSFORM TO THE FREQUENCY
      DOMAIN.
      N=9500
      FN=FLCAT(N)
      DELTAT=1./32.
      T=FN*DELTAT
      DELTAF=TWCP I/(FN*DELTAT)
      DO 20 J=1, N
        TIME(J)=DELTAT*FLCAT(J)
        FREQ(J)=DELTAF*FLCAT(J)
        XX(J)=(XX(J)-2048.)*5./2048.
        YY(J)=REAL(XX(J))
        VY(J)=(YY(J)-2048.)*5./2048.
        ZZ(J)=(ZZ(J)-2048.)*5./2048.
        'XX' IS THE X-COIL DATA, 'VY' IS THE Y-COIL DATA,
        'ZZ' IS THE Z-COIL DATA, AND 'TF' IS THE PROJECTION OF THE
        NORTH-SOUTH COMPONENT (XX) AND THE VERTICAL COMPONENT (ZZ)
        ON THE TOTAL GEOMAGNETIC FIELD VECTOR.
      CONTINUE
20  CONTINUE

```

```

DO 21 J=1,500
FRQ2(J)=ALOG10(FREQ(J))
21 CONTINUE
TIME SERIES DATA. SEE THE WRITEUP ON 'FOUR' FOR
FURTHER INFORMATION.
CALL FOURT(XX,N,1,-1,0,WORK)
CALL FOURT(YY,N,1,-1,0,WORK)
CALL FOURT(ZZ,N,1,-1,0,WORK)
THE NEXT BLOCK OF STATEMENTS APPLY THE SYSTEM (VOLTAGE TO
B-FIELD) TRANSFER FUNCTION TO THE TRANSFORMED
FREQUENCY
MAIN DATA. THIS BLOCK ENDS AT STATEMENT 5.
THE TRANSFER FUNCTION CONVERTS VOLTS TO NANOTESLAS (GAMMAS).
**WARNING** THIS TRANSFER FUNCTIONS YIELDS AN INACCURATE
PHASE. USE A DIFFERENT TRANSFER FUNCTION IF PHASE INFORMATION
NEEDED.
DO 9 L=1,N
FRQ=FREQ(L)
IF(FRQ.LE.25.)GO TO 1
XX(L)=XX(L)/28.
GO TO 8
1 IF(FRQ.LE.15.)GO TO 2
XX(L)=XX(L)/(105.5-3.14*FRQ)
YY(L)=YY(L)/(181.32-7.588*FRQ)
ZZ(L)=ZZ(L)/(177.26-7.484*FRQ)
GO TO 8
2 IF(FRQ.LE.10.)GO TO 3
XX(L)=XX(L)/(5.958*FRQ-30.97)
YY(L)=YY(L)/(7.166*FRQ-39.99)
ZZ(L)=ZZ(L)/(6.49*FRQ-32.35)
GO TO 8
3 IF(FRQ.LE.7.5)GO TO 4
XX(L)=XX(L)/(3.492*FRQ-6.31)
YY(L)=YY(L)/(4.252*FRQ-10.85)
ZZ(L)=ZZ(L)/(4.044*FRQ-7.89)
GO TO 8
4 IF(FRQ.LE.5.)GO TO 5
XX(L)=XX(L)/(2.6311*FRQ+0.14667)
YY(L)=YY(L)/(3.012*FRQ-1.55)
ZZ(L)=ZZ(L)/(3.184*FRQ-1.44)
GO TO 8
5 IF(FRQ.LE.3.)GO TO 6
XX(L)=XX(L)/(2.6311*FRQ+0.14667)
YY(L)=YY(L)/(2.702*FRQ)
ZZ(L)=ZZ(L)/(2.92*FRQ)
GO TO 8
6 XX(L)=XX(L)/(2.72*FRQ)
GO TO 7
7
8
9

```



```

8 CONTINUE
  TP(L)=(XX(L)*COSD + Y(L)*COSD1)*COS60 + ZZ(L)*COS30
5 CONTINUE
  IN THE NEXT BLOCK, ENDING WITH 30, THE MAGNITUDE OF THE COMPLEX
  FREQUENCY DOMAIN DATA IS TAKEN AND PLACED IN A REAL ARRAY. *ZX*
  FOR THE X-COIL, *ZY* FOR THE Y-COIL, *ZV* FOR THE Z OR VERTICAL
  COIL AND *ZT* FOR THE TOTAL FIELD PROJECTION. THIS DATA IS
  DIVIDED BY THE NUMBER OF SAMPLE POINTS AND SQUARED TO DETERMINE
  POWER.
  DO 30 I=1,N
    ZX(I)=ZX(I)+(CABS(XX(I))/FN)**2
    ZY(I)=ZY(I)+(CABS(YX(I))/FN)**2
    ZV(I)=ZV(I)+(CABS(ZZ(I))/FN)**2
    ZT(I)=ZT(I)+(CABS(TF(I))/FN)**2
  CONTINUE
30 CONTINUE
  THE FOLLOWING BLOCK AVERAGES THE DATA PCINTS ADDED IN BLOCK 30
  ABOVE BY THE NUMBER OF RUNS THROUGH THE DO LOOP ENDING WITH 70.
  AT THIS POINT THE POWER CURVES ARE CONVERTED INTO POWER SPECTRAL
  DENSITY.
  DO 33 I=1,N
    ZX(I3)=ZX(I3)*T/FNR
    ZY(I3)=ZY(I3)*T/FNR
    ZV(I3)=ZV(I3)*T/FNR
    ZT(I3)=ZT(I3)*T/FNR
  CONTINUE
23 CONTINUE
  THE NEXT STATEMENTS, THROUGH 204, ARE USED IN CURVE FITTING
  THE POWER SPECTRAL DENSITY OF THE TOTAL FIELD PROJECTION
  AND IN CALCULATING A MAD ACTIVITY INDEX.
  DO 37 I=3,42
    PX(I-2)=FREC(I)
    PY(I-2)=ZT(I)
  CONTINUE
27 H2=8
  M2=9
  WRITE(6,201)
201 FORMAT(11)
  CALL CH8FT(PX,PY,40,PC,M2,RX,RH,R)
  DO 38 I=1,M2
    PD(I)=PC(I)/FLOAT(I)
  CONTINUE
28 DO 39 K=1,4
  DO 46 LL=1,3
    XL=0.
  DO 47 I=1,9
    XU=XU+PD(I)*{FU(L)**I}
    XL=XL+PD(I)*{FL(K)**I}

```

MAD01500
 MAD01510
 MAD01520
 MAD01530
 MAD01540
 MAD01550
 MAD01560
 MAD01570
 MAD01580
 MAD01590
 MAD01600
 MAD01610
 MAD01620
 MAD01630
 MAD01640
 MAD01650
 MAD01660
 MAD01670
 MAD01680
 MAD01690
 MAD01700
 MAD01710
 MAD01720
 MAD01730
 MAD01740
 MAD01750
 MAD01760
 MAD01770
 MAD01780
 MAD01790
 MAD01800
 MAD01810
 MAD01820
 MAD01830
 MAD01840
 MAD01850
 MAD01860
 MAD01870
 MAD01880
 MAD01890
 MAD01900
 MAD01910
 MAD01920
 MAD01930
 MAD01940
 MAD01950
 MAD01960
 MAD01970

```

47 CONTINUE
IF(XU.LE.XL IGO TO 71
GO TO 72
71 M2=M2-1
M3=M3-1
CALL CHBFT(PX,PY,40,PC,M2,RX,RH,R)
DO 73 I=1,M2
PD(I)=PC(I)/FLOAT(I)
73 CONTINUE
XU=0.
XL=0.
DO 74 I=1,M2
XU=XU+PD(I)*{FU(LL)**I}
XL=XL+PD(I)*{FL(K)**I}
74 CONTINUE
XU=SQRT(XU-XL)
72 WRITE(6,204)XU,FL(K),FU(LL)
204 FORMAT(10X,'MAG INDEX= ',F10.4,1X,'GAMMAS',/,10X,'B ANDPASS:',/,'2X',
F5.2,/,TO,'F5.2','HERTZ',/)
45 CONTINUE
39 DO 31 I=3,96
PX1(I-2)=FREQ(I)
PY1(I-2)=ZT(I)
31 CONTINUE
M2=8
M3=9
CALL CHBFT(PX1,PY1,94,PC,M2,RX,RH,R)
DO 34 I=1,M3
PD(I)=PC(I)/FLOAT(I)
34 CONTINUE
DC 35 K=1,4
XU=0.
XL=0.
DO 36 I=1,9
XU=XU+PD(I)*{FU(4)**I}
XL=XL+PD(I)*{FL(K)**I}
36 CONTINUE
IF(XU.LE.XL IGO TO 75
GO TO 76
75 M2=M2-1
M3=M3-1
CALL CHBFT(PX1,PY1,94,PC,M2,RX,RH,R)
DO 77 I=1,M3
PD(I)=PC(I)/FLOAT(I)
IM=I-1
77 CONTINUE
XU=0.

```

MAD02460
MAD02470
MAD02480
MAD02490
MAD02500
MAD02510
MAD02520
MAD02530
MAD02540
MAD02550
MAD02560
MAD02570
MAD02580
MAD02590
MAD02600
MAD02610
MAD02620
MAD02630
MAD02640
MAD02650
MAD02660
MAD02670
MAD02680
MAD02690
MAD02700
MAD02710
MAD02720
MAD02730
MAD02740
MAD02750
MAD02760
MAD02770
MAD02780
MAD02790
MAD02800
MAD02810
MAD02820
MAD02830
MAD02840
MAD02850
MAD02860
MAD02870
MAD02880
MAD02890
MAD02900
MAD02910
MAD02920
MAD02930

```

XL=0.      I=1,M3
DC 78      XU=XL+PD(I)*(FU(4)**I)
           XL=XL+PD(I)*(FL(K)**I)
78 CONTINUE
76 XMI=SQRT(XU-XL)
   WRITE(6,204)XMI,FL(K),FU(4)
35 CONTINUE
   THE NEXT DO LOOP CONVERTS THE B-FIELD POWER SPECTRAL DENSITY
   INTO DECIBELS REFERENCED TO 1 NANOTESLA (GAMMA) **2/HERTZ.
DO 32 I=1,N
  ZX(I)=10.*ALOG10(ZX(I))
  ZY(I)=10.*ALOG10(ZY(I))
  ZV(I)=10.*ALOG10(ZV(I))
  ZT(I)=10.*ALOG10(ZT(I))
32 CONTINUE

C          VERSATEC PLOT OF B - FIELD SPECTRA
C
NPTS=10./DELTA F +1.
NP02=NPTS/2 +1
* NPTS DETERMINES NUMBER OF POINTS NECESSARY IN ORDER FOR
  THE 0 TO 10 HERTZ RANGE TO BE PLOTTED.
* NP02 IS FOR THE 0 TO 5 HERTZ RANGE.
  FOR THE FOLLOWING 'ITB' AND 'RTB' VALUES REVIEW THE WRITE-UP
  FOR THE SUBROUTINE PROCEDURE 'CRAMP'.
ITB(3)=20
ITB(4)=8
ITB(12)=0
RTB(1)=0.0
RTB(2)=0.0
RTB(3)=ALAB(1)
READ(5,3000)ITILE
CALL DRAWP(NPTS,FRQ2,ZX,ITB,RTB)
RTB(3)=ALAB(2)
READ(5,3000)ITILE
CALL DRAWP(NPTS,FRQ2,ZY,ITB,RTB)
RTB(3)=ALAB(3)
READ(5,3000)ITILE
CALL DRAWP(NPTS,FRQ2,ZV,ITB,RTB)
ITB(3)=10
ITB(12)=1
RTB(3)=ALAB(4)
READ(5,3000)ITILE
CALL DRAWP(NP02,FRQ2,ZT,ITB,RTB)
3000 FORMAT(6A8)
      STOP
      END

```


MAD03420
MAD03430
MAD03440
MAD03450
MAD03460
MAD03470
MAD03480
MAD03490
MAD03500
MAD03510
MAD03520
MAD03530
MAD03540
MAD03550
MAD03560
MAD03570
MAD03580
MAD03590
MAD03600
MAD03610
MAD03620
MAD03630
MAD03640
MAD03650
MAD03660
MAD03670
MAD03680
MAD03690
MAD03700
MAD03710
MAD03720
MAD03730
MAD03740
MAD03750
MAD03760
MAD03770
MAD03780
MAD03790
MAD03800
MAD03810
MAD03820
MAD03830
MAD03840
MAD03850
MAD03860
MAD03870
MAD03880
MAD03890

```

100      CONTINUE
C      IF (IRR.EQ.0) GO TO 150
      IRR=IRR+1
      IF (IRR.LT.IRS) GO TO 120
      WRITE (6,110)
      FORMAT ('I STOPPED IN SUB RD BECAUSE OF IRR.GT.',I6,' AT L110')
110      IRR=IRR
      STOP
      CONTINUE
120      WRITE (6,130) IREC,IRR
      FORMAT (' RESYNC AT FRAME ',I6,' WITH TOTAL ERRORS ',I7)
130      IER=0
      IRR=IRR
      GO TO 50
150      CONTINUE
      RETURN
900      WRITE (6,910) IUN,IREC
510      FORMAT ('1 END CF UNIT ',I3,' AT REC ',I7)
      STOP
      END

      FUNCTION ISHIFT (IN,NPLC)
      RETURNS SHIFTED VALUE OF I*2 WORD IN
      -VE LEFT,+VE RIGHT SHIFT

      INTEGER * 2 IN
      IP=IN
      IF (IP.LT.0) IP=IP+65536
      IF (NPLC.LT.0) GC TO 30
      ISHIFT=IP/(2*1ABS(NPLC))
      RETURN
      ISHIFT=IP*(2*1ABS(NPLC))
      IF (ISHIFT.GT.65535) ISHIFT=MOD(ISHIFT,65536)
      RETURN
      END
      FUNCTION IMASK (IN,IBL,IBR)
      MASK I*2 WORD IN OUTSIDE BITS IBL & IBR

      INTEGER * 2 IN,IO
      IO=IN
      IF (IBR.EQ.0) GO TO 50
      IT=ISHIFT(IN,IBR)
      IO=IT
      IP=ISHIFT(IO,IBL-15-IBR)
      IO=IP
      IMASK=ISHIFT(IO,15-IBL)
      RETURN
50

```


MAD04380
MAD04390
MAD04400
MAD04410
MAD04420
MAD04430
MAD04440
MAD04450
MAD04460
MAD04470
MAD04480
MAD04490
MAD04500
MAD04510
MAD04520
MAD04530
MAD04540
MAD04550
MAD04560
MAD04570
MAD04580
MAD04590
MAD04600
MAD04610
MAD04620
MAD04630
MAD04640
MAD04650
MAD04660
MAD04670
MAD04680
MAD04690
MAD04700
MAD04710
MAD04720
MAD04730
MAD04740
MAD04750
MAD04760
MAD04770
MAD04780
MAD04790
MAD04800
MAD04810
MAD04820
MAD04830
MAD04840
MAD04850

MENTS IN DATA MUST BE SET TO 0.0.

WORK A 1-DIMENSIONAL REAL*4 ARRAY USED FOR WORKING STORAGE.
ITS LENGTH SHOULD BE TWICE THE LARGEST ARRAY DIMENSION
NN(I), I=1,2,...,NDIM, WHICH IS NOT A POWER OF TWO. IN
PARTICULAR, IF ALL NN(I) ARE POWERS OF TWO, NO WORK SPACE
IS NEEDED AND WORK MAY BE REPLACED BY ZERO IN THE CALLING
SEQUENCE.

REMARKS

IF AN INVERSE TRANSFORM (ISIGN=+1) IS PERFORMED UPON AN ARRAY
OF TRANSFORMED (ISIGN=-1) DATA, THE ORIGINAL DATA WILL REAP-
PEAR, MULTIPLIED BY NN(I)*NN(2)*...*NN(NDIM).

FOR A MULTI-DIMENSIONAL ARRAY THE (J1,J2,...,JNDIM)
COMPONENT OF THE TRANSFORM IS GIVEN BY
SUM(DATA(I1,I2,...,INDIM)*W1**((I1-1)*(J1-1))*
W2**((I2-1)*(J2-1))*...*WNDIM**((INDIM-1)*(JNDIM-1))
HERE THE SUM RANGES OVER ALL POSSIBLE VALUES OF THE I'S
AND W1=EXP(ISIGN*2*PI*SQRT(-1)/NN(I)), ETC.

THE ARRAY OF INPUT DATA MUST BE IN COMPLEX FORMAT.
HOWEVER, IS ALL IMAGINARY PARTS ARE ZERO (I.E. THE DATA
ARE DISGUISED REAL). RUNNING TIME IS CUT UP TO FORTY PER-
CENT. (FOR FASTEST TRANSFORM OF REAL DATA, NN(I) SHOULD BE E-
VEN.) THE TRANSFORM VALUES ARE ALWAYS COMPLEX AND ARE RETURNED
IN THE ORIGINAL ARRAY OF DATA, REPLACING THE INPUT DATA.
LENGTH OF EACH DIMENSION OF THE DATA ARRAY MAY BE ANY INTEGER.
THE PROGRAM RUNS FASTER ON COMPOSITE INTEGERS THAN ON PRIMES,
AND IS PARTICULARLY FAST ON NUMBERS RICH IN FACTORS OF TWO.

TIMING IS IN FACT GIVEN BY THE FOLLOWING FORMULA. LET NTOI BE
THE TOTAL NUMBER OF POINTS (REAL OR COMPLEX) IN THE DATA ARRAY,
THAT IS, NTOI=NN(1)*NN(2)*...*NN(NDIM). DECOMPOSE NTOI INTO ITS PRIME
FACTORS, SUCH AS 2**K2 * 3**K3 * 5**K5 * ... * 5**K5. LET SUM2 BE THE
SUM OF THE FACTORS OF TWO IN NTOI, THAT IS, SUM2 = 2**K2. LET
SUMF BE THE SUM OF ALL OTHER FACTORS OF NTOI, THAT IS, SUMF =
3**K3 * 5**K5 * ... * 5**K5. THE TIME TO + NTOI*(T1+T2*SUM2+T3*SUMF). CN
THESE NTOI DATA IS T = TO + NTOI*(T1+T2*SUM2+T3*SUMF). T = 3000+
CDC 3300 (FLOATING POINT ADD TIME = SIX MICROSECONDS). T = 3000+
NTOI*(600+40*SUM2+175*SUMF) MICROSECONDS ON COMPLEX DATA.

THE SAVINGS OFFERED BY THIS PROGRAM CAN BE DRAMATIC. A ONE-DI-
MENSIONAL ARRAY 4000 IN LENGTH WILL BE TRANSFORMED IN 4000*(600+
40*(2+2+2+2)+175*(5+5+5)) = 14.5 SECONDS VERSUS ABOUT 4000*
4000*175 = 2800 SECONDS FOR THE STRAIGHTFORWARD TECHNIQUE.

CC

MAD04860
MAD04870
MAD04880
MAD04890
MAD04900
MAD04910
MAD04920
MAD04930
MAD04940
MAD04950
MAD04960
MAD04970
MAD04980
MAD04990
MAD05000
MAD05010
MAD05020
MAD05030
MAD05040
MAD05050
MAD05060
MAD05070
MAD05080
MAD05090
MAD05100
MAD05110
MAD05120
MAD05130
MAD05140
MAD05150
MAD05160
MAD05170
MAD05180
MAD05190
MAD05200
MAD05210
MAD05220
MAD05230
MAD05240
MAD05250
MAD05260
MAD05270
MAD05280
MAD05290
MAD05300
MAD05310
MAD05320
MAD05330

THE FAST FOURIER TRANSFORM PLACES THREE RESTRICTIONS UPON THE DATA.
1. THE NUMBER OF INPUT DATA AND THE NUMBER OF TRANSFORM VALUES MUST BE THE SAME.
2. BOTH THE INPUT DATA AND THE TRANSFORM VALUES MUST REPRESENT EQUISPACED POINTS IN THEIR RESPECTIVE DOMAINS OF TIME AND FREQUENCY. CALLING THESE SPACINGS DELTAT AND DELTAF, IT MUST BE TRUE THAT $\text{DELTAF} = 2\pi / (\text{NN}(1) * \text{DELTAT})$. OF COURSE, DELTAT NEED NOT BE THE SAME FOR EVERY DIMENSION.
3. CONCEPTUALLY AT LEAST, THE INPUT DATA AND THE TRANSFORM OUTPUT REPRESENT SINGLE CYCLES OF PERIODIC FUNCTIONS.

THERE ARE NO ERROR MESSAGES OR ERROR HALTS IN THIS PROGRAM. THE PROGRAM RETURNS IMMEDIATELY IF NCM OR ANY NN(I) IS LESS THAN ONE.

FOR MOST APPLICATIONS FOURT, IF COMPILED UNDER FORTRAN H, IS COMPARABLE IN SPEED AND ACCURACY TO THE IMSL FFT SUBROUTINES. WITH CERTAIN PATHOLOGICALLY ILL-CONDITIONED DATA THE ACCURACY OF FOURT MAY BE SERIOUSLY DEGRADED, BUT THE SAME CAN PROBABLY BE SAID OF ANY EXTANT FFT ROUTINE. WORK SPACE REQUIRED BY FOURT MAY BE GREATER OR LESS THAN THAT REQUIRED BY THE IMSL ROUTINES, GENERAL EASIER TO USE APPLICATION. FOURT IS MORE FLEXIBLE AND IN GENERAL EASIER TO USE THAN THE IMSL ROUTINES. FOURT ALONE PROVIDES THE CAPABILITY OF TRANSFORMING A MULTI-DIMENSIONAL ARRAY WITH A SINGLE CALL.

THIS IS THE FASTEST AND MOST VERSATILE VERSION OF THE FFT KNOWN TO THE AUTHOR. A PROGRAM CALLED FOUR2 IS AVAILABLE THAT ALSO PERFORMS THE FAST FOURIER TRANSFORM AND IS WRITTEN IN USASI BASIC FORTRAN. IT IS ABOUT ONE THIRD AS LONG AND RESTRICTS THE DIMENSIONS OF THE INPUT ARRAY (WHICH MUST BE COMPLEX) TO BE POWERS OF TWO. ANOTHER PROGRAM, CALLED FOUR1, IS ONE TENTH AS LONG AND RUNS TWO THIRDS AS FAST ON A ONE-DIMENSIONAL COMPLEX ARRAY WHOSE LENGTH IS A POWER OF TWO.

REFERENCE--
IEEE AUDIO TRANSACTIONS (JUNE 1967), SPECIAL ISSUE ON THE FFT.

EXAMPLE 1. THREE-DIMENSIONAL FORWARD FOURIER TRANSFORM OF A COMPLEX ARRAY DIMENSIONED 32 BY 25 BY 13 IN FORTRAN IV.
DIMENSION DATA(32,25,13),WORK(50),NN(3)
COMPLEX DATA

DATA NN/32,25,13/

DO I=1,32

DC I J=1,25

DC I K=1,13

DATA(I,J,K)=COMPLEX VALUE

1

MAD05820
MAD05830
MAD05840
MAD05850
MAD05860
MAD05870
MAD05880
MAD05890
MAD05900
MAD05910
MAD05920
MAD05930
MAD05940
MAD05950
MAD05960
MAD05970
MAD05980
MAD05990
MAD06000
MAD06010
MAD06020
MAD06030
MAD06040
MAD06050
MAD06060
MAD06070
MAD06080
MAD06090
MAD06100
MAD06110
MAD06120
MAD06130
MAD06140
MAD06150
MAD06160
MAD06170
MAD06180
MAD06190
MAD06200
MAD06210
MAD06220
MAD06230
MAD06240
MAD06250
MAD06260
MAD06270
MAD06280
MAD06290

```

20  GO TO 10
30  IDIV=3
    INON2=IF
    IQUOT=M/IDIV
    IREM=M-IDIV*IQUOT
    IF(IQUOT-IDIV) 60, 31, 31
31  IF(IREM) 40, 22, 40
32  IFACT(IF)=ICIV
    IF=IF+1
    M=IQUOT
    GO TO 30
40  IDIV=IDIV+2
    GO TO 30
50  GC TO 30
    INON2=IF
    IF(IREM) 60, 51, 60
51  NTWO=NTWO+NTWO
    GO TO 70
60  IFACT(IF)=M

SEPARATE FOUR CASES--
1. COMPLEX TRANSFORM OR REAL TRANSFORM FOR THE 4TH, 9TH, ETC.
   DIMENSIONS.
2. REAL TRANSFORM FOR THE 2ND OR 3RD DIMENSION. METHOD--
   TRANSFORM HALF THE DATA, SUPPLYING THE OTHER HALF BY CON-
   JUGATE SYMMETRY.
3. REAL TRANSFORM FOR THE 1ST DIMENSION, N ODD. METHOD--
   SET THE IMAGINARY PARTS TO ZERO.
4. REAL TRANSFORM FOR THE 1ST DIMENSION, N EVEN. METHOD--
   TRANSFORM A COMPLEX ARRAY OF LENGTH N/2 WHOSE REAL PARTS
   ARE THE EVEN NUMBERED REAL VALUES AND WHOSE IMAGINARY
   PARTS ARE THE ODD NUMBERED REAL VALUES. SEPARATE AND SUP-
   PLY THE SECOND HALF BY CONJUGATE SYMMETRY.

70  ICASE=1
    IFMIN=1
    IIRNG=NPI
    IF(IDIM-4) 71, 100, 100
    IF(IFORM) 72, 72, 100
71  ICASE=2
72  IIRNG=NPI*(1+NPREV/2)
    IF(IDIM-1) 73, 73, 100
73  ICASE=3
    IIRNG=NPI
    IF(NTWO-NPI) 100, 100, 74
74  ICASE=4
    IFMIN=2
    NTWO=NTWO/2
    N=N/2

```

MAD06300
MAD06310
MAD06320
MAD06330
MAD06340
MAD06350
MAD06360
MAD06370
MAD06380
MAD06390
MAD06400
MAD06410
MAD06420
MAD06430
MAD06440
MAD06450
MAD06460
MAD06470
MAD06480
MAD06490
MAD06500
MAD06510
MAD06520
MAD06530
MAD06540
MAD06550
MAD06560
MAD06570
MAD06580
MAD06590
MAD06600
MAD06610
MAD06620
MAD06630
MAD06640
MAD06650
MAD06660
MAD06670
MAD06680
MAD06690
MAD06700
MAD06710
MAD06720
MAD06730
MAD06740
MAD06750
MAD06760
MAD06770

```

NP2=NP2/2
NTOT=NTOT/2
I=1
DO 80 J=1,NTOT
  DATA(J)=DATA(I)
  I=I+2
C
C
C
C
  SHUFFLE DATA BY BIT REVERSAL, SINCE N=2**K. AS THE SHUFFLING
  CAN BE DONE BY SIMPLE INTERCHANGE, NO WORKING ARRAY IS NEEDED
C
  IF(NTWG-NP2)200,110,110
  NP2HF=NP2/2
  J=1
  DO 150 I2=1,NP2,NF1
    IF(J-I2)120,130,130
    I1MAX=I2+NP1-2
    DO 125 I1=I2,I1MAX,2
      DO 125 I3=I1,NTOT,NP2
        J3=J+I3-I2
        TEMPR=DATA(I3)
        TEMPI=DATA(I3+1)
        DATA(I3)=DATA(I3)
        DATA(I3+1)=TEMPR
        DATA(J3)=TEMPR
        DATA(J3+1)=TEMPI
      M=NP2HF
      IF(J-M)150,150,145
      J=J-M
      N=M/2
      IF(M-NP1)150,140,140
      J=J+M
      GO TO 300
C
C
C
  SHUFFLE DATA BY DIGIT REVERSAL FOR GENERAL NC ARRAY IS NEEDED
C
  NWORK=2*N
  DO 270 I1=1,NP1,2
    DO 270 I3=I1,NTOT,NP2
      J=I3
      DO 260 I=1,NWORK,2
        IF(ICASE-3)210,220,210
        WORK(I)=DATA(J)
        WORK(I+1)=DATA(J+1)
      GC TO 230
      WORK(I)=DATA(J)
      WORK(I+1)=0.
      IFP2=NP2
      IF=IFMIN
C
C
C
  200
  210
  220
  230

```

[illegible]

MAD07260
MAD07270
MAD07280
MAD07290
MAD07300
MAD07310
MAD07320
MAD07330
MAD07340
MAD07350
MAD07360
MAD07370
MAD07380
MAD07390
MAD07400
MAD07410
MAD07420
MAD07430
MAD07440
MAD07450
MAD07460
MAD07470
MAD07480
MAD07490
MAD07500
MAD07510
MAD07520
MAD07530
MAD07540
MAD07550
MAD07560
MAD07570
MAD07580
MAD07590
MAD07600
MAD07610
MAD07620
MAD07630
MAD07640
MAD07650
MAD07660
MAD07670
MAD07680
MAD07690
MAD07700
MAD07710
MAD07720
MAD07730

42C W3R=W2R*WR-W2I*WI
W3I=W2R*WI+W2I*WR
DC 530 I1=1,IIRNG,2
KMIN=I1+IPAR*H
IF(MMAX-NP1)430,440,440
KMIN=I1
KDI=IPAR*MMAX
KSTEP=4*KDI
IF(KSTEP-NT)460,460,530
DC 520 K1=KMIN,NTCT,KSTEP
K2=K1+KDI
K3=K2+KDI
K4=K3+KDI
IF(MMAX-NP1)470,470,480
U1R=DATA(K1)+DATA(K2)
U1I=DATA(K1+1)+DATA(K2+1)
U2R=DATA(K3)+DATA(K4)
U2I=DATA(K3+1)+DATA(K4+1)
U3R=DATA(K1)-DATA(K2)
U3I=DATA(K1+1)-DATA(K2+1)
IF(1SIGN)471,472,472
U4R=DATA(K3+1)-DATA(K4+1)
U4I=DATA(K4)-DATA(K3)
GO TO 510
471 U4R=DATA(K4+1)-DATA(K3+1)
U4I=DATA(K3)-DATA(K4)
GC TO 510
472 T2R=W2R*DATA(K2)-W2I*DATA(K2+1)
T2I=W2R*DATA(K2+1)+W2I*DATA(K2)
T3R=WR*DATA(K3)-WI*DATA(K3+1)
T3I=WR*DATA(K3+1)+WI*DATA(K3)
T4R=W3R*DATA(K4)-W3I*DATA(K4+1)
T4I=W3R*DATA(K4+1)+W3I*DATA(K4)
U1R=DATA(K1)+T2R
U1I=DATA(K1+1)+T2I
U2R=T3R+T4R
U2I=T3I+T4I
U3R=DATA(K1)-T2R
U3I=DATA(K1+1)-T2I
IF(1SIGN)49C,500,500
49C U4R=T3I-T4I
U4I=T4R-T3R
GC TO 510
500 U4R=T4I-T3I
U4I=T3R-T4R
51C DATA(K1)=U1R+U2R
DATA(K1+1)=U1I+U2I
DATA(K2)=U3R+U4R

MAD07740
MAD07750
MAD07760
MAD07770
MAD07780
MAD07790
MAD07800
MAD07810
MAD07820
MAD07830
MAD07840
MAD07850
MAD07860
MAD07870
MAD07880
MAD07890
MAD07900
MAD07910
MAD07920
MAD07930
MAD07940
MAD07950
MAD07960
MAD07970
MAD07980
MAD07990
MAD08000
MAD08010
MAD08020
MAD08030
MAD08040
MAD08050
MAD08060
MAD08070
MAD08080
MAD08090
MAD08100
MAD08110
MAD08120
MAD08130
MAD08140
MAD08150
MAD08160
MAD08170
MAD08180
MAD08190
MAD08200
MAD08210

```

520 DATA(K2+1)=U3I+U4I
    DATA(K3)=U1R-U2R
    DATA(K3+1)=U1I-U2I
    DATA(K4)=U3R-U4R
    DATA(K4+1)=U3I-U4I
    K0IF=KSTEP
    KMIN=4*(KMIN-11)+11
    GO TO 450
530 CCNTINUE
    M=M+LMAX
    IF(M-MMAX)540,540,570
540 IF(I SIGN)550,560,560
550 TEMPR=WR
    WR=(WR+WI)*RTHLF
    WI=(WI-TEMPR)*RTHLF
    GO TO 410
560 TEMPR=WR
    WR=(WR-WI)*RTHLF
    WI=(TEMPR+WI)*RTHLF
    GO TO 410
570 CCNTINUE
    IPAR=3-IPAK
    MPAX=MPAX+HMAX
    GO TO 360

    MAIN LOOP FOR FACTORS NOT EQUAL TO TWO. APPLY THE TWIDDLE FAC-
    TOR W=EXP(I SIGN*2*PI*SQRT((-1)*(J1-1)*(J2-J1)/(IFP1+IFP2))),
    THEN PERFORM A FOURIER TRANSFORM OF LENGTH IFACT(IF), MAKING USE
    OF CONJUGATE SYMMETRIES.

    IF(NTWO-NP2)605,700,700
    IFP1=NTWC
    IF=INON2
    NPIHF=NPI/2
    IFP2=IFACT(IF)*IFP1
    JIMIN=NPI+1
    IF(JIMIN-IFP1)615,615,640
    DO 635 J1=JIMIN,IFP1,NPI
    THETA=-TWCP1*FLOAT(J1-1)/FLOAT(IFP2)
    IF(I SIGN)625,620,620
    THETA=-THETA
    WSTPR=COS(THETA)
    WSTPI=SIN(THETA)
    WR=WSTPR
    WI=WSTPI
    J2MIN=J1+IFP1
    J2MAX=J1+IFP2-IFP1
    DO 635 J2=J2MIN,J2MAX,IFP1

```

MAD08220
MAD08230
MAD08240
MAD08250
MAD08260
MAD08270
MAD08280
MAD08290
MAD08300
MAD08310
MAD08320
MAD08330
MAD08340
MAD08350
MAD08360
MAD08370
MAD08380
MAD08390
MAD08400
MAD08410
MAD08420
MAD08430
MAD08440
MAD08450
MAD08460
MAD08470
MAD08480
MAD08490
MAD08500
MAD08510
MAD08520
MAD08530
MAD08540
MAD08550
MAD08560
MAD08570
MAD08580
MAD08590
MAD08600
MAD08610
MAD08620
MAD08630
MAD08640
MAD08650
MAD08660
MAD08670
MAD08680
MAD08690

```

IIMAX=J2+IIRNG-2
DO 630 I1=J2,IIMAX,2
DO 630 J3=I1,NTOT,IFP2
  TEMPR=DATA(J3)
  DATA(J31)=DATA(J3)*WR-DATA(J3+1)*WI
  DATA(J3+1)=TEMPR*WI+DATA(J3+1)*WR
  TEMPR=WR
  WR=WR*WSTPR-WI*WSTPI
  WI=TEMPR*WSTPI+WI*WSTPR
  THETA=-TWCPJ/FLOAT(IFACT(IF))
  IF(ISIGN)650,645,645
  THETA=-THETA
  WSTPR=COS(THETA)
  WSTPI=SIN(THETA)
  J2RNG=IFP1*(1+IFACT(IF)/2)
  DO 695 I1=1,IIRNG,2
  DO 695 I3=I1,NTOT,NP2
    J2MAX=I3+J2RNG-IFP1
    DO 690 J2=I2,J2MAX,IFP1
    J1MAX=J2+IFP1-NP1
    DO 680 J1=J2,J1MAX,NP1
    J3MAX=J1+NP2-IFP2
    DO 680 J3=J1,J3MAX,IFP2
    JMIN=J3-J2+I3
    JMAX=JMIN+IFP2-IFP1
    I=1+(J3-I3)/NP1HF
    IF(J2-I3)655,655,665
    SUMR=0.
    SUMI=0.
    DO 660 J=JMIN,JMAX,IFP1
    SUMR=SUMR+DATA(J)
    SUMI=SUMI+DATA(J+1)
    WORK(I)=SUMR
    WORK(I+1)=SUMI
    GO TO 680
    ICONJ=1+(IFP2-2*J2+I3+J3)/NP1HF
    J=JMAX
    SUMR=DATA(J)
    SUMI=DATA(J+1)
    OLD SI=0.
    OLD SI=0.
    J=J-IFP1
    TEMPR=SUMR
    SUMR=TWOWR+SUMR-OLD SR+DATA(J)
    TEMPI=SUMI
    SUMI=TWOWR+SUMI-OLD SI+DATA(J+1)
    OLD SR=TEMPR
    OLD SI=TEMPI

```

63C

635

640

645

650

655

66C

665

67C

MAC08700
MAC08710
MAC08720
MAC08730
MAC08740
MAC08750
MAC08760
MAC08770
MAC08780
MAC08790
MAC08800
MAC08810
MAC08820
MAC08830
MAC08840
MAC08850
MAC08860
MAC08870
MAC08880
MAC08890
MAC08900
MAC08910
MAC08920
MAC08930
MAC08940
MAC08950
MAC08960
MAC08970
MAC08980
MAC08990
MAC09000
MAC09010
MAC09020
MAC09030
MAC09040
MAC09050
MAC09060
MAC09070
MAC09080
MAC09090
MAC09100
MAC09110
MAC09120
MAC09130
MAC09140
MAC09150
MAC09160
MAC09170

```

J=J-IFP1
IF(J-JMIN)675,675,670
TEMPR=WR*SUMR-OLD$R+DATA(J)
TEMPI=WI*SUMI
WORK(I)=TEMPR-TEMPI
WORK(I*CONJ)=TEMPR+TEMPI
TEMPR=WR*SUMI-OLD$I+DATA(J+1)
TEMPI=WI*SUMR
WORK(I+1)=TEMPR+TEMPI
WORK(I*CONJ+1)=TEMPR-TEMPI
CONTINUE
IF(J2-I3)685,685,686
WR=WSIPR
WI=WSIPI
GO TO 690
TEMPR=WR
WI=WR*WSTPR-WI*WSTPI
WI=TEMPR*WSTPI+WI*WSTPR
TWOVR=WR+WR
I=1
I2MAX=I3+NP2-NP1
DO 695 I2=I3,I2MAX,NP1
DATA(I2)=WORK(I)
DATA(I2+1)=WORK(I+1)
I=I+2
IF=IF+1
IFP1=IFP2
IF(IFP1-NP2)610,700,700
COMPLETE A REAL TRANSFORM IN THE 1ST DIMENSION, N EVEN, BY CON-
JUGATE SYMMETRIES.
GO TO (900,800,900,701),ICASE
NHALF=N
N=N+N
THEIA=-TWCPI/FLOAT(N)
IF(ISIGN)702,702,702
THEIA=-THEIA
WSTPR=COS(THEIA)
WSTPI=SIN(THEIA)
WR=WSIPR
WI=WSIPI
IMIN=3
JMIN=2*NHALF-1
GO TO 725
J=JMIN
DO 720 I=IMIN,NTOT,NP2
SUMR=(DATA(I)+DATA(J))/2.

```


MAD09180
MAD09190
MAD09200
MAD09210
MAD09220
MAD09230
MAD09240
MAD09250
MAD09260
MAD09270
MAD09280
MAD09290
MAD09300
MAD09310
MAD09320
MAD09330
MAD09340
MAD09350
MAD09360
MAD09370
MAD09380
MAD09390
MAD09400
MAD09410
MAD09420
MAD09430
MAD09440
MAD09450
MAD09460
MAD09470
MAD09480
MAD09490
MAD09500
MAD09510
MAD09520
MAD09530
MAD09540
MAD09550
MAD09560
MAD09570
MAD09580
MAD09590
MAD09600
MAD09610
MAD09620
MAD09630
MAD09640
MAD09650

```

SUMI=(DATA(I+1)+DATA(J+1))/2.
DIFR=(DATA(I)-DATA(J))/2.
DIFI=(DATA(I+1)-DATA(J+1))/2.
TEMPI=WR*SUMI+WI*DIFR
TEMPJ=WI*SUMI-WR*DIFR
DATA(I)=SUMR+TEMPI
DATA(J)=SUMR-TEMPJ
DATA(I+1)=DIFI+TEMPI
DATA(J+1)=-DIFI+TEMPJ
J=J+NP2
IMIN=IMIN+2
JMIN=JMIN-2
TEMPR=WR
WR=WR*WSTPR-WI*WSTPI
WI=TEMPR*WSTPI+WI*WSTPR
IF(IMIN-JMIN)710,73C,740
IF(I-SIGN)731,740,740
DO 735 I=IMIN,NTOT,NP2
DATA(I+1)=DATA(I+1)
NP2=NP2+NP2
NTOT=NTOT+NTOT
J=NTOT+1
IMAX=NTOT/2+1
IMIN=IMAX-2*NHAF
I=IMIN
GO TO 755
DATA(J)=DATA(I)
DATA(J+1)=-DATA(I+1)
I=I+2
J=J-2
IF(I-IMAX)750,760,760
DATA(J)=DATA(IMIN)-DATA(IMIN+1)
DATA(J+1)=0.
IF(I-J)77C,780,78C
DATA(J)=DATA(I)
I=I-2
J=J-2
IF(I-IMIN)775,775,765
DATA(J)=DATA(IMIN)+DATA(IMIN+1)
DATA(J+1)=0.
IMAX=IMIN
GO TO 745
DATA(1)=DATA(1)+DATA(2)
DATA(2)=0.
GO TO 900

```

COMPLETE A REAL TRANSFORM FOR THE 2ND OR 3RD DIMENSION BY
CONJUGATE SYMMETRIES.

```

C      800      IF(I1RNG-NP11805,500,900
C      805      DO 860 I3=1,NTOT,NP2
C          I2MAX=I3+NP2-NP1
C          DO 860 I2=I2,I2MAX,NP1
C              IMIN=I2+I1RNG
C              IMAX=I2+NP1-2
C              JMAX=2*I3+NP1-IMIN
C              IF(I2-I31820,820,810
C                  JMAX=JMAX+NP2
C              IF(IDIM-21850,850,830
C                  J=JMAX*NP0
C                  DO 840 I=IMIN,IMAX,2
C                      DATA(I)=DATA(J)
C                      DATA(I+1)=-DATA(J+1)
C                      J=J-2
C                  J=JMAX
C                  DO 860 I=IMIN,IMAX,NP0
C                      DATA(I)=DATA(J)
C                      DATA(I+1)=-DATA(J+1)
C                      J=J-NP0
C                  END CF LOOP ON EACH DIMENSION
C      860
C      500      AFO=NP1
C      910      NP1=NP2
C      520      NPREV=N
C          RETURN
C          END
C          SUBROUTINE CHBFT
C      PURPOSE:
C      SUBROUTINE CHBFT EVALUATES THE COEFFICIENTS OF AN MTH ORDER
C      POLYNOMIAL  $P(X)=A(1)+A(2)*X+A(3)*X^2+...+A(M+1)*X^M$  SUCH
C      THAT THE MAXIMUM ERROR  $ABS(P(X(1))-Y(1))$  IS A MINIMUM OVER
C      THE N (N.GT.M+1) SAMPLE POINTS  $X(I), Y(I), I=1,2,...,N$ . THE
C       $X(I)$  MUST FORM A STRICTLY MONOTONIC SEQUENCE: 1.E.,
C       $X(1), LT, X(2), LT, X(3), LT, ..., X(N)$ . THIS SUBROUTINE IS A
C      CONVERSION FROM ALGOL TO FORTRAN OF ALGORITHM 318, CHEBYSHEV
C      CURVE-FIT FROM COMMUNICATIONS OF THE ACM VOL.10, NUMBER 12,
C      DECEMBER, 1967. THE AUTHOR OF THE ALGOL VERSION WAS
C      J. BOOTHROYD FROM THE UNIVERSITY OF TASMANIA.
C      USAGE:
C      CALL CHEFT (X,Y,N,A,M,RX,RH,R)
C      DESCRIPTION OF PARAMETERS:
C      X -ARRAY OF ABSCISSAE DIMENSIONED REAL*4 X(N)

```

[illegible]

MAD10620
MAD10630
MAD10640
MAD10650
MAD10660
MAD10670
MAD10680
MAD10690
MAD10700
MAD10710
MAD10720
MAD10730
MAD10740
MAD10750
MAD10760
MAD10770
MAD10780
MAD10790
MAD10800
MAD10810
MAD10820
MAD10830
MAD10840
MAD10850
MAD10860
MAD10870
MAD10880
MAD10890
MAD10900
MAD10910
MAD10920
MAD10930
MAD10940
MAD10950
MAD10960
MAD10970
MAD10980
MAD10990
MAD11000
MAD11010
MAD11020
MAD11030
MAD11040
MAD11050
MAD11060
MAD11070
MAD11080
MAD11090

```

DC 4 J=1,MPLUS1
I1=MPLUS2
A11=A(I1)
RHI1=RH(I1)
I=MPLUS1
5 DENCM=RX(I1)-RX(I-J+1)
AI=A(I)
RHI=RH(I)
A(I1)=(A11-AI)/DENOM
RHI1)=(RHI1-RHI)/DENOM
I1=I
AI1=AI
RHI1=RHI
I=I-1
IF(I-J) 4,5,5
4 CONTINUE
EQUATE (M+1) THE DIFFERENCE TO ZERO TO DETERMINE H
H=-A(MPLUS2)/RH(MPLUS2)
WITH H KNOWN, COMBINE THE FUNCTION AND DEVIATION DIFFERENCES
DC 6 I=1,MPLUS2
6 A(I)=A(I1)+RHI(I)*H
J=M
7 XJ=RX(J)
I=J
AI=A(I)
JPLUS1=J+1
DO 8 I1=JPLUS1,MPLUS1
AI1=A(I1)
A(I1)=AI-XJ*AI1
AI=AI1
I=I1
8 J=J-1
IF(J-1) 9,7,7
9 CONTINUE
IF THE REFERENCE DEVIATION IS NOT INCREASING MONOTONICALLY
THEN EXIT
HMAX=ABS(H)
IF(HMAX.GT.PKEVH) GO TO 29
A(MPLUS2)=-HMAX
RETURN
FIND THE INDEX, IMAX, AND VALUE, HIMAX, OF THE LARGEST ABSOLUTE
ERROR FOR ALL SAMPLE POINTS
29 A(MPLUS2)=HMAX
PREVH=HMAX
IMAX=P(1)
HIMAX=H
J=1

```

```

C
C
C
110 CONTINUE
IF (I-1/2*2).NE.0) NEXTI=-H
IF (HIMAX#NEXTI.GE.0) GO TO 115
IF (IMAX.GE.R(1)) GO TO 116
J1=MPLUS2
J=M
117 R(J1)=R(J)
J1=J
IF (J-1) 118, 117, 117
118 R(1)=IMAX
GO TO 2
116 IF (IMAX.LE.R(MPLUS2)) GO TO 120
J=1
DO 121 J1=1,MPLUS2
R(J1)=R(J1)
121 R(MPLUS2)=IMAX
GC TO 2
115 R(1)=IMAX

```

```

MAD11100
MAD11110
MAD11120
MAD11130
MAD11140
MAD11150
MAD11160
MAD11170
MAD11180
MAD11190
MAD11200
MAD11210
MAD11220
MAD11230
MAD11240
MAD11250
MAD11260
MAD11270
MAD11280
MAD11290
MAD11300
MAD11310
MAD11320
MAD11330
MAD11340
MAD11350
MAD11360
MAD11370
MAD11380
MAD11390
MAD11400
MAD11410
MAD11420
MAD11430
MAD11440
MAD11450
MAD11460
MAD11470
MAD11480
MAD11490
MAD11500
MAD11510
MAD11520
MAD11530
MAD11540
MAD11550
MAD11560
MAD11570

```

THIS POINT, EXCHANGE POINT HAVING AN ERROR OF THE NEAREST REFERENCE POINT

MAD11580
MAD11590
MAD11600
MAD11610
MAD11620
MAD11630
MAD11640
MAD11650
MAD11660
MAD11670
MAD11680
MAD11690
MAD11700
MAD11710
MAD11720
MAD11730
MAD11740

```

GO TO 2
12C R(1-1)=IMAX
GO TO 2
END
//GO.SYSIN DD *
LA MESA VILLAGE, 18 AUG 82 0507-0636 LOCAL.
PSD CF X COIL, AMP IN DB REF NT**2/HZ
LA MESA VILLAGE, 18 AUG 82 0507-0636 LOCAL.
PSD CF Y COIL, AMP IN DB REF NT**2/HZ
LA MESA VILLAGE, 18 AUG 82 0507-0636 LOCAL.
PSD CF Z COIL, AMP IN DB REF NT**2/HZ
LA MESA VILLAGE, 18 AUG 82 0507-0636 LOCAL.
PSD CF TOTAL FIELD, AMP IN DB REF NT**2/HZ
//GO.FT20F001 DD UNIT=3400-4,VOL=SER=GMDT4A,DISP=(CLD,KEEP),
// LABEL=(1,1,1,1)
// DCB=(RECFM=FB,LRECL=32,BLKSIZE=512,DEN=2)
//GO.SYSOUMP DD SYSOUT=A

```

LIST OF REFERENCES

1. Naval Oceanography Office, Washington, D. C., Technical Report TR-218, The Influence of the Natural Environment on MAD Operations, by James A. Brennan and Thomas M. Davis, 1969.
2. Chapman, Sydney, "Perspective," pp 3-28 in Physics of Geomagnetic Phenomena, Matsushita, S., and Campbell, W. H., editors, Academic Press, New York, 1967.
3. Parker, E. N., Cosmical Magnetic Fields: Their Origin and Their Activity, Clarendon Press, Oxford, 1979.
4. Air Force Cambridge Research Laboratories, L. G. Hanscom Field, Bedford, Massachusetts, Report AFRL-72-0570, The Geomagnetic Field, by David J. Knecht, 1972.
5. Air Force Geophysics Laboratory, L. G. Hanscom Field, Bedford, Massachusetts, Report AFGL-79-0192, Proceedings of the Air Force Geophysics Laboratory Workshop on Geomagnetism: April 6-7, 1979, edited by R. C. Sagallyn, R. O. Hutchinson, and S. Gussenhoven, p. 47, 1979.
6. Jacobs, J. A., Geomagnetic Micropulsations, Springer-Verlag, New York, 1970.
7. Vestine, E. H., "Main Geomagnetic Field," pp 181-234 in Physics of Geomagnetic Phenomena, Matsushita, S., and Campbell, W. H., editors, Academic Press, New York, 1967.
8. Haymes, Robert C., Introduction to Space Science, John Wiley and Sons, Inc., New York, 1971.
9. Nagata, Takesi, and Ozima, Minoru, "Paleomagnetism," pp 103-180 in Physics of Geomagnetic Phenomena, Matsushita, S., and Campbell, W. H., editors, Academic Press, New York, 1967.
10. Kern, John W., "Magnetosphere and Radiation Belts," pp 1037-1109 in Physics of Geomagnetic Phenomena, Matsushita, S., and Campbell, W. H., editors, Academic Press, New York, 1967.
11. Matsushita, S., "Solar Quiet and Lunar Daily Variation Fields," pp 301-424 in Physics of Geomagnetic Phenomena, Matsushita, S., and Campbell, W. H., editors, Academic Press, New York, 1967.

12. Reid, George C. "Ionospheric Disturbances," pp 627-662 in Physics of Geomagnetic Phenomena, Matsushita, S., and Campbell, W. H., editors, Academic Press, New York, 1967.
13. Matsushita, S. "Geomagnetic Disturbances and Storms," pp 793-819 in Physics of Geomagnetic Phenomena, Matsushita, S., and Campbell, W. H., editors, Academic Press, New York, 1967.
14. Naval Air Development Center, Warminster, Pennsylvania, Report NADC-EL-47-50, Magnetic Airborne Detection Frequency Responses, by J. E. Anderson, 1949.
15. U. S. National Defense Research Committee, Washington, D. C., Summary Technical Report of Division 6, Volume 1, A Survey of Subsurface Warfare in World War II, Appendix H, Preliminary Memorandum on Magnetic Detection of Submarines from Moving Ships or Airplanes, by L. B. Slichter, 1940.
16. U. S. National Defense Research Committee, Washington, D. C., Summary Technical Report of Division 6, Volume 5, Magnetic Airborne Detector Program, edited by J. S. Coleman, 1946.
17. Operations Evaluation Group, Navy Department, Washington, D. C., OEG Report No. 51, Antisubmarine Warfare in World War II, by Charles M. Sternhell and Alan M. Thorndike, 1946.
18. Price, Alfred, Aircraft Versus Submarine, Naval Institute Press, 1973.
19. Operations Evaluation Group, Navy Department, Washington, D. C., OEG Report No. 54, Methods of Operations Research, by Philip M. Morse and George E. Kimball, 1946.
20. Chilton, F., Wood, L., and Buntzen, R., "Electric and Magnetic Sensing Systems: Applications," chapter 10 of Applications of Remote Sensing to Ocean Surveillance, AGARD Lecture Series No. 88, North Atlantic Treaty Organization, Advisory Group for Aerospace Research and Development, London, 1977.
21. Texas Instruments Incorporated, Dallas, Texas, Report No. C2-61009-2, MAD Signal Processing Study, Analytical Report No. 2 (Final), Volume 1, 1961.
22. Lockheed-California Company, Burbank, California, Lockheed Orion Service Digest, Issue 26, Magnetic Anomaly Detection - AN/ASQ-81 MAD System, 1972.

23. Lockheed-California Company, Burbank, California, Lockheed Orion Service Digest, Issue 28, Magnetic Anomaly Detection - The Total System in Relation to Compensation, 1973.
24. Personal communication between the author and Dr. A. Ochadlick, Naval Air Development Center, Warminster, Pennsylvania, and Naval Postgraduate School, Monterey, California.
25. Weaver, J. T., "Magnetic Variations Associated with Ocean Waves and Swell", Journal of Geophysical Research, v. 70, No. 8, pp. 1927-1929, April 1965.
26. Nishida, A., Geomagnetic Diagnosis of the Magnetosphere, Springer-Verlag, New York, 1978.
27. Lincoln, J. Virginia, "Geomagnetic Indices," pp 66-100 in Physics of Geomagnetic Phenomena, Matsushita, S., and Campbell, W. H., editors, Academic Press, New York, 1967.
28. Bartels, J., "The geomagnetic measures for the time-variations of solar corpuscular radiation, described for use in correlation studies in other geophysical fields," pp 227 - 236, in the Annual of the International Geophysical Year, Volume 4, part IV, Pergamon Press, Oxford, 1957.
29. Air Force Global Weather Central, Offutt Air Force Base, Nebraska, Report Number AFGWC/TN-80/002, Geomagnetic Index Calculation and Use at AFGWC, by Robert D. Prochaska, 1980.
30. Commander, Air Test and Evaluation Squadron One, Patuxent River, Maryland, Report VX1 OTG 261-4-78, Patuxent River, Maryland, Recommended P3-C MAD (Magnetic Anomaly Detection) Compensation Management Program and Procedures, 1978.
31. Personal communication between the author and LCDR F. Shapley, Fleet Numerical Oceanographic Center, Monterey, California.
32. Joint USAF-NOAA Space Environment Services Center, Boulder, Colorado, Preliminary Report and Forecast of Solar-Geophysical Data, Issue 348, 4 May 1982.
33. Naval Oceanography Office, Washington, D. C., Technical Report TR-250, The Effect of Geomagnetic Micropulsations on MAD Systems, by James A. Brennan and Kuno Smits, 1975.

34. Mayaud, P. N., Derivation, Meaning, and Use of Geomagnetic Indices, Geophysical Monograph 22, American Geophysical Union, Washington, D. C., 1980.
35. Fraser-Smith, A. C., and Heinz, Otto, A Proposed MAD Index of Geomagnetic Activity, Abstract for the First International Symposium of the Society of Madmen, 1982.
36. Air Force Cambridge Research Laboratories, Bedford, Massachusetts, Report No. AFCL-71-0144, Study of the Characteristics of ULF-ELF Fluctuations of the Geomagnetic Field, by George L. Mason, 1971.
37. Naval Air Development Center, Warminster, Pennsylvania, Technical Memorandum NADC-202219:ARO, Correlation of K index with geomagnetic noise in the MAD band pass, by Andrew R. Ochadlick, Jr., 1976.
38. Miller, Irwin, and Freund, John E., Probability and Statistics for Engineers, Second Edition, Prentice-Hall, Inc., Englewood Cliffs, New Jersey, 1977.
39. McDevitt, Gerald R., and Homan, B. Bert, Low Frequency Geomagnetic Fluctuations (.04 to 25 Hz) on Land and on the Floor of Monterey Bay, M.S. Thesis, Naval Postgraduate School, Monterey, 1980.
40. Beard, Michael W. Power Spectra of Geomagnetic Fluctuations Between 0.02 and 20 Hz, M.S. Thesis, Naval Postgraduate School, Monterey, 1981.
41. McKinley, Gary M. and Santos, Robert M. Characteristics of Geomagnetic Power Spectra on Land and Sea in the Period Range 0.2 to 400 seconds, M.S. Thesis, Naval Postgraduate School, Monterey, 1980.
42. Fraser-Smith, A. C., "Short-term prediction and a new method of classification of Pc 1 pulsation occurrences", Planet. Space Sci., Volume 28, 739-747, 1980.
43. Fraser-Smith, A. C., "Long-term prediction of Pc 1 geomagnetic pulsations: Comparison with observations", Planet. Space Sci., Volume 29, 715-719, 1981.

BIBLIOGRAPHY

Ames, Morgan P., Jr., and Vehslage, Louis M., Low Frequency Geomagnetic Fluctuations (0.025 to 20 Hz) on the Floor of Monterey Bay, M.S. Thesis, Naval Postgraduate School, Monterey, 1981.

Regan, Robert D., and Cain, Joseph C., The Use of Geomagnetic Field Models in Magnetic Surveys, NASA Report TM-X-70777, Goddard Space Flight Center, Greenbelt, Maryland, 1974.

Yannuzzi, Edward, Evaluation of Magnetic Airborne Detecting Set AN/ASQ-81, Report No. NADC-AE-619, Naval Air Development Center, Warminster, Pennsylvania, 1966.

INITIAL DISTRIBUTION LIST

	No. Copies
1. Defense Technical Information Center Cameron Station Alexandria, Virginia 22314	2
2. Library, Code 0142 Naval Postgraduate School Monterey, California 93940	2
3. Chairman ASW Academic Group, Code 71 Naval Postgraduate School Monterey, California 93940	1
4. Dr. Otto Heinz, Code 61Hz Department of Physics Naval Postgraduate School Monterey, California 93940	2
5. Dr. Andrew R. Ochadlick, Jr., Code 610c Department of Physics Naval Postgraduate School Monterey, California 93940	2
6. Dr. Paul Moose, Code 62Me Department of Electrical Engineering Naval Postgraduate School Monterey, California 93940	1
7. Dr. Michael Thomas, Code 61To Department of Physics Naval Postgraduate School Monterey, California 93940	1
8. LT Jeffrey M. Schweiger, USN 44 Roundabout Road Smithtown, New York 11787	3
9. LT Wade D. Dwyer, USN Commander, Helicopter ASW Wing One P.O. Box 92 Naval Air Station Jacksonville, FL 32212	1
10. LCDR Ken Peters, USN Commander, Patrol Wings, Atlantic Naval Air Station Brunswick, ME 04011	1
11. Commander, Patrol Wings U.S. Pacific Fleet Naval Air Station Moffett Field, CA 94035	1
12. Dr. A. C. Fraser-Smith Radio Science Laboratory Stanford Electronics Laboratories Stanford University Stanford, CA 94305	1

13. Dr. David M. Bubenik 1
Assistant Director,
Electromagnetic Sciences Laboratory
SRI International
333 Ravenswood Avenue
Menlo Park, CA 94025

14. Dr. Robert N. McDonough, 8-368 2
The Johns Hopkins University
Applied Physics Laboratory
Johns Hopkins Road
Laurel, MD 20801

15. Commander, Anti-Submarine Warfare Wing, 1
U.S. Pacific Fleet
Naval Air Station, North Island
San Diego, CA 92135

16. Mr. Robert D. Smith (AIR-5490) 1
Naval Air Systems Command
Washington, D.C. 20361

17. Commander, Sea Based ASW Wings, Atlantic 1
Naval Air Station
Box 102
Jacksonville, FL 32212

18. Mr. John Shannon 1
Naval Air Development Center (Code 3012)
Warminster, PA 18974

19. Mr. Edward Yanzuzzi 1
Naval Air Development Center (Code 30)
Warminster, PA 18974

20. Chief of Naval Research
Department of the Navy
800 North Quincy Street
Arlington, VA 22217
Code 100C1 1
Code 460 1
Code 464 1
Code 480 1

21. Mr. Gracen Joiner 1
Chief of Naval Research (Code 414)
Department of the Navy
800 North Quincy Street
Arlington, VA 22217

22. Mr. William Andahazy 1
Naval Ship Research & Development Center
Annapolis Laboratory
Annapolis, MD 21402